GEOMAR
Helmholtz-Zentrum für Ozeanforschung Kiel

ANTHROPOGENIC EMISSIONS OF GREENHOUSE GASES FROM THE SEAFLOOR INTO THE NORTH SEA

DISSERTATION
zur Erlangung des Doktorgrades
der Mathematisch-Naturwissenschaftlichen Fakultät
der Christian-Albrechts-Universität zu Kiel

LISA VIELSTÄDTE
Kiel, 2015

Referent: ..... Prof. Dr. Klaus Wallmann

Koreferent: ..... Priv. Doz. Dr. Mark Schmidt

Tag der mündlichen Prüfung: 22.02.2016

Zum Druck genehmigt: 22.02.2016

Der Dekan

Erklärung

Hiermit erkläre ich, dass die vorliegende Doktorarbeit selbständig, abgesehen von der Beratung durch den Betreuer, erstellt wurde. Weder diese noch eine ähnliche Arbeit wurden an einer anderen Abteilung oder Hochschule im Rahmen eines Prüfungsverfahrens vorgelegt, veröffentlicht oder zur Veröffentlichung vorgelegt. Ferner versichere ich, dass die Arbeit unter Einhaltung der Regeln guter wissenschaftlicher Praxis der Deutschen Forschungsgemeinschaft entstanden ist.

Kiel, den 15. Dezember 2015

Lisa Vielstädte

Acknowledgements

This study was realized under supervision of Dr. Matthias Haeckel and Prof. Dr. Klaus Wallmann. In the beginning, I would like to thank Matthias for his professional support, his readiness for discussion, and for the pleasant and amicable working atmosphere throughout the period of my PhD. Thank you, Matthias!

I sincerely thank Prof. Dr. Klaus Wallmann for accepting me as a PhD student within the Research Unit Marine Geosystems and for acting as a co-supervisor and referee for this dissertation. Klaus had always an open ear and many times he gave helpful advise. Thank you, Klaus!

I would also like to thank Dr. Marcus Dengler for being a member of my Thesis Committee. Marcus provided valuable insights into phyiscal oceanography which considerably helped to improve the progress in plume dispersion modelling. Thank you, Marcus!

Moreover, I am grateful to Prof. Dr. Daniel F. McGinnis for fruitful cooperation and for supporting me in the very beginning of my PhD. He provided first valuable insights into bubble dissolution modelling. Thank you, Dan!

Special thanks go to Dr. Jens Karstens, who supported me with seismic data analysis. He also joint me at the International Conference "Gas in Marine Sediments" in Taipei and various ECO2 project meetings. It was always a pleasure to discuss and have him by my side! Thank you, Jens!

I would also like to thank Prof. Dr. Jens Greinert and Prof. Dr. John Pohlman who saw the potential of integrating my studies on gas bubble dissolution into their work. This work resulted in a manuscript and two conference talks, which I could contribute to as a co-author.

In this context, I would also like to thank Prof. Dr. Rachael James for involving me into her work. This cooperation resulted into a co-authorship of a review paper on effects of climate change on methane emissions from the seafloor sediments in the Arctic Ocean.

During my PhD, I took part in five seagoing expeditions. I would like to owe thanks to the crews and masters of RV Alkor and RV Celtic Explorer as well as the teams of ROV Kiel 6000 and Phoca for their valuable support during the cruises CE12010 and AL412. I gratefully thank Dr. Peter Linke and Sergiy Cherednichenko who designed the Gas Release Experiment providing extensive data for this dissertation. Special thanks go to Meike Dibbern, Matthias Haeckel, and Dirk Schroller for their support during onboard geochemical analysis. I also gratefully acknowledge the research diving team, Nikolaus Bigalke, Christian Howe, and Matthias Kreuzburg for excellent collaboration and support during our expeditions to natural CO_2 seeps offshore Panarea Island. Without their outstanding expertise much of the work

would have not been possible.

Further, I would also like to thank the DFG-funded Cluster of Excellence "The Future Ocean", the projects ECO2, MIDAS, and SUGAR for financing my PhD studies and for giving me the possibility to present the progress of my work at various international project meetings, workshops, and conferences.

I also want to thank all my colleagues and friends at GEOMAR for the friendly atmosphere. Special thanks go to Christian Deusner and Dirk Schroller who shared an office with me. Thank you for the nice conversation, the friendly working climate, and for tolerating the chaos on my desk!

Special thanks go to my friends and family for always supporting me. In particular, I want to thank Jana Wellendorf for her valuable support in the final phase of my PhD and Björn Klein for his encouragement and the affectionate companionship during the past years.

Abstract

Leakage from hydrocarbon wells is of concern because the primary fugitive component of oil and gas is methane (CH_4) – a potent greenhouse gas (GHG) which has a significant warming potential. Current regulations only target the leakage of produced fossil fuels from surface oil and gas installations (wellhead, pumps, controllers etc.), commonly identified by testing of sustained casing pressure. Because operators and regulators stop assessing well integrity after well abandonment and do not consider shallow gas migration along the outside of wells, fugitive CH_4 emissions are currently underestimated. Understanding GHG emissions from the hydrocarbon-industry requires a profound knowledge of all types of leakage, including well integrity failure and shallow gas migration from both active and abandoned wells. Consequently, the present thesis investigates the leakage of shallow gas along hydrocarbon wells; one of the missing emission sources in GHG inventories.

In the North Sea, and in other hydrocarbon-prolific areas of the world shallow gas pockets are frequently observed in the sedimentary overburden above the deep hydrocarbon reservoirs. When drilling wells for oil and gas exploration and production, these shallow gas accumulations are penetrated, thereby fracturing the sediment surrounding the well providing a highly permeable escape route for the shallow gas.

Chapter II provides the first qualitative and quantitative data on this type of leakage in the North Sea. It presents geochemical and seismic analysis of anthropogenic gas emissions at three abandoned wells in the Central North Sea and estimates the emitted seabed and atmospheric methane fluxes. The data are interpreted with respect to the geology at the wells and compared to other anthropogenic emissions at the blowout site (22/4b) and natural methane seepage in the North Sea. High methane concentrations, low abundance of higher hydrocarbons, and light $\partial^{13}C$-signatures in the emanating gas, a geochemical signature that significantly differs from the deep hydrocarbon reservoirs, clearly point towards a shallow, biogenic emissions source. Quantitative data further indicate that the methane emissions at the three investigated wells are comparable to those at major natural seeps in the North Sea and thus, constitute an unconsidered, but potentially significant methane source.

To further investigate the relevance of these anthropogenic methane fluxes, a North Sea-wide quantification of drilling-induced CH_4 emissions is provided in Chapter III. Quantifications are based on the extrapolation of observed gas emissions at the three leaky wells investigated in Chapter II and by correlating seismically mapped shallow gas pockets with 55 well paths in a representative area of the Central North Sea. Seismic evidence of numerous wells poking through shallow gas pockets indicates that one third of the existing well may leak methane.

The resulting methane input into the entire North Sea from this leakage is extrapolated to be almost 10-times larger than the other known methane sources (rivers, Wadden Sea, and natural seeps). It may account for a large fraction of the methane export into the North Atlantic and the atmospheric degassing flux which exceed the known sources by one order of magnitude. Together with other anthropogenic emissions from the blowout site (22/4b), the calculated methane input from shallow gas leakage largely closes the CH_4 budget of the North Sea.

The findings of Chapter II and III indicate that shallow gas leakage is likely a widespread phenomenon in the North Sea. This conclusion has important implications for Carbon Capture and Storage (CCS) since it implies that leakage from a carbon dioxide (CO_2) storage site can potentially occur along any type of well (production, exploration, or abandoned), as long as it penetrates the subsurface CO_2 plume.

As a consequence Chapter IV focuses on the Sleipner CO_2 storage site in the Central North Sea and investigates hypothetic, but probably realistic leakage of CO_2 along a well that penetrates the subsurface CO_2 plume and leaks into the ~80 m deep water column, using a combination of experimental field data and numerical modelling. The data are interpreted with respect to potential environmental consequences and leak detection. The results demonstrate that the impact and detectability of such leakage at low rates (<55 t yr^{-1} of CO_2) would be very localized, i.e. a few tens to one hundred meter around the gas release spot which is arguably not significant on a regional scale. Strong tidal currents and cycles, both prominent in the North Sea, significantly diminish the spreading of low-pH water masses into the far field of a leak by efficiently diluting elevated pCO_2 levels with background concentrations. The consequences of a single well leaking CO_2 are thus, found to be insignificant in terms of storage performance, environmental impact, and a climate control point of view.

Considering the millions of oil and gas wells drilled world-wide and the prospective implementation of CCS at a scale that would have significant impact on global CO_2 emissions, the leakage of gas along wells may become a wide-spread phenomenon contributing to future anthropogenic emissions of carbon-based greenhouse gases (CH_4 and prospectively CO_2), particularly onshore where gas is directly emitted into the atmosphere. This thesis stresses that pressure-based testing of well integrity is not sufficient for identifying and quantifying gas emissions (CH_4 or CO_2) along hydrocarbon wells. Therefore, it is important to improve our surveying and monitoring efforts and adapt the respective regulatory frameworks (national and international).

Kurzfassung

Undichte Kohlenwasserstoff-Bohrungen sind besorgniserregend, da die primär flüchtige Komponente von Öl und Gas Methan (CH_4) ist – ein starkes Treibhausgas welches erheblich zur globalen Klimaerwärmung beiträgt. Derzeitige Regulierungen verpflichten die Betreiber und Aufsichtsbehörden ausschließlich dazu die Freisetzung produzierter Kohlenwasserstoffe zu fahnden. Dieses wird üblicherweise durch spezielle Drucktests am Bohrkopf festgestellt. Die Integrität stillgelegter Bohrlöcher und die mögliche Migration von flachem Gas entlang der Bohrloch-Außenseite sind daher weitesgehend unbekannt. Dies führt zu einer Unterschätzung der flüchtigen CH_4 Emissionen in die Atmosphäre. Ein umfassendes Verständnis dieser industriellen CH_4 Emissionen erfordert detaillierte Kenntnisse über alle Leckagearten, einschließlich solcher, die durch das Integritätsversagen und der Migration von flachem Gas verursacht werden, sowohl von aktiven als auch stillgelegten Bohrlöchern. Die vorliegende Arbeit beschäftigt sich daher mit einem der in den Treibhausgasinventaren fehlenden industriellen Emissionsquellen: das Austreten von flachem Gas entlang Öl- und Gasbohrungen.

In der Nordsee, wie auch in anderen Kohlenwasserstoff-reichen Gebieten der Welt, kommen flache Gasakkumulationen sehr häufig in den Sedimenten über den tiefen Kohlenwasserstoffvorkommen vor. Beim Bohren für die Öl- und Gasexploration und -Produktion werden diese flachen Gasansammlungen durchbohrt und die umliegenden Sedimente gestört und zerklüftet, wodurch sich durchlässige Wegsamkeiten für das umliegende flache Gas bilden.

Kapitel II beinhaltet die ersten qualitativen und quantitativen Daten zu dieser Art der Leckage in der Nordsee. Es präsentiert geochemische und seismische Analysen anthropogener Gasaustritte entlang von drei stillgelegten Bohrlöchern in der zentralen Nordsee und schätzt die emittierten Methanflüsse am Meeresboden und in die Atmosphäre ab. Die Daten werden im Hinblick auf die lokale Geologie an den Bohrlöchern interpretiert und mit anderen anthropogenen Emissionen an dem Gas-Blowout (22/4b) sowie natürlichen Methanaustritten in der Nordsee verglichen. Hohe Methan-Konzentrationen, geringe Mengen an höheren Kohlenwasserstoffen und leichte $\partial^{13}C$-Werte in den austretenden Gasen, eine Signatur deutlich unterschiedlich derer tiefer Kohlenwasserstoff-Reservoire, weisen auf eine biogene Gasquelle im flachen Untergrund hin. Quantitative Daten zeigen, dass die von den drei untersuchten Bohrlöchern freigesetzten Methanemissionen mit denen natürlicher Methanaustritte in der Nordsee vergleichbar sind. Die erhobenen Daten zeigen, dass die Migration von flachem Gas einen unbeachteten, aber potenziell bedeutsamen Methaneintrag in die Nordsee darstellt.

Um die Relevanz dieser anthropogenen Methan-Austritte weiter zu untersuchen, beschäftigt sich Kapitel III mit der Nordseeweiten Quantifizierung der Bohrloch-induziereten CH_4-Emissionen. Die Quantifizierung basiert auf der Extrapolation der gemessenen Gasflüsse an den drei undichten Bohrlöchern, die in Kapitel II untersucht wurden, und der seismischen Kartierung von flachen Gasvorkommen, die mit dem Verlauf von 55 Bohrpfaden in einem repräsentativen Bereich der zentralen Nordsee korreliert werden. Die Korrelation deutet darauf hin, dass ein Drittel der Bohrlöcher durch flaches Gas gebohrt wurden und folglich potentielle Wegsamkeiten für die Migration des flachen Gases bilden. Der sich aus dieser Art der Leckage ergebende Methaneintrag in die gesamten Nordsee ist fast 10-mal größer als die anderen bekannten Methanquellen (Flüsse, Wattenmeer, und natürliche Seeps) und könnte somit erheblich zu den 20-fach größeren Methansenken, der Export in den Nordatlantik und die Entgasung in die Atmosphäre, beitragen. Zusammen mit den anthropogenen Emissionen des Gas-Blowouts (22/4b) kann der berechnete Methaneintrag das CH_4 Budget der Nordsee weitestgehend schließen.

Die erhobenen Daten aus Kapitel II und III lassen vermuten, dass die Migration von flachem Gas entlang von Bohrlöchern ein in der Nordsee weit verbreitetes Phänomen ist. Diese Beobachtung liefert wichtige Implikationen für die geologische Speicherung von CO_2 (kurz CCS), weil sie impliziert, dass das verpresste CO_2 möglicherweise entlang eines jeden Bohrlochs (Produktion, Exploration, oder stillgelegt) und ungeachtet dessen Integrität aus der Speicherstätte austreten kann, so lange dieses das unterirdische CO_2-Vorkommen durchdringt.

Folglich befasst sich Kapitel IV mit dem CO_2 Speicherungsprojekt „Sleipner“, das in der zentralen Nordsee operiert, und es untersucht das hypothetische, aber realistische Austreten von CO_2 entlang eines Bohrlochs, welches die unterirdische CO_2-Ansammlung durchdringt und in die ~ 80 m tiefe Wassersäule leckt. Die Arbeit beruht auf experimentellen und numerischen Daten, die im Hinblick auf die potentiellen Umweltauswirkungen und die Detektierbarkeit einens undichten Bohrlochs bei Sleipner interpretiert werden. Die experimentellen und numerischen Ergebnisse beweisen, dass die Detektierbarkeit und die Umweltauswirkungen einer solchen Leckage mit geringen Gasflüssen (< 55 t CO_2 yr^{-1}) auf einen kleinen Bereich (einige zehner- bis einhundert Meter) um das Leck herum begrenzt sein werden. Diese räumliche Beeinflussung ist in einem regionalen Kontext der Nordsee nicht relevant. Die Ausbreitung von Wassermassen mit einem CO_2-induzierten, niedrigen pH Wert wird durch die Nordseeweiten starken Strömungen und Gezeiten reduziert, indem diese die erhöhten CO_2 Werte effizient mit Hintergrundkonzentrationen mischen. Die Folgen eines einzigen undichten Bohrlochs werden daher als unbedeutend im Hinblick auf die CO_2 Speicher-Performance, Umweltauswirkungen und den Klima Schutz eingeschätzt.

Angesichts der Millionen von Öl- und Gasbohrungen weltweit und der zukünftigen Implementation von CCS in einem Ausmaß, das einen erheblichen Einfluss auf die globalen CO_2 Emissionen hätte, könnte die Leckage von Gas entlang von Bohrlöchern ein weit verbreitetes Phänomen werden, das zu den prospektiven, anthropogenen Emissionen der Kohlenstoffbasierten Treibhausgase (CH_4 und zukünftig CO_2) beiträgt, vor allem an Land, wo die Gasaustritte direkt in die Atmosphäre gelangen. Diese Dissertation betont, dass das Druck-basierte Testen der Bohrloch-Integrität unzureichend ist um Gasaustritte (CH_4 und CO_2) entlang von Kohlenwasserstoffbohrungen zu identifizieren und quantifizieren. Eine optimierte Überwachung und Anpassung entsprechender Regelwerke (national und international) sind daher unerlässlich.

Contents

I. General Introduction

I.1 Anthropogenic greenhouse gas emissions into the atmosphere

I.1.1 The carbon-based greenhouse gases CO_2 and CH_4

Anthropogenic greenhouse gas (GHG) emissions have been in the focus of scientific research in the last decades because rapidly increasing atmospheric GHG concentrations are suspected to induce global climate warming (Cook et al., 2013; Crowley, 2000), which is one of the major challenges for the global community in the next decades to centuries (Cias et al., 2013). GHGs strongly influence the radiative properties of the atmosphere, as they increase the capacity to adsorb long-wave radiation emitted from the earth surface. The carbon-based GHGs, that are carbon dioxide (CO_2) and methane (CH_4), are the two most abundant and important GHGs in the atmosphere, making up roughly 0.04 and 0.00018% (or 400 ppm and 1.85 ppm) of the total amount of atmospheric gases, respectively (see esrl.noaa.gov). Aside differences in their abundance, the carbon-based GHGs differ in their warming potential and atmospheric life-times: on short time scales CH_4 has an at least 20-fold higher warming potential as compared to the same amount of CO_2. However, CH_4 has an atmospheric life-time of only about 7 years whereas CO_2 persists in the atmosphere over a much longer period of time.

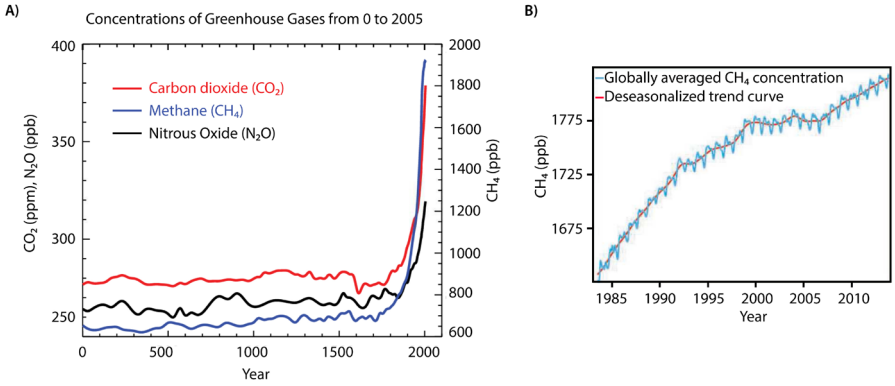

Figure I.1: A) Atmospheric concentrations of the carbon-based greenhouse gases, carbon dioxide (CO_2) and methane (CH_4), and nitrous oxide (N_2O) over the past 2,000 years (IPCC, 2007). **B**) Globally averaged atmospheric methane concentrations over the past three decades showing a quick rise before 1992, stagnant concentrations between 1999 and 2006, and the renewed increase of methane in the atmosphere since 2007 (modified after Nisbeth et al., 2014).

Since pre-industrial times (defined as 1750), atmospheric concentrations of carbon-based GHGs have increased incessantly by 40% for CO_2 and 150% for CH_4 (Fig. I.1), now reaching values that exceed those reconstructed from ice core records dating back 800,000 years (Cias et al., 2013; IPCC, 2014). This rapid increase is decidedly attributed to anthropogenic sources

with industrial CO_2 emissions accounting for about 78% of the total GHG emissions increase during the last 40 years (IPCC, 2014). Moreover, around two-thirds of the total CH_4 emissions are caused by human-actions (Nisbet et al., 2014; Cias et al., 2013 based on top-down estimates). The human-induced change in the atmospheric composition, with which major tropospheric, terrestrial, and oceanic sinks cannot compete with, primarily results from emissions associated with energy use (primarily contributing to atmospheric CO_2) and urbanization and land use changes (e.g. deforestation for CO_2 and agriculture for CH_4) (Karl and Trenberth, 2003).

The burning of fossil fuels (coal, oil, gas) is the primary source for the growth in atmospheric CO_2, also slightly contributing to other atmospheric GHGs, i.e. CH_4 and nitrous oxide (N_2O). Energy-related emissions other than fossil fuel combustion significantly contribute to the acceleration of "old or fossil" CH_4 (^{14}C-free) in the atmosphere, primarily due to the fugitive loss of natural gas (containing ~90% of CH_4) from hydrocarbon equipment leaks, gas venting and flaring, fossil fuel treatment and transportation. Based on the Emission Database for Global Atmospheric Research (EDGAR v.4.2) roughly 20% of the total anthropogenic CH_4 sources are attributed to fugitive emissions from oil and gas production. It should however be noted that, while some of these fugitive emission sources are intended (e.g. vent and flare systems), and therefore relatively well characterized, the quantity and composition of accidental or unintended emissions (e.g. equipment leaks during production and transportation) are subjected to significant uncertainty, as mentioned by the IPCC Guidelines for National Greenhouse Gas Inventories (2006).

Poor understanding of the quantity and composition of fugitive emissions is reflected by its debated role in controlling global atmospheric CH_4 concentrations. Stagnant CH_4 concentrations in the atmosphere between 1999 and 2006 and the renewed increase of CH_4 in the atmosphere since 2007 (Fig. I.1b) have been linked to decreasing fugitive emissions from the hydrocarbon industry (Kirschke et al., 2013 and references therein) and to the subsequent intensification of shale gas and oil extraction by hydraulic fracturing in the United States (Nisbet et al., 2014; Kirschke et al. 2013), respectively. However, this inference is debated because atmospheric CH_4 has become more depleted in ^{13}C since 2007, an indication that growth is dominated by ^{12}C-richer emissions from biogenic sources such as wetlands and ruminants (Nisbet et al., 2014 and references therein).

Considering that the human impact on the global climate system is already apparent by increasing global temperatures on land and in the oceans, partial melting of the Greenland and Antarctic ice sheets, ocean acidification, extreme weather events, and a global mean sea level rise of 19 cm during the last century, (IPCC, 2014) there is a strong need of human efforts to better understand GHG emissions so that appropriate mitigation strategies can be developed and implemented in order to control climate change.

I.1.2 The ocean's role in anthropogenic GHG emissions

The oceans play a key role in global warming because they constitute a net sink for atmospheric carbon, having absorbed ~30% of the anthropogenic CO_2 emissions throughout the industrial era (IPCC, 2014). While this has a positive impact on the magnitude of global warming, increasing levels of dissolved inorganic carbon (DIC) in the oceans are changing the chemistry of seawater and making it more acidic, which poses risks for marine ecosystems. From a climate control point of view, there is concern that due to complex feedback mechanisms in the carbon-climate system, this oceanic uptake of atmospheric CO_2 may substantially decline primarily as a consequence of the weakening of the ocean thermohaline circulation in the event of ongoing climate warming (Sarmiento and Le Quéré, 1996). This is supported by coupled climate models revealing that a weakening of the Atlantic Meridional Overturning Circulation (AMOC), is very likely to occur (IPCC, 2014 Chapter 3).This reduction would have a major impact on the future growth rate of atmospheric CO_2 because the AMOC is associated with the production of about half of the global ocean's deep waters in the northern North Atlantic and responsible for most of the meridional transport of heat and carbon (IPCC, 2014). Observations of changes in the AMOC are too short to provide evidence for any long-term trend, showing however interannual variability (IPCC, 2014 Chapter 3).

One idea to extent the oceanic sink in a manner that avoids ocean acidification is to capture CO_2 from industrial sources and store it in marine sediments 1-3 kilometers below the

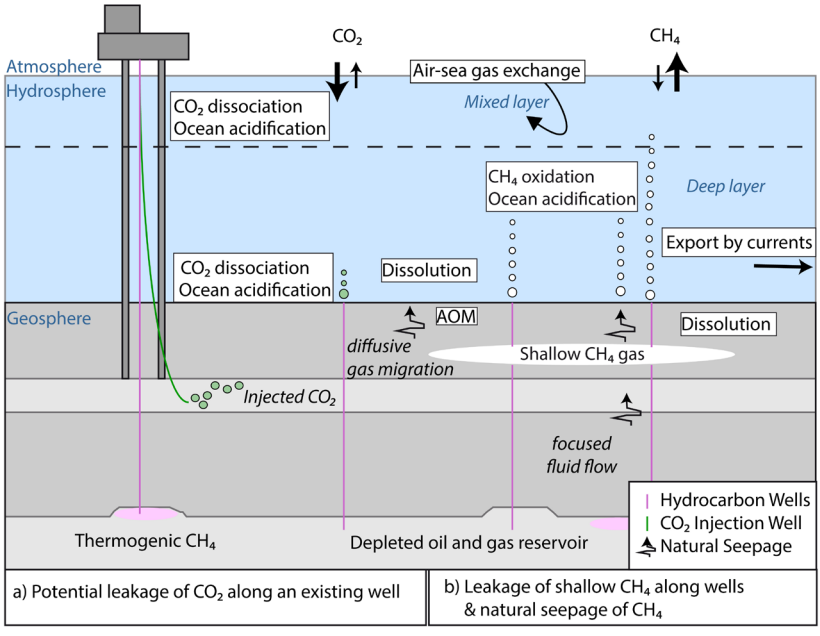

Figure I.2: Scheme illustrating anthropogenic and natural GHG emissions (CH_4 and prospectively CO_2) from the seabed into the Ocean (natural, hydrothermal venting of CO_2 is not shown). Further processes controlling the fate of seeping (or leaking gases) during upward migration through the sediment, through the water column, and up towards the atmosphere are shown. Bold arrows illustrate that the ocean is a net source for atmospheric CH_4 and a net sink for atmospheric CO_2.

seafloor. However, there is concern that CO_2 might escape from the storage reservoir and leak into the ocean posing risk for marine ecosystems or may be mixed back into the atmosphere causing climate damage. Studying the suitability of marine sediments to constitute an "extra" oceanic sink for atmospheric CO_2 is an important step in mitigating climate change.

Aside from the prospective implementation of submarine CCS at a scale that would have a significant impact on reducing anthropogenic CO_2 emissions, substantial amounts of carbon (i.e. in the form of CH_4) are already stored in marine sediments and submarine gas hydrates (i.e. >455 Gt of methane-bound carbon; Wallmann et al., 2012). These quantities of CH_4 originate from mainly two distinctly different processes 1) the microbial (anaerobic) degradation of shallow, organic-rich sediments (termed biogenic CH_4) or 2) the thermal breakdown of organic compounds in deeply buried sediments (termed thermogenic CH_4). Minor amounts of CH_4 in the oceans are abiogenic in origin and are derived by inorganic processes operating deep within the Earth's crust and underlying mantle (Kvenvolden, 2005). Only a fraction of the sedimentary CH_4 migrates upwards to the seafloor and reaches the water column. The microbial process of anaerobic oxidation of CH_4 (AOM) constitutes the most efficient sink for seeping CH_4, efficiently removing it from marine sediments before it reaches the sediment-water-interface (Hinrichs and Boetius, 2002 and references therein). Due to higher vertical advection velocities of migrating bubbles in marine sediments as compared to diffusive fluxes, rising CH_4 bubbles can by-pass this microbial filter and directly transport CH_4 into the water column, where gas bubbles are prone to dissolution during their ascent. Here, dissolved CH_4 is subjected to advective transport by ocean currents and oxidation by microbes where aerobic metabolism can be efficient under some circumstances (Steinle et al., 2015). Thus, depending on the gas ebullition type (i.e. diffusive or bubble flux) and the oceanic setting (i.e. water depth, stratification, and microbial oxidation potential) only a fraction of the seeping gas may reach the atmosphere, either via direct bubble transport or via the diffusive sea-air gas exchange which finally transports CH_4 dissolved in the surface mixed layer to the atmosphere (Fig. I.2).

As a result, global oceanic CH_4 fluxes are small, contributing roughly 2% to the global atmospheric CH_4 emissions. While all of this oceanic CH_4 contribution, meanwhile included in global GHG inventories (Cias et al., 2013), is currently attributed to natural seabed sources, that are mud volcanoes, natural seeps, and oceanic ridges, some must also result from leaking oil and gas wells.

Poor understanding of oceanic methane sources is due to the challenge for oceanic GHG emission studies to detect (all) sources at the seabed and attributing observed gas flares or CH_4 concentrations in seawater to multiple potential seabed sources, both natural and anthropogenic. Attribution is complicated by the fact that anthropogenic emissions from leaky wells can look like natural gas seepage because many of the abandoned wells

"disappeared" with no evidence of their existence at the seafloor.

I.2 Anthropogenic CH_4 emissions from hydrocarbon wells

As a result of extensive hydrocarbon exploration the world hosts several millions of wells (onshore and offshore), many believed to be leaking CH_4 which is the primary fugitive component of fossil fuels and has a significant warming potential. Gas leakage from hydrocarbon wells can arise from two different mechanisms: (1) the failure of well material, (primarily) leading to uncontrolled gas migration from the reservoir or (2) the drilling-induced disturbance and fracturing of sediments around the wellbore, leading to unintended release of gas (from the deep reservoir or any other hydrocarbon accumulation in the shallower subsurface) along the outside of the well (Fig. I.3).

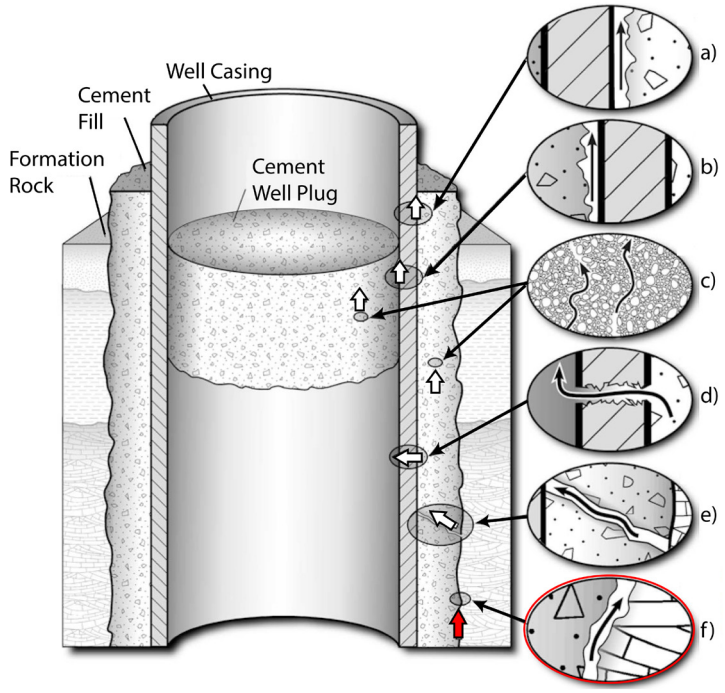

Figure I.3: Scheme illustrating possible leakage pathways through (white arrows) and along (red arrow) an abandoned well: **a**) Between casing and cement; **b**) between cement plug and casing; **c**) through the cement pore space as a result of cement degradation; **d**) through casing as a result of corrosion; **e**) through fractures in cement; and **f**) between cement and rock along the outside of the well (modified after Gasda et al., 2004).

Present regulations only target leakage of produced fossil fuels and formation fluids from the reservoir, primarily due to human and environmental safety reasons (e.g. U.S. Mineral Management Service, Norwegian NORSOK). Therefore, the petroleum industry considers the potential failure of well material (e.g. damaged casing steel and poorly bonded or

degraded cement), typically identified by diagnostic testing of sustained casing pressure (SCP) (Brufatto, et al., 2003; Wojtanowicz, 2001; Davies et al., 2014). Available data on such well integrity issues is published by operating companies and governmental authorities and provides an uncertain estimate of 2-75% of all wells (onshore and offshore, Davies et al., 2014) being compromised and potentially at risk for leakage. The problem with this kind of pressure tests is that they lack information on the integrity of plugged and abandoned wells whose wellheads were cut off so that pressure tests cannot be conducted. In addition, SCP cannot detect shallow gas leakage through fractured and disturbed sediments in the surrounding of the well because it doesn't influence the pressure in the well annulus. As such, shallow gas migration along the outside of wells and gas leakages through abandoned wells are badly quantified. Both leakage types currently represent missing emission sources in GHG inventories, particularly because data on emission factors (e.g. leakage rates) and activities (well counts), used in GHG inventories to calculate fugitive emissions, is not available (EPA, 2015).

Poorly identified and quantified leakages from the oil and gas industry likely result in an underestimation of fugitive CH_4 emissions, particularly onshore where gas is directly emitted into the atmosphere. This is supported by growing evidence for increased CH_4 emissions primarily in evolving unconventional gas production areas in the United States relative to national GHG inventories (Allen et al., 2013; Alvarez et al., 2012; Caulton et al., 2014; Miller et al. 2013; Schneising et al., 2014; Zhang et al., 2014; Brandt et al., 2014; Kang et al., 2014). These emissions are generally attributed to leakage of the produced fossil fuel from the infrastructure and equipment during various operation steps (Allen et al., 2013) and after well abandonment (Kang et al., 2014), but some must also result from shallow, biogenic sources as indicated by ^{12}C-richer isotopic signatures in the emanating CH_4 (Kang et al., 2014).

I.2.1 Shallow gas leakage along the outside of wells

In this thesis shallow gas leakage is defined as the migration of CH_4 along the outside of the well originating from a shallow gas accumulation in the upper 1,000 m of the sediment that the well has been drilled through. Although shallow gas migration is mentioned as a potential emission source (UNFCCC, 2009; IPCC, 2006), it is not considered in national and global GHG inventories, because the quantities of these unintended releases are difficult to predict.

Shallow gas migration along a well can either be driven by overpressure, buoyancy or a combination of both. Overpressure-driven leakage is usually related to drilling incidents where large amounts of shallow gas are suddenly released after drilling into an unnoticed, but highly pressurized gas pocket in the shallow subsurface. Such an incident occurred in 1990, when Mobile North LTD created a massive gas blowout in the Central UK North Sea

(57.922°N, 1.6325°E, WGS84) after drilling into an over-pressurized gas pocket about 360 m below the seafloor (Fig. I.4). The drilling site had to be abandoned after the incident and CH_4 emissions ("leakage") from the created seabed depression persisted over several decades (Rehder et al., 1998; Schneider von Deimling et al., 2007; Schneider von Deimling et al., 2015) representing the strongest gas seepage quantified to date (Leifer, 2015). Less persistent blowouts have been reported by the U.S. Mineral Management Service, where 39 blowouts occurred during drilling operations on the U.S. outer continental shelf in the period between 1992 and 2006 (Izon et al., 2007). The majority of these blowouts were due to shallow gas influx (Izon et al., 2007).

Figure I.4: Gas ebullition at the blowout well 22/4b in the British Sector of the North Sea after drilling into an unnoticed by highly pressurized shallow gas pocket in 1990 (Schneider von Deimling et al., 2015).

Smaller leaks can result from drilling through less-pressurized shallow gas pockets. In the absence of high overpressures, gas migration along a well can be best described by buoyancy-driven capillary invasion of drilling induced pathways where the gas has to exceed the capillary pressure to enter an initially water-saturated conduit (Clayton et al., 1994; Gurevich et al., 1993). Because drilling disturbs and fractures the sediment around a wellbore mechanically (Gurevich et al., 1993) it may create highly efficient pathways for the upward migration of gas drawing CH_4 from the surrounding sediment because of lower capillary pressure in the fracture (Bethke et al., 1991; Judd and Hovland, 2007).

The buoyant release of shallow gas along the outside of hydrocarbon wells results in significantly lower gas emissions compared to the blowout case, and is likely not related to fatalities, injuries or economic losses. Nonetheless, considering the millions of wells drilled world-wide and the ubiquitous gas accumulations in the shallow subsurface, smaller leaks of CH_4 are likely wide-spread potentially adding significant amounts of "extra" industry-related CH_4 into the ocean and/or to the atmosphere. Therefore, it is important to understand and quantify this type of CH_4 emission source so that appropriate mitigation (or compensation) strategies can be developed and implemented.

I.2.2 Geochemical tools to distinguish between reservoir and shallow gas leakage

As a result of different fractionation (kinetic isotope effects) and generation processes of biogenic and thermogenic methane, shallow gas leakage and reservoir leakage can often be distinguished by their isotopic signatures and molecular ratios, such as $\partial^{13}C$ of CH_4, ∂D of CH_4, and methane/(ethane+propane) ($C_1/(C_2+C_3)$). Shallow gas leakage of biogenic methane is enriched in light ^{12}C (-110‰<$\partial^{13}C$<-50‰ VPDB; Whiticar, 1999), depleted in D (-400‰<∂D<-150‰ SMOW), and contains only trace amounts of higher alkanes (C_1/C_{2+}>1,000). This is because methane producing organisms (methanogens) preferably use the light isotopes such as ^{12}C and ^{1}H for their metabolism and do not produce significant amounts of higher hydrocarbons. By contrast, leakage of thermogenic methane from the deep HC reservoir is depleted in ^{12}C (-50‰<$\partial^{13}C$<-20‰ VPDB; Whiticar, 1999) and has a high abundance of higher alkanes, with values $C_1/(C_2+C_3)$<100 (Wiese and Kvenvolden, 1993). With increasing maturity the $C_1/\sum C_{2+}$ ratio decreases and the isotopic signature of the thermogenic gas gets progressively heavier because at the late stages methane is the dominant product over other hydrocarbon gases and the available organic matter is enriched in ^{13}C due to earlier fractionation with preferential removal of ^{12}C (i.e. the ^{13}C-^{12}C bonds are stronger than the^{12}C-^{12}C bonds).

It should be noted that potential gas sources for shallow gas leakage include both upward migrated thermogenic gas principally from deeper thermally mature source rocks and biogenic methane originating from geologically young, organic-rich sediments, or a mixture of both sources. As such, shallow gas leakage must not be restricted to biogenic gas signatures making a distinct geochemical characterization of shallow and reservoir leakage challenging in some places.

I.3 Carbon Capture and Storage

Carbon Capture and Storage (CCS) is considered as a key technology in reducing CO_2 emissions into the atmosphere and thereby to slow down global warming. It aims at capturing the CO_2 arising from the (energy-related) combustion of fossil fuels and other industrial processes, transporting it and storing it in deep geological formations. The IEA World Energy Outlook (2014) estimated that the global consumption of fossil fuels continues to increase, with energy-related CO_2 emissions rising by 20% to 2040, which puts the world on a path consistent with a long-term global average temperature increase of 3.6°C. This would be far above the goal to stopping global warming at 2°C above preindustrial levels, a threshold value suggested to preventing dangerous/irreversible anthropogenic interference in the climate system (Cias et al., 2013). Therefore, significant CCS deployment at a global-scale (in addition to other mitigation options) is projected to be needed from 2020 to 2030 to achieving the 2-degree target (IEA, 2013).

CCS is a technically feasible method demonstrated by 55 CCS projects that have been established around the world by 2014 (Global CCS Institute, 2014). The capturing of CO_2 can be applied by three main principles: 1) post-combustion, where CO_2 is removed from waste-gas or natural gas combustion by wet scrubbing with aqueous amine solutions or 2) prior to combustion of coal and biomass by applying physical solvents to gasified fossil fuels, or (3) oxyfuel combustion of gas and coal using oxygen-enriched gas instead of air which results in final flue-gases that consists mainly of CO_2 (Gibbins and Chalmers, 2008). After separation, the captured CO_2 gas is typically cooled and compressed to a high density to facilitate both transport (if required via pipelines and/or ships) and storage (Metz et al., 2005). CO_2 storage is realized via one or several injection wells that typically are made of corrosion-resistant well material (steel and cement) to withstand the highly corrosive force of dissolved CO_2 in the formation water.

The storage of CO_2 is possible in several geological formations, such as depleted hydrocarbon reservoirs, deep, un-minable coal seams, and notably in deep saline aquifers, both onshore and offshore (Metz et al., 2005). From a climate control point of view, offshore CCS has the benefit that in the event of leakage, atmospheric CO_2 emissions would be reduced because the water column acts as a barrier for seeping gases from the seafloor.

Globally, the majority of gas storage projects are in depleted oil and gas reservoirs and saline formations (Metz et al., 2005). The former are promising for storing CO_2 because these structures tend to be geologically well understood with existing wellbore and seismic data helping to characterize the local geology and overburden, demonstrated their integrity and safety by containing hydrocarbons for a very long time, and may already have infrastructures in place (Metz et al., 2005). One downside of storing CO_2 in developed sites is the presence of pre-existing wells (Gasda et al., 2004; Nordbotten et al., 2005) which have been identified as posing a greater risk for gas leakage from CO_2 storage formations than geological features, such as faults or fractures (Bachu and Watson, 2009).

Saline aquifers offer the highest potential capacity for CO_2 globally because they are widespread in sedimentary basins throughout the world, both onshore and on the continental shelves (Michael et al., 2010; Metz et al., 2005). The three large-scale CCS projects Sleipner, Snøhvit and In Salah (all injecting CO_2 from natural gas production) make use of this storage reservoir and various commercial projects are planned for the future (Michael et al., 2010). In a saline aquifer the injected CO_2 will end-up either as a separated phase beneath the top seal (as in Sleipner), a residual gas saturated in the pore space, dissolved in the formation brine, or precipitated in the mineral phase (Michael et al., 2010). Although these trapping mechanisms for CO_2 are relatively well known, the rates and timing of the various process still have to be better constrained (Michael et al., 2010).

For every storage site, monitoring is required for purposes of managing, proving its integrity, and verifying the extent of CO_2 emissions reduction which has been achieved (Metz et al., 2005). The suitability of CCS as a climate change mitigation option will particularly depend on the long-term (> 1,000 years) containment of CO_2 in the reservoir.

I.4 The North Sea

I.4.1 Bathymetry and Hydrology

As part of the northwestern European continental shelf, the North Sea is a semi-enclosed shallow sea with an open northern and southern boundary to the North Atlantic Ocean, and an eastern connection to the Baltic Sea. The average water depth is 74 m, deepening from south to north (Otto et al., 1990). The Norwegian Channel (incl. the Skagerrak) along the east coast of Norway forms a prominent, deep intrusion in the shelf (Fig. I.5). Here, the water depth increases to 400 m in the Norwegian Channel and 750 m in the Skagerrak. In the southern region, the Dogger Bank forms a significant morphological high in the otherwise fairly flat bathymetry of the North Sea. The water depths south of the Dogger Bank are less than 50 m deep enabling continuous vertical mixing of water mases, whereas the deeper northern part is subjected to seasonal stratification (Thomas et al., 2005).

The hydrology of the North Sea is dominated by continuous water exchange across the northern opening to the North Atlantic Ocean (NAO) with minor inputs via the English Channel (Thomas et al., 2005 and references therein). As a consequence the main residual flow pattern is an anti-clockwise "u-shaped" circulation of North Atlantic Ocean water (Fig. I.5), entering the north-western boundaries of the North Sea via the Shetland Channel and Fair Island Channel, flowing along the Scottish/British coast to the Dutch, German, Danish, and Norwegian coast, and leaving along the Norwegian Trench, with residence times of less than one year (i.e. 0.75 years; Thomas et al., 2005 and references therein). Riverine input of freshwater and inflow of brackish water from the Baltic lead to local nutrient inputs, admixtures, and dilution of North Sea water masses. It should be noted that the hydrological characteristics described above are bulk patterns and the dispersion of a tracer (such as CH_4 and CO_2) may locally and temporally differ from this advection scheme.

I.4.2 Geological Setting and CH_4 sources

In terms of petroleum geology the North Sea is a complex buried graben structure that experienced extensional tectonics and failed rifting during the latest Jurassic and earliest Cretaceous time as well as various subsequent post-rifting events (Gautier, 2005). The North Sea Graben Province, which can be subdivided into three sub-basins, that are the Viking Graben in the north, the Central Graben in the south, and the Moray Firth/Witch Ground near the British coast, is one of the world's great petroleum provinces, ranked number 8

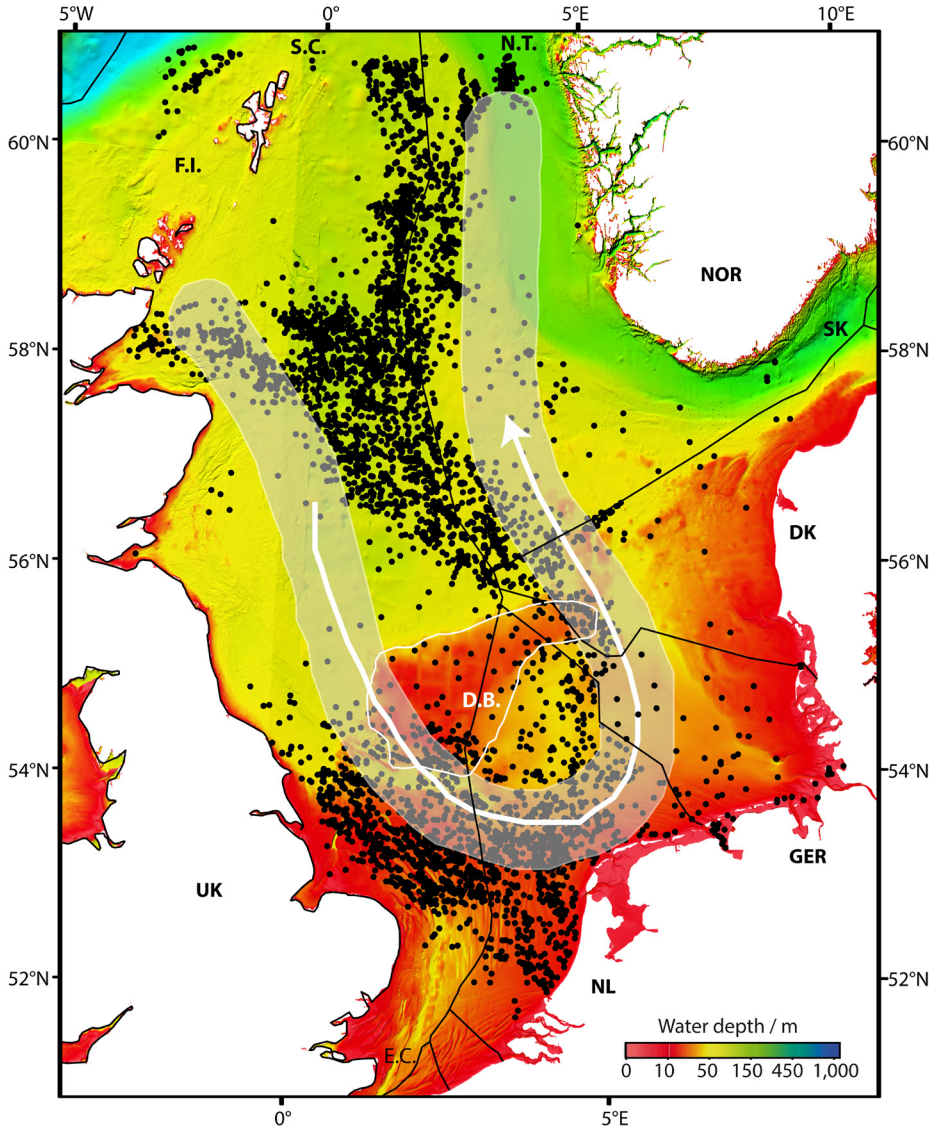

Figure I.5: Bathymetric map of the North Sea (EMODnet) showing the surface location of wells (black dots), and its hydrology (white arrow; after Thomas et al., 2005). The flow pattern of the North Sea is mainly dominated by inflow of North Atlantic Ocean water via the Faire Island Channel (F.I), minor inflow through the English Channel (E.C.), and outflow through the Norwegian Trench (N.T.). The arrow indicates the dominant anticlockwise circulation of North Atlantic Ocean water through the North Sea. The locationof the Dogger Bank (D.B.) is indicated (white rim).

among 76 world priority provinces in terms of volumes of discovered oil and gas (Gautier, 2005). The oil and gas accumulations found there occur in a variety of structural settings and within reservoir rocks of various ages (ranging from Devonian to Eocene), but almost all originates from marine, organic-rich shales (Kimmeridgian Shale) that were deposited during the period of intensive extension and rifting (Gautier, 2005). Aside from dominant Kimmeridgian Shales, pre-rifting Carboniferous coal deposits are economically important

source rocks for natural gas in the Southern North Sea (Gautier, 2005). After subsidence and continuous burial of Carboniferous coal measures and the Kimmeridgian Shale in most of the North Sea Graben Province, oil and gas generation began locally by Cretaceous time and has continued in various places ever since (Gautier, 2005). In addition to thermogenic sources, biogenic CH_4 originates from geologically young, organic-rich sediments, such as Quaternary peats and Lower-Middle Pleistocene delta sediments (primarily in the southern North Sea), and Tertiary lignites (Judd et al., 1997).

Vertical migration of hydrocarbons in the North Sea is often associated with tectonic stresses, salt doming, and depressurization of gas-holding sediments (after glaciation periods). While some of these natural conduits (i.e. faults, fractures, and gas chimneys) connect source rocks with suitable structural traps and reservoir rocks, others may reach the seafloor, leading to the natural losses of hydrocarbons (mainly gas) from the seafloor at some places. Drilling incidents and hydrocarbon wells, constituting additional man-made conduits for the upward migration of gas, (potentially) lead to additional, unintended releases of sedimentary CH_4 into the North Sea.

Various gas flares and pockmarks, as well as CH_4 supersaturations in the surface seawater of the open North Sea (with respect to atmospheric levels) have been reported in the scientific literature (Bange et al., 1994; Rehder et al.,1998; Schneider von Deimling et al., 2007; Judd and Hovland, 2007; Judd et al., 1997; Schroot et al., 2005), and originate from various potential seabed sources (natural and anthropogenic), which are however badly identified and quantified.

I.4.3 Shallow gas accumulations

In the North Sea, shallow gas accumulations are apparently abundant in unconsolidated sediments of Miocene-Holocene age (Schroot et al., 2005; Laier et al., 1990). Potential gas sources include upward migrated thermogenic gas principally from deeper thermally mature source rocks (i.e. Kimmerige Clay and Coal Measures) and biogenic methane originating from geologically young, organic-rich sediments, such as Quaternary peats and Lower-Middle Pleistocene delta sediments (primarily in the southern NS), and Tertiary lignites (Judd et al., 1997). Clay-rich sediments known as Nordland Shales (Horvig, 1982) largely act as a seal for upward migrating fluids, except for sections with pre-existing or pressure-induced fractures.

Shallow gas accumulations have been identified in industrial and scientific seismic data by tracking seismic anomalies that are indicative for the presence of gas, such as seismic turbidity (i.e. chaotic seismic reflections) and bright spots (i.e. reverse polarity high amplitude anomalies). While the former is indicative for the rather unfocused distribution of gas (<1% gas in pore space), the latter indicates the presence of free gas accumulations in the pore

space. Some of the identified gas accumulations are large enough (bright spots with diameters up to 10 km; Schroot et al., 2005) to be of commercial interest, but many others are smaller or have not yet been explored.

I.4.4 Well inventory and integrity

As a result of extensive hydrocarbon exploration since 1964, the North Sea hosts 15,781 wells (including sidetracked and multilateral wells, Fig. I.5). While most of these wells are inactive today and have been abandoned, around 4,447 are currently used for oil and gas production, and injection of formation waters or CO_2 (see Supp. Tab. III.3). Based on reported data on well integrity issues on the British and Norwegian Continental Shelf, 10 to 18% of the active wells (Davies et al., 2014 and references therein) and up to 38% of the temporarily abandoned wells (which still have their wellhead in place; Vignes, 2011) are being compromised and potentially at risk to leak.

I.4.5 The Sleipner CO_2 storage project

The Statoil operated CO_2 storage project "Sleipner" is located in the Norwegian Sector of the Central North Sea and is the world's first large-scale CCS project with an annual injection rate of ~1 Mt of CO_2 since 1996 (Fig. I.6). To meet the specifications of maximum 2.5% by volume of CO_2 in the sale gas, CO_2 is stripped from natural gas production containing 4-9.5% of CO_2 using a conventional amine process (Korbøl and Kaddour, 1995). The CO_2 tax, introduced in 1991 by the Norwegian authorities, was one of the triggers for Statoil to store the separated CO_2 underground by injection into a saline aquifer in ~700-1,000 m sediment depth, overlying the natural gas reservoir. CO_2 injection is realized by a single well, consisting of a high quality stainless steel tubing to prevent corrosion (Eiken et al., 2011). The injection point is located 1,012 m below sea level, some 200 m below the top of the storage reservoir (Chadwick et al., 2009; Arts et al., 2008), so that the injected CO_2 is in a supercritical phase.

The Utsira storage Formation (Fm.) is a highly elongated sand reservoir extending for more than 400 km from north to south and between 50-100 km from east to west (Torp and Gale, 2004), and has a thickness of about 250 m in the vicinity of the injection site (Arts et al., 2008). The sandstone formation is of Tertiary age and consists of mainly un-cemented fine grained, highly porous (35-40%; Torp and Gale, 2004), very permeable (1-3 Darcy; Arts et al., 2008), homogenous sand deposited on a shallow marine shelf (Korbøl and Kaddour, 1995). The Utsira Fm. is overlain by the ~800 m thick Nordland Fm., which lower 200-300 m consists of shale forming the main reservoir cap rock. Coarser sediments, such as silts and sand dominate the shallower parts of the Nordland Fm.

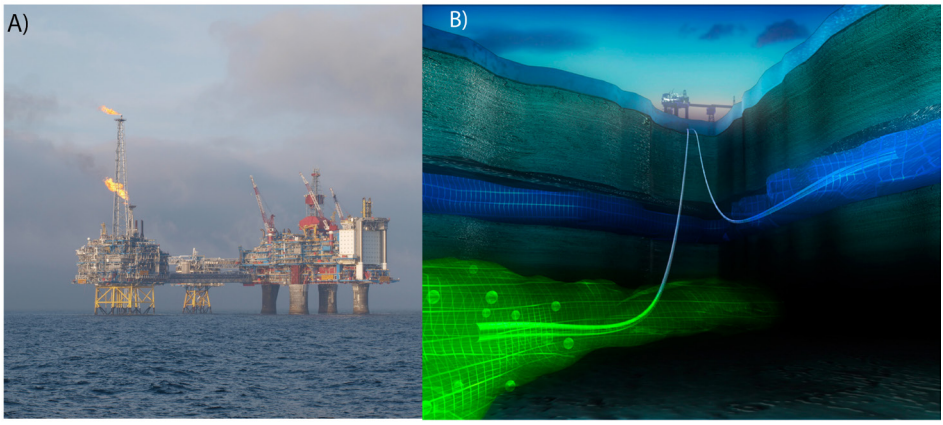

Figure I.6: A) Sleipner A Platform from which CO_2 is being injected into the Utsira storage formation (Picture: Jens Karstens). **B**) CO_2 is injected into a saline aquifer (blue) in ~900 m sediment depth overlying the deep hydrocarbon reservoir (green) (Picture: Statoil).

For the purpose of monitoring, Statoil uses a number of monitoring techniques, namely temperature and pressure monitoring at the injection wellhead (bottom hole pressure is not measured; Eiken et al., 2011), and repeated seismic and gravity surveys. A set of seven repeat 3-D seismic surveys, in 1994, 1999, 2001, 2002, 2004, 2006, and 2008, (Eiken et al., 2011; Chadwick et al., 2009) has shown that the buoyant CO_2 migrates upward from the injection point and accumulates under the overlying cap rock (Torp and Gale, 2004). Here, the CO_2 migration has a prominent north-ward trend and follows a linear topographic ridge at the top reservoir (Chadwick et al., 2009). Furthermore, three time-lapse seafloor gravity surveys have been carried out, in 2002, 2005 and 2009, namely to estimate the amount of CO_2 absorbed in the formation water, which is currently not feasible by seismic data (Eiken et al., 2011). In addition, the seafloor has been mapped with multibeam echo sounding, side-scan sonar, and ROV video footage. However, no seafloor changes (pockmarks, bubbles; Eiken et al., 2011) or systematic changes in the overburden (Chadwick et al., 2009) have been observed indicating that CO_2 is being contained within the storage reservoir at Sleipner.

References:

Allen, D.T., et al., 2013. Measurements of methane emissions at natural gas production sites in the United States. *Proc. Natl. Acad. Sci. U.S.A.* **110**, 17768-17773.

Alvarez, R.A., Pacala, S.W., Winebrake, J.J., Chameides, W.L., Hamburg, S.P., 2012. Greater focus needed on methane leakage from natural gas infrastructure. P*roc. Natl. Acad. Sci. U.S.A.* **109**, 6435-6440.

Arts, R.J., Chadwick, R.A., Eiken, O., Thibeau, S., Nooner, S., 2008. Ten years‘ experience of monitoring CO_2 injection in the Utsira Sand at Sleipner, offshore Norway. EAGE Special

Topic 26, 56-72.

Bachu, S., and Watson, T.L., 2009. Review of failures for wells used for CO_2 and acid gas injection in Alberta, Canada. *Energy Procedia* **1**, 3531-3537. doi:10.1016/j.egypro.2009.02.146.

Bange, H.W., Bartell, U.H., Rapsomanikis, S., Andreae, M.O., 1994. Methane in the Baltic and North Seas and a reassessment of the marine emissions of methane. *Glob. Biogeochem. Cycles* **8**, 465–480.

Brufatto, C., et al., 2003. From mud to cement - Building gas wells. *Oilfield Rev.* **15**, 62-76.

Behtke, C. M., Reed, J.D., Olzt, D.F., 1991. Long –range petroleum migration in the Illinois Basin. American Association of Petroleum Geologists (Bulletin) 75, 925-45.

Brandt et al., 2014. Methane Leaks from North American Natural Gas Systems. *Science* **343**, 733-735.

Caulton, D.R., et al. , 2014. Toward a better understanding and quantification of methane emissions from shale gas development. *Proc. Natl. Acad. Sci. U.S.A.* **111**, 6237-6242.

Chadwick, R.A., Noy, D., Arts, R.J., Eiken, O., 2009. Latest time-lapse seismic data from Sleipner yield new insights into CO_2 plume development. *Energy Procedia* **1**, 2103–2110. doi:10.1016/j.egypro.2009.01.274.

Ciais, P., et al., 2013. Climate Change 2013: The Physical Science Basis. Contribution of Working Group I to the Fifth Assessment Report of the Intergovernmental Panel on Climate Change, in: Stocker, T.F., Qin, D., Plattner, G.-K., Tignor, M., Allen, S.K., Boschung, J., Nauels, A., Xia, Y., Bex, V., Midgley, P.M. (Eds.). IPCC, Cambridge, UK, pp. 465-570.

Clayton, C.J., Hay, J., 1994. Gas migration mechanisms from accumulation to surface. *Bull. Geol. Soc. Den.* **41**, 12-23.

Cook, J., et al., 2013. Quantifying the consensus on anthropogenic global warming in the scientific literature. *Environ. Res. Lett.* **8** (2), 024024. doi:10.1088/1748-9326/8/2/024024.

Crowley, T.J., 2000. Causes of Climate Change Over the Past 1000 Years. *Science* **289**, 270–277. doi:10.1126/science.289.5477.270.

EDGAR v.4.2. CH_4 FT2010. http://edgar.jrc.ec.europa.eu/overview.php?v=42FT2010.

Eiken, O., et al., 2011. Lessons Learned from 14 years of CCS Operations: Sleipner, In Salah and Snøhvit. *Energy Procedia* **4**, 5541-5548.

EPA, 2015. Inventory of U.S. Greenhouse Gas Emissions and Sinks: 1990-2013. Chapter 3 Energy. http://www3.epa.gov/climatechange/Downloads/ghgemissions/US-GHG-Inventory-2015-Chapter-3-Energy.pdf.

Gasda S, Bachu S, Celia M., 2004. The potential for CO_2 leakage from storage sites in geological media: analysis of well distribution in mature sedimentary basins. *Environ. Geol.* **46** (67), 707–20.

Gautier L., 2005. Kimmeridgian Shales Total Petroleum System of the North Sea Graben Province: *U.S. Geol. Surv. Bull.* 2204-C, 24 p.

Gibbins, J., Chalmers, H., 2008. Carbon capture and storage. *Energy Policy* **36**, 4317–4322. doi:10.1016/j.enpol.2008.09.058.

Global CCS Institute, 2014. The Global Status of CCS: 2014, Melbourne, Australia. 199 pp.

Gurevich, A.E., Endres, B.L., Robertson Jr, J.O., Chilingar, G.V., 1993. Gas migration from oil and gas fields and associated hazards. *J. Petr. Sci. Eng.* **9**, 233-238.

Hinrichs, K.-U. and Boetius, A., 2002. *The anaerobic oxidation of methane: New insights in microbial ecology and biogeochemistry* In: Wever, G., Billett, D., Hebbeln, D., Jørgensen, B. B., Schlüter, M., and van Weering, T. C. E. Eds., Ocean Margin Systems. Springer-Verlag, Heidelberg.

Horvig, S., 1982. WDSS 40 01 16 7 2: Geological Completion Report Well 16/7-2. Esso Exploration and production Norway Inc.

IEA, 2013. Annual Report 2013. OECD Publishing. https://www.iea.org/publications/freepublications/publication/2013_AnnualReport.pdf.
IEA, 2014. World Energy Outlook 2014, Executive Summary. OECD Publishing. http://www.iea.org/textbase/npsum/weo2014sum.pdf.

IPCC, 2006. IPCC Guidelines for National Greenhouse Gas Inventories. Chapter 4 Fugitive Emissions.

IPCC, 2007. Changes in Atmospheric Constituents and in Radiative Forcing. In: Climate Change 2007: The Physical Science Basis. Contribution of Working Group I to the Fourth Assessment Report of the Intergovernmental Panel on Climate Change [Solomon, S., D. Qin, M. Manning, Z. Chen, M. Marquis, K.B. Averyt, M.Tignor and H.L. Miller (eds.)]. Cambridge University Press, Cambridge, United Kingdom and New York, NY, USA.

IPCC, 2014. Climate Change 2014: Synthesis Report. Contribution of Working Groups I, II and III to the Fifth Assessment Report of the Intergovernmental Panel on Climate Change [Core Writing Team, R.K. Pachauri and L.A. Meyer (eds.)]. IPCC, Geneva, Switzerland, 151 pp.

Izon, D., Danenberger, E.P., Mayes, M., 2007. Absence of fatalities in blowouts encouraging in MMS study of OCS incidents 1992-2006. Drilling Contractor.

Judd, A., Hovland, M., 2007. *Seabed fluid flow: the impact on geology, biology and the marine environment*. Cambridge University Press, Cambridge. doi:10.1017/cbo9780511535918.

Judd, A., et al., 1997. Contributions to atmospheric methane by natural seepage on the U.K. continental shelf. *Mar. Geol.* **140**, 427-455.

Kang et al., 2014. Direct measurements of methane emissions from abandoned oil and gas wells in Pennsylvania. *Proc. Natl. Acad. Sci. U.S.A.* **111**, 18173–18177.

Karl, T.R., Trenberth, K.E., 2003. Modern Global Climate Change. *Science* **302**, 1719-1723.

Kirschke et al, 2013. Three decades of global methane sources and sinks. *Nat. Geosci.* **6**, 813–823, doi: 10.1038/NGEO1955.

Korbøl, R., Kaddour, A., 1995. Sleipner vest CO_2 disposal-injection of removed CO_2 into the Utsira Formation. *Energy Conv. Manag.* **36**, 509–512.

Kvenvolden, K.A., Rogers, B.W., 2005. Gaia's breath—global methane exhalations. *Mar. Petrol. Geol.* **22**, 579–590. doi:10.1016/j.marpetgeo.2004.08.004.

Laier, T., Jørgensen, N.O., Buchardt, B., Cederberg, T., Kuijpers, A., 1992. Accumulation and seepages of biogenic gas in Northern Denmark. *Cont. Shelf Res.* **12** (10), 1173-1186.

Leifer, I., 2015. Seabed bubble flux estimation by calibrated video survey for a large blowout seep in the North Sea. *Mar. Petrol. Geol.* **68**, Part B, 743–752.

Metz, B., Davidson, O., De Coninck, H.C., Loos, M., 2005. IPCC special report on carbon dioxide capture and storage. Prepared by Working Group III of the Intergovernmental Panel on Climate Change. IPCC.

Michael, K., Golab, A., Shulakova, V., Ennis-King, J., Allinson, G., Sharma, S., Aiken, T., 2010. Geological storage of CO_2 in saline aquifers: A review of the experience from existing storage operations. *Int. J. Greenh. Gas Control* **4**, 659–667. doi:10.1016/j.ijggc.2009.12.011.
Miller, S.M., et al., 2013. Anthropogenic emissions of methane in the United States. *Proc. Natl. Acad. Sci. U.S.A.* **110**, 20018-20022.

Nisbet, E.G., Dlugokencky, E.J., Bousquet, P., 2014. Methane on the Rise-Again. *Science* **343**, 493-495.

Nordbotten, J.M., Celia, M.A., Bachu, S., Dahle, H.K., 2005. Semianalytical Solution for CO_2 Leakage through an Abandoned Well. *Environ. Sci. Technol.* **39**, 602-611.

NORSOK Standard D-010, 2004. http://www.standard.no/PageFiles/1315/D-010r3.pdf.

Otto, L., Zimmerman, J.T.F., Furnes, G.K. Mork, M., Seatre, R., Becker, G., 1990. Review of the phydical oceanography of the North Sea. *Neth. J. Sea Res.* **26** (2-4), 161-238.

Rehder, G., Keir, R.S., Suess, E., Pohlmann, T., 1998. The multiple sources and patterns of methane in North Sea waters. *Aquat. Geochem*. **4**, 403-427.

Sarmiento, J.L., Le Quéré, C., 1996. Oceanic Carbon Dioxide Uptake in a Model of Century-Scale Global Warming. *Science* **274**, 1346-1350.

Schneider von Deimling, J.,Brockhoff, J., Greinert, J., 2007. Flare imaging with multibeam systems: data processing for bubble detection seeps. *Geochem. Geophys. Geosys.* **8**.

Schneider von Deimling, J., Linke, P., Schmidt, M., Rehder. G., 2015. Ongoing methane discharge at well site 22/4b (North Sea) and discovery of a spiral vortex bubble plume motion. *Mar. Petr. Geol.* **68**, Part B, 718–730.

Schneising, O., et al., 2014. Remote sensing of fugitive methane emissions from oil and gas production in North American tight geologic formations. *Earth's Future* **2**, 548-558.

Schroot, B.M., Klaver, G.T., Schüttenhelm, R.T.E., 2005. Surface and subsurface expressions of gas seepage to the seabed- examples from the Southern North Sea. *Mar. Petrol. Geol.* **22**, 499-515.

Steinle et al., 2015. Water column methanotrophy controlled by a rapid oceanographic switch. *Nat. Geosci.* **8**, 378–382.

Thomas, H., et al., 2005. The carbon budget of the North Sea. *Biogeosciences* **2**, 87-96.

Torp, T.A., Gale, J., 2004. Demonstrating storage of CO_2 in geological reservoirs: The Sleipner and SACS projects. *Energy* **29**, 1361-1369.

UNFCCC, 2009. UNFCCC Resource Guide: For preparing the national communications of non-annex I parties. Module 3 National Greenhouse Gas Inventories.

Vignes, B., 2011. Contribution to Well Integrity and Increased Focus on Well Barriers from a Life Cycle Aspect (PhD thesis). University of Stavanger.
Wallmann et al., 2012. The Global Inventory of Methane Hydrate in Marine Sediments: A Theoretical Approach. *Energies* **5**, 2449-2498.

Whiticar, M.J., 1999. Carbon and hydrogen isotope systematics of bacterial formation and oxidation of methane. *Chem. Geol.* **161**, 291-314.

Wiese, K., Kvenvolden, K.A., 1993. Introduction to Microbial and Thermal Methane. The Future Of Energy Gases. *U.S. Geol. Surv. Prof. Paper* 1570.

Wojtanowicz, A.K., Nishikiwa, S., Rong, X., 2001. Diagnostic and remediation of sustained casing pressure in wells. Mineral. Manag. Serv.

Zhang, Y., Zhao, H., Zhai, W., Zang, K., Wang, J., 2014. Enhanced methane emissions from oil and gas exploration areas to the atmosphere – The central Bohai Sea. *Mar. Pollut. Bull.* **81**, 157-165.

Quantification of methane emissions at abandoned gas wells in the Central North Sea

Lisa Vielstädte [a,*], Jens Karstens [a], Matthias Haeckel [a], Mark Schmidt [a], Peter Linke [a], Susan Reimann [a], Volker Liebetrau [a], Daniel F. McGinnis [b,c], Klaus Wallmann [a]

[a] *Helmholtz Centre for Ocean Reserach, Kiel, Germany*

[b] *IGB, Leibniz Institute of Freshwater Ecology and Inland Fisheries, Berlin, Germany*

[c] *Institute F.-A. Forel, Earth and Environmental Sciences, Faculty of Sciences, University of Geneva, Geneva, Switzerland*

Published in 2015 in Marine and Petroleum Geology, doi.org/10.1016/j.marpetgeo.2015.07.030

Abstract

As a result of extensive hydrocarbon exploration, the North Sea hosts several thousand abandoned wells; many believed to be leaking methane. However, how much of this greenhouse gas is emitted into the water column and ultimately reaches the atmosphere is not known. Here, we investigate three abandoned wells at 81-93 m water depth in the Norwegian sector of the North Sea, all of which show gas seepage into the bottom water. The isotopic signature of the emanating gas points towards a biogenic origin and hence to gas pockets in the sedimentary overburden above the gas reservoirs that the wells were drilled into. Video-analysis of the seeping gas bubbles and direct gas flow measurements resolved initial bubble sizes ranging between 3.2 and 7.4 mm in diameter with a total seabed gas flow between 1 and 19 tons of CH_4 per year per well. Estimated total annual seabed emissions from all three wells of ~24 tons are similar to the natural seepage rates at Tommeliten, suggesting that leaky abandoned wells represent a significant source of methane into North Sea bottom waters. However, the bubble-driven direct methane transport into the atmosphere was found to be negligible (< 2%) due to the small bubble sizes and the water depth at which they are released.

* Corresponding Author. *E-mail address*: lvielstaedte@geomar.de (L. Vielstädte).

II.1. Introduction

Methane contributes significantly to the atmospheric pool of radiative (greenhouse) gases, suspected to induce global climate change (Crutzen and Zimmermann, 1991; Hartmann et al., 2013; Lelieveld et al., 1993). Marine methane emissions may contribute around 20 Tg yr^{-1} (Etiope et al., 2008; Kvenvolden and Rogers, 2005; Bange et al., 1994) to the global atmospheric methane budget (i.e. 542±56 Tg yr^{-1} based on top-down estimates, Ciais et al., 2013), most of it, about 75%, being released from coastal and shelf areas (e.g. Bange et al., 1994). The highest amount of marine methane is produced by methanogenesis in the deeper sediment layers of productive coastal areas (Scranton and McShane 1991; Hovland et al., 1993), which may result in the build-up of free-gas accumulations in the shallow subsurface (Hovland and Judd, 1988; Judd and Hovland, 2007). Such gas pockets constitute a potential risk in connection with drilling operations, because they may be associated with high pore pressures. In 1990, Mobile North LTD created a massive gas blowout in the central UK North Sea (57.922°N, 1.6325°E, WGS84) after drilling into an over-pressurized gas pocket about 360 m below the seafloor. The drilling site had to be abandoned after the incident and methane emissions ("leakage") from the created seabed depression persisted over several decades (Rehder et al., 1998; Schneider von Deimling et al., 2007; Schneider von Deimling et al., 2015) representing the strongest gas seepage quantified to date (Leifer, 2015). Smaller methane leaks can result from drilling through less-pressurized gas pockets and the numerous abandoned offshore wells penetrating such gas accumulations may constitute efficient pathways to release gas from the sedimentary strata to the hydrosphere and finally to the atmosphere (Gurevich et al., 1993; Gasda et al., 2004). Although leakage rates are probably orders of magnitude lower compared to a blowout scenario like well 22/4b, leaks along abandoned wells are much more likely to occur. As monitoring generally is not required after proper well abandonment (Gasda et al., 2004), quantitative data on both, the number of leaking wells, and their leakage rates are rare. Most of the available data are related to well integrity surveys that are performed by operating companies and governmental authorities to reduce the risk of major accidents, primarily for the population, environment and economic values, however their focus is mostly on active (production and injection) wells. E.g. on the Norwegian Continental Shelf, 18% of active wells are reported to have integrity issues (Vignes et al., 2006). However, studies in the Gulf of Mexico showed that the majority of integrity issues were related to shut-in or temporarily abandoned wells, rather than to active wells (Wojtanowicz et al., 2001). Thus, even though leakage from abandoned wells poses a lower risk of major accidents for people and economic aspects, it may constitute a relevant source for methane into the ocean.

A large fraction of the released methane will dissolve in the water column, disperse by currents, and is subsequently oxidized by microbes (e.g., Ward et al., 1987; Jones, 1991). Transfer of

methane into the atmosphere is possible by both diffusive and turbulent air-sea gas exchange as well as bubble-mediated transport (Leifer and Patro, 2002; Wanninkhof, 1992). The latter is the most efficient way of transferring seabed methane to the atmosphere (McGinnis et al., 2006), which may enhance local sea-air fluxes, particularly in shallow shelf seas. In this study we focus on the North Sea, which acts as a net source for atmospheric methane (Bange et al., 1994). Current flux estimates (Bange et al., 1994; Rehder et al., 1998) seem to be too low, because methane fluxes from estuaries and marine seeps are not adequately represented (Bange et al., 2006) and possible contributions from abandoned wells have not been studied at all.

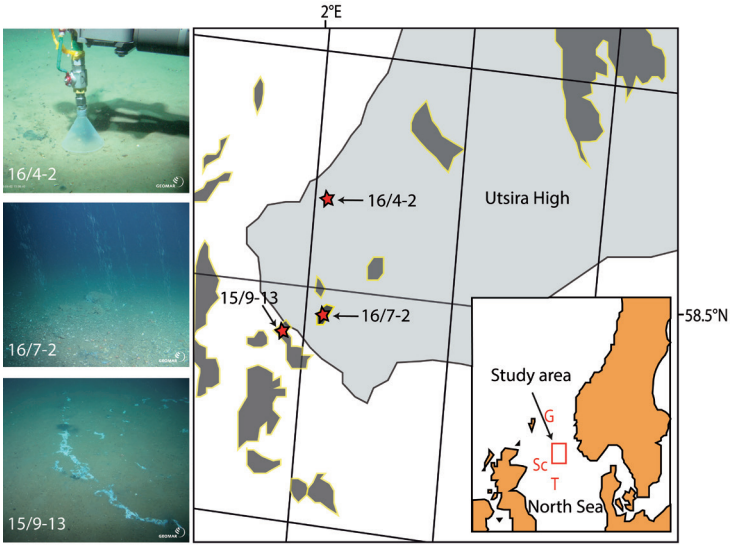

Figure II.1: Map of the study area showing the Utsira High as the major structural element, the locations of deep hydrocarbon reservoirs (dark gray; based on Fact Map of the Norwegian Petroleum Directorate), and the locations of the investigated abandoned wells (red stars); Lower right corner: Regional map of the North Sea Basin showing the location of the study area (red box), and natural seep sites discussed in this paper (red letters: T: Tommeliten, Sc: Scanner Pockmark, G: Gullfaks). Left: Pictures showing gas flow measurement at well 16/4-2, the most intensive leakage at well 16/7-2, and bacterial mats related to CH_4 leakage at well 15/9-13.

To our knowledge, this is the first public study aiming to quantify methane leakage from abandoned wells in the North Sea. For this purpose, we investigated three abandoned wells that show continuous bubble release into the water-column during two research cruises in 2012 and 2013. Further, we determine the source of leaking gases and possible migration pathways driving the seabed emissions at leaky wells. Applying a numerical gas bubble dissolution model, we estimate the resulting direct methane flux across the sea surface and finally, methane emissions at the abandoned wells are compared to natural methane seepage as well as other methane sources in the North Sea.

II.1.1 Study area

The three wells are located on the south-western flank of the Utsira High in the Norwegian sector of the North Sea (Fig. II.1). The area hosts hydrocarbon-rich Paleocene sediments mainly in the Heimdal Formation, which are charged by Jurassic source rocks (Justwan and Dahl, 2005). The main objectives of the three wells were to delineate hydrocarbon accumulations found in the Heimdal Formation (15/9-13, Normann and Østby, 1982), to prove the presence of a high-risk stratigraphic trap in the Heimdal Formation (16/7-2, Horvig, 1982), and to test a possible small closure at the Top Heimdal Formation (16/4-2, Hydro, 1990). In all cases, the target depths of the wells were deeper than 3,000 m below the seafloor (mbsf) corresponding to Jurassic (i.e. 16/4-2, Hydro, 1990) and Permian (i.e. 15/9-13 and 16/7-2, Normann and Østby, 1982; Horvig, 1982) stratigraphic units. Well 16/4-2 was permanently plugged and abandoned as a dry well (Hydro, 1990), while the other two boreholes proved gas in the Heimdal Formation but were subsequently plugged and abandoned (Normann and Østby, 1982; Horvig, 1982). Shallow gas is mostly present within Nordland Group sediments in the upper Cenozoic sequences. The Utsira Formation, the Top Pliocene, and an 11-m thick sand layer above the Top Utsira Formation constitute important sand layers, which are separated by impermeable layers of shale or mudstones (Fig. II.2), thus creating fairly good conditions for the trapping and accumulation of shallow gas (Karstens and Berndt, 2015). The Utsira Formation overlies marine mudstones at the base

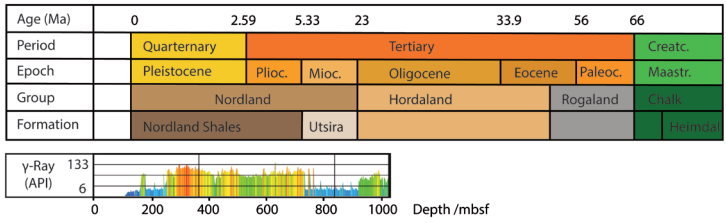

Figure II.2: Lithostratigraphic overview of the study area showing the geochronology of groups and formations present in the study area (Cretac.= Cretaceous, Maastr.= Maastrichian Fm., Paleoc.= Paleocene, Mioc.= Miocene, Plioc.= Pliocene). Gamma Ray logs (Norwegian Petroleum Directorate) are based on well 15/9-13 and indicate the sedimentology of the Nordland Group, where high values represent clay (yellow to red), intermediate values represent a mixture of clay and sand (green), and low values represent permeable sand layers (blue).

of the Nordland Group and is dominated by medium-grained sand intersected with some stringers of clay (Eidvin and Rundberg, 2007; Normann and Østby, 1982). While Utsira sands were deposited in a high-energetic shelf environment (Galloway, 2001; 2002), the depositional environment changed from a shallow to a deeper marine environment in the Early Pliocene, which was accompanied by the deposition of finer sediments. The interval

from 300 mbsf down to the Utsira Formation thus consist of clay-rich sediments known as Nordland Shales (Fig. II.2; Horvig, 1982) largely acting as a seal for upward migrating fluids, except for sections with pre-existing or pressure-induced fractures. The uppermost 300 m of the Nordland Group consists mostly of sand with some inter-bedded clay also containing gas in the vicinity of some wells (Horvig, 1982).

II.2. Methodology

Geochemical sampling and video investigations were performed at three leaky abandoned wells during cruises on board the research vessels RV Celtic Explorer (CE12010, July-August 2012) and RV Alkor (AL412, March 2013). In addition, an industrial 3-D seismic data set (ST98M3, Statoil ASA) covering the area around the three wells of interest was analyzed for gas accumulations and possible vertical migration pathways in the sedimentary strata around the boreholes. Furthermore, well reports and well-logs of the Norwegian Petroleum Directorate (NPD) were investigated for the characterization of the sediments in the uppermost 1,200 mbsf.

II.2.1. Sediment and gas sampling

During the Celtic Explorer expedition CE12010, surface sediments were collected with ROV-deployed push-cores (PC). For dissolved gas analysis, 3 ml of wet sediment was sub-sampled in 2-cm intervals and filled into 20-ml headspace vials. 6 ml of saturated NaCl solution and an additional 1.5 g of NaCl were added and the vials sealed tight with butyl-rubber stoppers. The samples were stored refrigerated for onshore analyses. Prior to storage in the cold room, the vials were shaken vigorously for half an hour to release dissolved gases into the headspace. In addition, free gas was sampled directly in the bubble stream with ROV-operated special gas samplers as described by Rehder and Schneider von Deimling (2008) and Pape et al. (2010). The gas sampler consists of a stainless steel cylinder with a PVC funnel attached to it to facilitate gas bubble sampling (Fig. II.1 and Supp. Fig. II.1). Onboard, subsamples of pressurized gas were transferred into pre-evacuated headspace glass vials of 20 and 100 ml volume until the pressure in the vials was ~1,020 mbar.

In the GEOMAR home laboratory, methane and higher alkane concentrations in the free gas samples and in head space vials were determined with a gas chromatograph GC 8000top (CE instruments) equipped with a FID detector and a capillary column (RT-Alumina Bond-KCl, 50 m, 0.53 mm). Stable carbon isotope composition of methane was determined by using a continuous flow GC-Isotope Ratio Mass Spectrometer combination. Methane was separated from other hydrocarbons in a Thermo Trace GC (isotherm at 60°C, He-carrier gas, ShinCarbon 1.5 m packed column). The subsequent conversion of methane to carbon

dioxide was conducted in a Ni/Pt combustion furnace at 1,150°C. The $^{13}C/^{12}C$-ratios of the produced CO_2 were determined by a Thermo MAT253 isotope ratio mass spectrometer. All isotope ratios are reported in the ∂-notation with respect to Vienna Pee Dee Belemnite (VPDB). Analytical precision of the reported concentrations and isotopic composition is ± 3% and ± 0.3 ‰, respectively.

Sediment porewater was extracted by squeezing wet sediment at low pressure (<5 bar) through 0.45 µm Whatman regenerated cellulose filters. 2 ml aliquots were treated with 10 µL of HgCl to inhibit further microbial degradation and stored cool until analysis. Onshore, the stable carbon isotope composition of dissolved inorganic carbon (DIC), referred to as ∂^{13}DIC was determined at the University of Bremen using a Finnigan MAT 251 mass spectrometer with an analytical accuracy of <0.07‰. Total alkalinity was determined by titration with 0.02 N HCl using a mixture of methyl red and methylene blue as indicator. The titration vessel was bubbled with argon to strip any CO_2 and H_2S produced during the titration. The IAPSO seawater standard was used for calibration; analytical precision and accuracy are both ~2%.

Carbonate pieces from the sediment surface were sampled with the ROV KIEL 6000 at well 16/7-2 and were cleaned of remaining sediment by washing with site specific seawater. The detailed sub-sampling was conducted after cleaning with MilliQ-water and drying at room temperature. All sub-samples were taken with a hand-held mini-driller from freshly cut or broken surfaces of solid material, after discarding first drill steps as a surface cleaning procedure. Onshore, samples were analyzed for their stable carbon isotope composition using a Thermo Fisher Scientific 253 Mass Spectrometer coupled to a CARBO KIEL online carbonate preparation line. $\partial^{13}C$ values are reported with respect to the VPDB scale.

II.2.2. Video based quantification of gas emissions

ROV videos were analyzed by two approaches to determine the gas flow emitted into the water column at the three abandoned wells: (1) measuring the time for filling up the funnel of the gas sampler and (2) quantifying the gas bubble size spectrum at individual seepage spots.

II.2.2.1. Gas flow measurements

The *in situ* gas flow was quantified at single bubble streams of well 16/4-2 and well 15/9-13 using the ROV-operated gas sampler with attached funnel (Fig. II.1 and Supp. Tab. II.1). Both, the time, t, to fill the funnel with gas and its corresponding volume, V_F, were determined based on video using the software ImageJ (Farreira and Rasband, 2012). The gas volume accumulating in the funnel was calculated from the resulting volume of the cone frustum, $V_F = h \cdot \pi/3 \cdot (r_B^2 + r_B \cdot r_T + r_T^2)$, where r_B and r_T are the radii of the base plane and top

plane, respectively, and h is the distance between both planes, $h=(m^2-r_T^2+2r_T \cdot r_B-r_B^2)^{0.5}$ (Supp. Fig. II.1, Supp. Tab. II.1). The lateral height of the funnel had a length of m=12.5 cm and was used as scale in the images. The optically-derived gas volume required correction, due to imprecise size measurements of a 3-D object in its 2-D projection. The ratio between optically-derived and known funnel volume, F_{corr} was used to correct the gas volume (Supp. Tab. II.1). The resulting gas flow, Q_F, is:

$$Q_F = \frac{V_F}{t} \cdot F_{corr} \qquad \text{Eq. II.1}$$

The correction factor ranged between 0.88 and 1.33 including optical failures described above and uncertainties in pixel accuracy during measurements with ImageJ (Supp. Tab. I.1). The error in determining the time for filling the funnel is about 1 s, resulting in an error of the gas flow of < 2.7 cm^3/s, i.e. less than 2.5%.

II.2.2.2 Bubble size spectra

The image editing software ImageJ (Farreira and Rasband, 2012) was applied to the ROV video sequences, which also were used for the funnel measurements, to determine the respective initial (seafloor) gas bubble sizes (e.g. Leifer and MacDonald, 2003; Römer et al., 2012; Sauter et al., 2006). These size spectra are required to calculate the dissolution rate, the bubble rise velocity, and the resulting gas transfer into the atmosphere. For calibration of bubble sizes, the bottom plane of the funnel (diameter = 150 mm) was used as a scale. A video sequence of 5 s, corresponding to 125-150 individual frames, was analyzed frame by frame. The video sequence was first converted to grayscale and was subsequently processed to enhance the contrast. Unfortunately, contrast and pixilation noise remained rather poor making a computer based automatic measurement routine impractical. Hence, ellipses were manually overlaid to individual bubbles leaving the seafloor and were marked as overlays. The overlays were allocated to individual bubbles to track them and analyze their changes in size in subsequent frames. If bubbles had a very irregular shape, they were outlined manually before using the ellipse fitting object of ImageJ (i.e. 10 of 71 measurements at well 16/7-2). For each bubble, the major and minor axes, angle, perimeter, area, circularity, as well as frame number were recorded. The corresponding bubble volume, $V_0 = 4/3 \cdot \pi \cdot r_{eq}^2$, was calculated from the equivalent spherical radius, $r_{eq} = (a^2 \cdot b)^{1/3}$ based on the major, a, and the minor half axes, b, of the fitted ellipse.

If bubbles were measured in several frames, their average radius was used to level out the trajectory and shape oscillations of the bubble during its ascent (Clift et al., 1978). All determined bubble volumes were added to calculate the total gas volume flow over a period of 5 s.

The methodological error of bubble size measurements was estimated in two ways:

1) The volume flow derived from the bubble size spectra was compared to the flow constrained by the funnel measurements. The funnel-derived flow is integrated over much longer time and hence, regarded as more precise. Consequently, the bubble size spectra were corrected to match the funnel-derived flow values.

2) Multiple bubble measurements in sequential video frames were used to quantify the error caused by oscillation or wobbling of the gas bubble in the real 3-D space which cannot be correctly represented in a 2-D image. The video can only provide a snapshot of current bubble shape and size projected onto a plane.

II.2.3 Gas bubble dissolution model

A numerical model was developed to simulate the shrinking of a gas bubble due to dissolution in the water column, its expansion due to decreasing hydrostatic pressure in the course of its ascent and gas stripping, and the final gas transport into the atmosphere. The model solves a set of coupled ordinary differential equations (ODEs) describing these processes for each of the involved gas species (CH_4, N_2, and O_2; Eq. II.2) and the bubble rise velocity (Eq. II.3), where time solves as the only independent variable. Thermodynamic and transport properties of the gas components, such as molar volume, gas compressibility, and gas solubility in seawater, were calculated from respective equations of state (Duan et al., 1992; Duan and Mao, 2006; Geng and Duan, 2010; Mao and Duan, 2006), and empirical equations for diffusion coefficients (Boudreau, 1997), mass transfer coefficients (Zheng and Yapa, 2002), and bubble rise velocities (Wüest et al., 1992), taking into account local pressure, temperature and salinity conditions as measured by CTD casts. Implemented equations and values are provided in Table II.2. The ODE system is solved using finite difference methods implemented in the NDSolve object of Mathematica (i.e. LSODA, Sofroniou and Knapp, 2008).

The mass exchange of gas components across the bubble-surface is generally described as (e.g., McGinnis and Little, 2002; Leifer and Patro, 2002; Wüest et al., 1992):

$$\frac{dN_i}{dt} = 4\pi r_{eq}^2 \cdot K_{L,i}(C_{a,i} - C_{eq,i}) \qquad \text{Eq. II.2}$$

where i is the ith gas species, N, is the amount of gas in the bubble, $4 \pi r_{eq}^2$ is the surface area of the equivalent spherical bubble, K_L is the specific mass transfer rate between gas phase and aqueous phase, C_a is the dissolved gas concentration, and C_{eq} is the gas solubility. All of the above variables are functions of the water depth, z, i.e. pressure, temperature and salinity (see Tab. II.2 for details and references). The change of the vertical bubble position is related to the bubble rise velocity, v_b (Tab. II.2):

Table II.1: Location, water depth, and bottom water temperature of the abandoned wells and CTD cast 12.

Site/Gear	Latitude/ °N	Longitude/ °E	Water depth/ m	BW Temperature/ °C
16/4-2	58.596	2.028	93	5.1
16/7-2	58.473	2.033	83	7.8[a]
15/9-13	58.373	1.932	81	7.8[a]
CTD12	58.406	2.024	80	7.8

[a] Based on measurements of CTD12

$$\frac{dz}{dt} = v_b \qquad \text{Eq. II.3}$$

Model simulations were performed based on boundary conditions obtained from Sea-Bird 9 plus CTD data of August 2012 (Tab. II.1) and run for 21 different initial bubble sizes (1.7 to 3.7 mm radius, in accordance with the results of the measured bubble spectra), initially containing only methane. The measured initial bubble size distribution is assumed to be representative and the mass transfer of gases other than CH_4, N_2, and O_2, as well as the development of upwelling flows were considered to be negligible. Simulated water depths of 81, 83, and 93 m correspond to those of the investigated wells. The numerical simulation of gas transport by a single rising bubble is justified because only single bubble streams were observed at the wells with very little to no interaction between the bubbles, or plume dynamics. The bubble-mediated methane flow into the atmosphere was calculated from the remaining amount of CH_4 in the bubble, when it reaches the sea surface, N_S, i.e.

$$N_S(r_0, z) = N_0(r_0, z_0) - \int_{t=0}^{tmax} dN(r_0, z)\, dt \qquad \text{Eq. II.4}$$

where N_0 is the initial amount of methane in the bubble and *tmax* is the time required by the gas bubble to travel from the seafloor (z_0) to the sea surface and is determined numerically by the bubble dissolution model. The residual methane depends on the initial bubble size (r_0) and water depth (z) and was normalized to the corresponding N_0. The relative amount of methane at the sea surface with respect to the initial bubble methane content, $\Omega(r_0,z)=N_S(r_0,z)/N_0(r_0,z_0)$, is referred to as the transport efficiency of a single gas bubble. At seep sites, where bubbles are of uniform size, the atmospheric gas flow can be easily quantified by multiplying the bubble transport efficiency with the seabed gas flow. However, if gas bubbles show a size spectrum, $\Omega(\Psi,z)$ has to be calculated for each bubble size and weighted by its volumetric contribution, V_0, to the total emitted gas bubble volume, V_Ψ. Integrating this weighted bubble transport efficiency over the entire bubble size spectrum and multiplying it by the seabed gas flow at the investigated well, Q_{well}, gives the total gas flow into the atmosphere:

Table II.2: Parameterization of numerical model.

Parameterization	Range	Variance	Reference
[a] Diffusion coeff.: D_i / m^2 s^{-1}			
$D_{O2}=1.05667\cdot10^{-9}+4.24\cdot10^{-11}\cdot T$	T:0-25°C	$1.00\cdot10^{-21}$	Boudreau, 1997
$D_{N2}=8.73762\cdot10^{-10}+3.92857\cdot10^{-11}\cdot T$	T:0-25°C	$2.94\cdot10^{-23}$	Boudreau, 1997
$D_{CH4}=7.29762\cdot10^{-10}+3.31657\cdot10^{-11}\cdot T$	T:0-25°C	$5.70\cdot10^{-24}$	Boudreau, 1997
Mass transfer coefficient: $K_{L,i}$ / m s^{-1}			
$K_L=0.013(v_b\cdot10^2/(0.45+0.4\ r\cdot10^2))^{0.5}\cdot D_i^{0.5}$	r≤2.5 mm		Zheng and Yapa,2002
$K_L=0.0694\ D_i^{0.5}$	2.5<r≤6.5 mm		Zheng and Yapa,2002
$K_L=0.0694\ (2r\cdot10^{-2})^{-0.25}\cdot D_i^{0.5}$	R<6.5 mm		Zheng and Yapa,2002
Fit to CTD data as function of z			
$T(z)=8+7/(1+e^{0.375\ (-21.7512+z)})$	Z: 0.100 m	$3.99\cdot10^{-2}$	
$S(z)=35.12-0.67/(1+e^{0.4125\ (-20.1595+z)})$	Z: 0-100 m	$4.97\cdot10^{-4}$	
Density of SW: φ_{SW}/ kg m^{-3}			
$\varphi_{SW}(z)=1027.7-2.150/(1+e^{0.279\ (-21.612+z)})$	Z: 0-100 m	$6.8\cdot10^{-3}$	Unesco,1981
Bubble rise velocity: vb / m s^{-1}			
$v_b=4474\ r^{1.357}$	r<0.7 mm		Wüest et al., 1992
$v_b=0.23$	0.7≤r<5.1 mm		Wüest et al., 1992
$v_b=4.202\ r^{0.547}$	r≥5.1 mm		Wüest et al., 1992
Gas solubility: c_i / mM			
cN2=0.622+0.0721·z	Z:0-100m	$2.5\cdot10^{-3}$	Mao and Duan, 2006
cO2=1.08+0.1428·z	Z:0-100m	$9.8\cdot10^{-3}$	Geng and Duan, 2010
cCH4=1.44+0.1671·z	Z:0-100 m	$2.4\cdot10^{-2}$	Duan and Mao, 2006
CH_4 molar volume: MV_{CH4} / L mol^{-1}			
$MV_{CH4}=1/(0.0418+0.0044\cdot z)$	Z:0-100 m	$3.0\cdot10^{-2}$	Duan et al., 1992
Hydrostatic Pressure: P_{hydro}/ bar			
$P_{hydro}=1.013+\varphi_{SW}\cdot g\cdot z$			

[a] The parameterization of the diffusion coefficients is based on a seawater salinity of 35 PSU. Pressure effects have been neglected because at the given water depths (<100 m) the resulting error is less than 1%.

$$F_{Atm}(\psi,z)=\frac{Q_{well}}{MI}\int_{r(min)}^{r(max)}\frac{N_S\ (r_0,z)}{N_0\ (r_0,z_0)}\cdot\frac{V_0\ (r_0)}{V_\psi}\ dr \qquad \text{Eq. II.5}$$

where, *r(min)*, and *r(max)* are the minimum and maximum radii of the bubble size spectrum *Ψ*, respectively, and *MI* is the measurement interval between individual bubble sizes (i.e. 0.1 mm). V_0 and V_ψ refer to optical size measurements at individual gas streams of the investigated wells, which were conducted to determine the combined bubble size spectrum considered to be representative for the three wells. As Eq. II.5 assumes that there is no change in the weighted volumetric contribution of each bubble size to the total emitted bubble volume (i.e. $V_0(r_0)/V_\psi$=*const.*), the relative distribution of bubble sizes is considered to be constant, although the release frequency of bubbles may change due to a variability of the seabed gas flow. This means that an increase in the gas flow increases the rate of bubble formation, but not their size distribution, as generally validated for seeps with a low gas flow (Dewar et al., 2013; Leifer et al., 2004). The numerical accuracy of the model, determined from mass balance errors, was better than 99.9%.

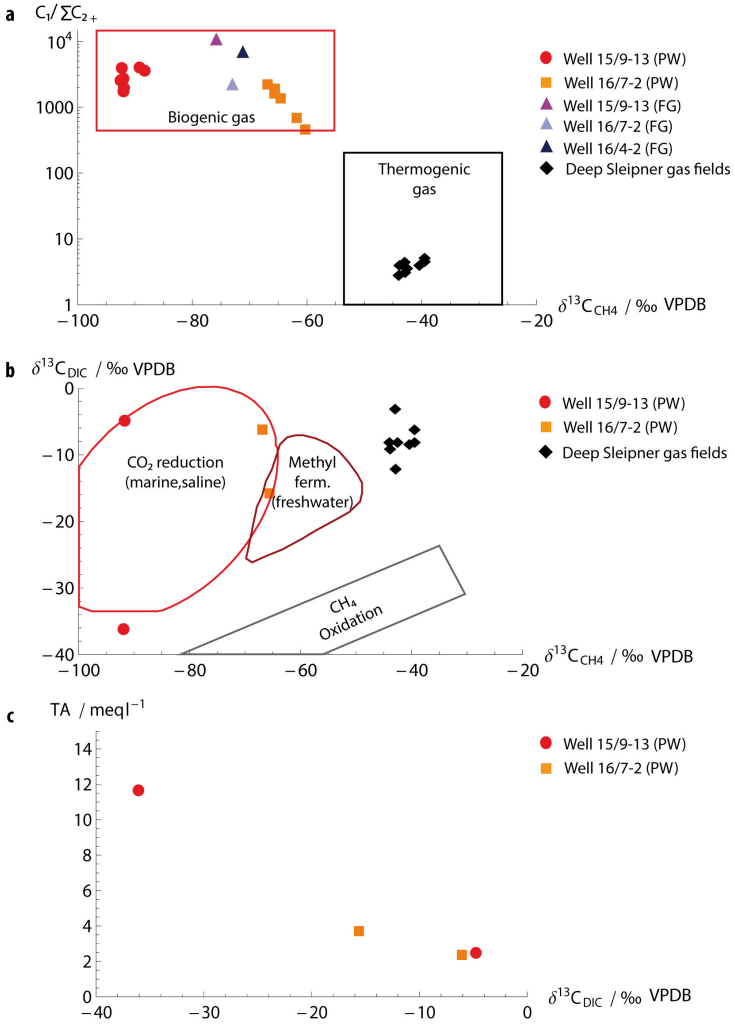

Figure II.3: a) Bernard diagram of the molecular and isotopic gas composition (after Bernard et al., 1978) indicating the gas source of the gas at abandoned wells (red dots: porewater (PW) at well 15/9-13, orange rectangle: porewater at well 16/7-2, triangles: free seep gas (FG) at wells 15/9-13, 16/7-2, and 16/4-2) and the deep hydrocarbon reservoirs in the area (black diamonds; James, 1990). (**b**) Cross-plot of $\partial^{13}C$ of DIC versus $\partial^{13}C$ of CH_4 in the porewater at well 16/7-2 (orange rectangles), well 15/9-13 (red dots), and the deep hydrocarbon reservoirs (black diamonds; James, 1990). (**c**) Cross-plot of total alkalinity (TA) and $\partial^{13}C$ of DIC indicating microbial anaerobic oxidation of methane.

II.3 Results

II.3.1 Gas composition and isotopic signatures

The seep gas at the wells consists mainly of methane (85-89 Vol.%) with minor contents of ethane (69-365 ppmV) and propane (2-17 ppmV). Higher hydrocarbons, such as n-butane, n-pentane, and n-hexane, were not present; iso-butane (5.5 ppmV) was only detected at well 16/4-2 (Fig. II.3a). The remaining gas components making up 11-15 Vol.% are assumed to consist of N_2 and O_2, which were not determined in our analyses, but were likely stripped

from ambient seawater during the time of filling the funnel with gas, i.e. 10 minutes. The volume ratio of methane and higher hydrocarbons, $C_1/\sum C_{2+}$ of the expelled gas is 2,300-11,100 and the $\partial^{13}C$ value of the methane is -71 to -70‰ VPDB (Fig. II.3a).

The dissolved methane in the surface sediments shows a slightly larger variation in the $\partial^{13}C$ signature of -92.5 ‰ at well 15/9-13 to -60.3‰ at well 16/7-2. Likewise, DIC in the porewater carries a $\partial^{13}C$ signature ranging between -36.07 and -15.63‰ VPDB at 5 cm sediment depth (Fig. II.3b) and between -4.76 and -6.07‰ VPDB in the bottom water. Corresponding total alkalinity values at wells 15/9-13 and 16/7-2 are 11.7 and 3.8 meq L^{-1} at 5 cmbsf and 2.5 and 2.4 meq L^{-1} in the bottom water, respectively (Fig. II.3c).

II.3.2 Leakage site characteristics

II.3.2.1 The Nature of surface sediments

Surface sediments at the investigated wells were overall sandy with minor admixtures of clay, particularly at wells 15/9-13 and 16/4-2. At well 16/7-2 sediments were generally coarser.

Carbonates were found only at well 16/7-2, both in the surface sediments and at the seafloor. Their stable carbon isotopic signature, $\partial^{13}C$, of -14 to -3‰ VPDB is rather heavy and corresponds well with the observed carbon isotopic signature of the DIC in ambient porewaters (see Section II.3.1).

II.3.2.2 The nature of methane seepage

Active bubble emissions and patchy bacterial mats were characteristic leakage features at the investigated wells (Fig. II.1). The total seepage area was roughly estimated to cover ~10 m^2 of seabed at each well, thus significantly exceeding the actual well diameter of ~76 cm (Horvig, 1982; Normann and Østby, 1982). Bubbles generally pinched-off as single bubble streams from tiny depressions in the sandy sediments. Seepage activity varied substantially between the studied wells, evident by the significantly different numbers of total vents per well: 39 individual bubble streams were observed at well 16/7-2, whereas only 2 and 8 seep spots were found at wells 15/9-13 and 16/4-2, respectively (Tab. II.3).

II.3.3 Seabed methane emissions

Results of the funnel-derived gas flow measurements at individual bubble streams of well 16/4-2 and well 15/9-13 are shown in Table II.3. At well 16/7-2 the gas flow was derived from bubble size measurements (see section II.3.4, and Tab. II.3). To allow comparison of the gas emissions, measured at different locations (i.e. 58.373° N and 1.932° E; 58.473° N and 2.033° E; and 58.596° N and 2.028° E, see Tab. II.1) and at variable water-depths (i.e. 81, 83, and 93 m at well 15/9-13, 16/7-2, and 16/4-2, respectively), *in situ* gas flows measured at 7.8 °C and 5.1 °C were expressed in standard conditions, referred as STP (P = 1 bar;

Table II.3: Quantification of seabed- and direct atmospheric gas emissions at abandoned wells.

Well	Seabed				Atmosphere	
	In situ Q per vent/ L min^{-1}	Q (STP) per vent/ L min^{-1}	Number of vents	Q per well[a]/ t CH_4 yr^{-1}	F_{Atm} per well/ %	F_{Atm} per well/ kg CH_4 yr^{-1}
16/4-2	0.15/0.17[b]	1.6/1.8[b,e]	8	4	0.4	16
16/7-2	0.15[c]	1.4[f]	39	19	1.3	250
15/9-13	0.09	0.9[g]	2	1	1.5	15
Total			49	24	1.2	280
Abs. error (1σ)	0.03	0.4		6[d]		76[d]
Rel. error (1σ)	25	27	122			

[a] based on the average gas flow of 1.4 L min^{-1} at STP (25°C, 1bar)
[b] based on replicate gas flux measurements at well 16/4-2
[c] derived from bubble size, due to lack of direct funnel measurements
[d] based on a spatial variability of 27.1%
[e] measured at high tide
[f] measured at low tide
[g] measured 2 h after low tide

T = 298.15 K). The standard gas flows, *Q*, ranged from 0.9 to 1.8 L min^{-1} (STP) with an average gas flow of 1.4 (±0.4) L min^{-1} (STP) at the sampled bubble streams (Tab. II.3). This corresponds to a relative variability of 27%, which was (due to lack of information) also assumed to be equivalent to the spatial variability at a single well. Thus, based on the average *Q* and the number of individual bubble streams at the wells, the total seabed methane gas flow was estimated to range between 2.8 L min^{-1} and 55 L min^{-1} (STP), corresponding to an annual methane release of 1.0-19 t yr^{-1} $well^{-1}$ assuming no larger variability over prolonged times. Estimates of the methane release were highly variable and were controlled clearly by the number of seep spots per well. Based on the relative variability of 27%, the total annual methane release of all three wells was estimated to be 24 (±6) tons.

Uncertainties in the estimation of the seabed methane flow arise from five different factors: (1) uncertainty in estimating the total number of vents, (2) error in funnel-based flow measurements (<2.5%), (3) uncertainty due to variability in methane emission rates at individual gas streams (27%), (4) unknown temporal variability of the gas flux on time scales larger than hours, and (5) uncertainty based on the initial assumption that expelled gas consists only of methane. The latter may result in an overestimation of seabed methane emissions, because measured compositional CH_4 data were lower (85-89 Vol.%). Nevertheless, we propose that it is acceptable to assume that seep gases consist only of methane, because N_2 and O_2 uptake as well as methane dissolution during the time for filling-up the funnel (i.e. 10 minutes) likely reduced the methane content in our gas samples. The uncertainty in the quantified number of vents is expected to be small because the counting of individual seep

spots in the video material was repeated several times. However, single vents, particularly at well 16/7-2, where gas bubbling was most active, could have been missed due to the low contrast and resolution of the videos, or simply because vents were outside the area covered during the ROV dives.

II.3.4 Bubble size measurements

Bubble sizes measured from video ranged from 3.2 to 16 mm in diameter (Fig. II.4). Except for the measurements at well 16/7-2, where bubbles were observed to escape from below a carbonate rock, bubbles were emitted from sandy sediments with an average release frequency of 27 s^{-1}. At well 16/7-2, larger bubbles were expelled into the water column because gas accumulated below a carbonate rock, thus forming significantly larger bubbles of 7.2 -16 mm in diameter compared to those directly released from the sandy sediments into the water column, i.e. 3.2- 7.4 mm in diameter.

According to the rather low gas flow, bubble emissions were classified as minor bubble plumes, typically showing narrow size distributions with peaks for radii of 2.4 and 2.7 mm at wells 15/9-13 and 16/4-2, respectively. These can be described by a simple Gaussian function, as suggested by Leifer and Culling (2010) (Fig. II.4). The combined bubble size distribution, Ψ, was determined from 274 size measurements, combining bubble size measurements at well 16/4-2 and well 15/9-13 (Fig. II.4d). Bubble measurements at well 16/7-2 were excluded for the determination of the combined size spectrum because bubble sizes were strongly affected by gas accumulating below a carbonate rock. Given that gas flow at individual seeps is low and assuming that initial bubble formation is controlled by the mechanical properties of the surface sediments (Dewar et al., 2013), Ψ is proposed to be representative for bubbles released from the fine to medium-grained clayey sand found at the investigated wells.

The averaged uncertainty in optical size measurements arising from the 2-D projection of a 3-D oscillating volume was estimated to be 12.4%, based on multiple measurements of the same bubbles in subsequent video frames. The error significantly increased with an increasing amount of large bubbles, which is in agreement with enhanced shape oscillations (wobbling) as bubbles become larger. Furthermore, bubble size measurements at wells 15/9-13 and 16/4-2 both resulted in an *in situ* gas flow of 0.10 L min^{-1}, which differed from funnel-derived gas flows of 0.09 and 0.17 L min^{-1}, respectively. Thus, bubble sizes were corrected by 1–14% to match direct gas flow measurements, indicating that small bubbles might have been missed, and/or that the scale was in front of the measured bubbles, both of which resulting in an under-estimation of bubble size-derived gas emissions. At well 16/7-2 video-data of funnel-derived gas flow measurements were not available. However, due to the lower release

frequency, the tracking of bubbles in following frames was easier, and allowed measuring each bubble several times, which reduced the error in the bubble size-derived gas flow at this particular well.

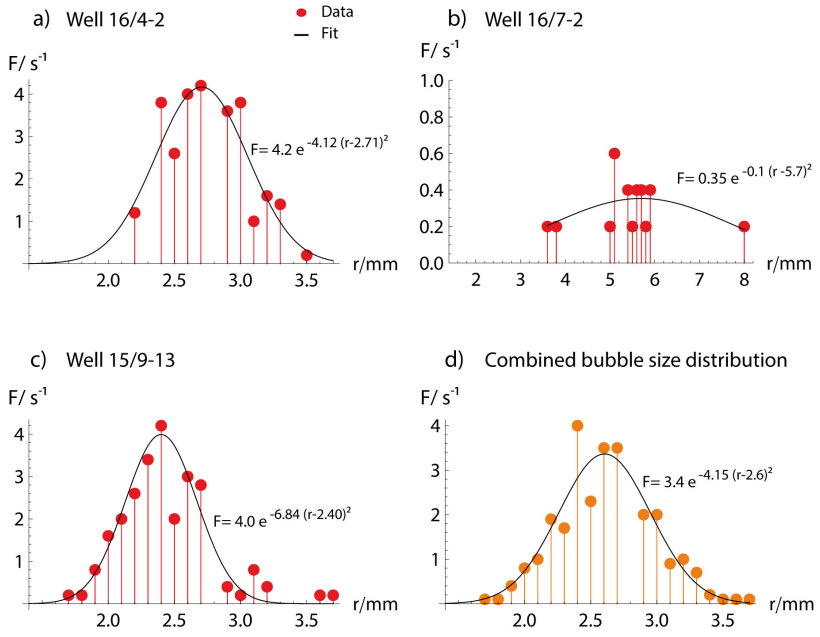

Figure II.4: Measured bubble release frequency (F) versus bubble radius (r), and Gaussian fits for the bubble size distribution of single streams at the investigated wells (**a-c**). **d**) Combined bubble size distribution based on measurements at wells 15/9-13 and 16/4-2. Gaussian functions were fitted to the data using the non-linear least-squares fitting algorithm "NonlinearModelFit" of Mathematica. The variance, s^2, of the fits is 0.53, 0.002, 0.31, and 0.18 for the bubble size distributions at wells 16/4-2, 16/7-2, 15/9-13, and the combined spectrum, respectively.

II.3.5 Contribution to atmospheric methane via direct bubble transport

The bubble-driven methane transport to the sea-surface strongly depends on the initial bubble size and the leakage depth. Numerical simulations show that the largest bubble of the size spectrum (r_{eq} = 3.7 mm) that is released from the shallowest well (i.e. well 15/9-13 at 81 mbsl) has the highest methane transport efficiency, nonetheless losing about 93% of its initial methane content on its way from the seafloor towards the sea-surface. Hence, the majority of the methane leaking from the seabed will dissolve in seawater before bubbles reach the atmosphere. Based on the determined bubble size distribution Ψ, which was found to be characteristic for the investigated abandoned wells, we calculated the direct seabed methane contribution to the atmosphere for each investigated well using Equation II.5. Any additional contributions to (or from) the atmosphere arising from the diffusive air-sea gas exchange have not been quantified in this study.

Our results show that the transport efficiency, $\Omega(\Psi)$, decreases with increasing water depth, but is always below 2% (Tab. II.3): i.e. 1.5%, 1.3%, and 0.4% for the water depths of 81, 83, and 93 m of the respective three abandoned wells. Assuming that the observed seepage activity and the bubble size distribution are representative, this corresponds to an atmospheric methane emission of 15, 250, and 16 kg yr^{-1}, at wells 15/9-13, 16/7-2 and 16/4-2, respectively. Hence, at all three wells, combined bubbles were estimated to transport around 280 kg of seabed methane to the atmosphere each year, most of it being emitted at well 16/7-2.

Uncertainties in atmospheric emission estimates arise from two different factors: (1) spatial and temporal variability in seabed emissions, and (2) seasonal changes of sea water conditions. Based on CTD casts obtained in March 2013, the latter was found to be negligible for the investigated wells, enhancing the CH_4 transport efficiency of bubbles by less than 0.2% in winter, as determined by numerical modeling. Based on the relative spatial variability of seep emissions of 27%, the respective uncertainty in the total atmospheric methane release was estimated to be 280 (±76) kg yr^{-1}. Some uncertainties due to the unknown temporal variability of leakage rates on time scales longer than hours and related changes of the bubble-chain dynamics remain. However, enhanced bubble rise velocities have not been observed at the investigated seeps, neither at low nor at high tide, suggesting that the atmospheric gas transport from the three wells is probably not affected by upwelling.

II.4 Discussion

II.4.1 Gas origin

The methane leaking at the investigated abandoned wells is clearly of biogenic origin, as indicated by a $\partial^{13}C$ of CH_4 lighter than -70‰ VPDB and a $C_1/\sum C_{2+}$ ratio larger than 1,000 (Fig. II.3a). Hence, the source depth is shallower than 2 km, considering a regional geothermal gradient of ~30°C km^{-1} and an upper temperature limit of microbial methanogenesis of 55-60°C (Rice, 1992). This interpretation is corroborated by literature values of the gases in the deep hydrocarbon reservoirs in the area showing significantly lower $C_1/\sum C_{2+}$ ratios of 2.9 - 5.3 and heavier stable isotopic values, i.e. $\partial^{13}C_{CH4}$= -39 to -44‰ VPDB, clearly identifying their thermogenic origin (James, 1990) (Fig. II.3a).

The slightly larger variation in the $\partial^{13}C$ signature of the dissolved methane in the surface sediments at wells 15/9-13 and 16/7-2 suggests two different carbon pools of the seeping methane. While the $\partial^{13}C_{CH4}$ values measured at well 15/9-13 ($\partial^{13}C_{CH4} \approx$ -90‰ VPDB) are produced by microbial CO_2 reduction related to a marine carbon pool, less negative values at well 16/7-2 (i.e. $\partial^{13}C_{CH4}$ > -67‰ VPDB) point towards microbial fermentation of methylated substrates of a fresh-water carbon pool (Fig. II.3b). The latter may originate from

fluvial or glacial sediment deposits, both common in the North Sea.
The corresponding $\partial^{13}C_{DIC}$ of -15.6‰ VPDB and a slightly increased TA value of 3.8 meq L^{-1} at well 16/7-2 and even more so the $\partial^{13}C_{DIC}$ of -36.07‰ VPDB and the elevated TA value of 11.7 meq L^{-1} at well 15/9-13, both indicate that methane is oxidized by anaerobic microbial consortia in the ambient surface sediments (Fig. II.3b,c).

In order to further constrain the origin of the leaking gas, we correlate the well paths of the three boreholes with geological information described in Well-Reports (Horvig, 1982; Normann and Østby, 1982; Hydro, 1990) and with the locations of gas pockets in the subsurface sediment. The latter have been mapped as high-amplitude anomalies in the seismic data (Karstens and Berndt, 2015) (Fig. II.5).

The well-paths of 15/9-13 and 16/7-2 both penetrate sand-dominated layers with a high density of seismic bright spots, indicating a focused gas distribution forming distinct gas pockets in ~600 and ~750 mbsf (Fig. II.5a,b). The seismic indications of free gas are in good agreement with observations in the well completion report of well 16/7-2 (Horvig, 1982). In particular, Lower Pliocene sediments at a depth of 750 m were described to contain thin gas-bearing sand stringers. However, evidence for gas was found also in shallower sediment depths, such as 715 mbsf, 687 mbsf, 539 mbsf, and 242 mbsf (Horvig, 1982). Thus, leaking gases might originate from different shallow source areas, with a biogenic signature in common.

For well 16/4-2, the seismic data do not reveal prominent bright spots in the direct vicinity of the well-path, but the near-surface sediments (Fig. II.5c, 0.1 – 0.4 s two-way-travel time TWT) show seismic turbidity, which might indicate an unfocussed distribution of gas (Judd and Hovland, 1992). Hence, the presence of free gas in the pore space is less constrained by the seismic data at well 16/4-2 than at 15/9-13 and 16/7-2. Well 16/4-2 further penetrates a topographic high at the Top Pliocene (Fig. II.5c; 0.5 s TWT), which may facilitate buoyancy-controlled gas migration towards the well.

II.4.2 The nature of gas migration along an abandoned well

In the absence of high overpressures, gas migration along an abandoned well can be best described by buoyancy-driven capillary invasion of well-induced pathways where the gas has to exceed the capillary pressure to enter an initially water-saturated conduit (Clayton et al., 1994; Gurevich et al., 1993). The capillary resistance that needs to be overcome generally decreases with increasing pore-space (sediments) or width (fracture), making a water-saturated clay totally impermeable for non-overpressured gas (i.e. due to the very large capillary pressure of ~300 kPa, Wheeler et al., 1990; Judd and Hovland, 2007), unless there are pre-existing cracks and fractures.

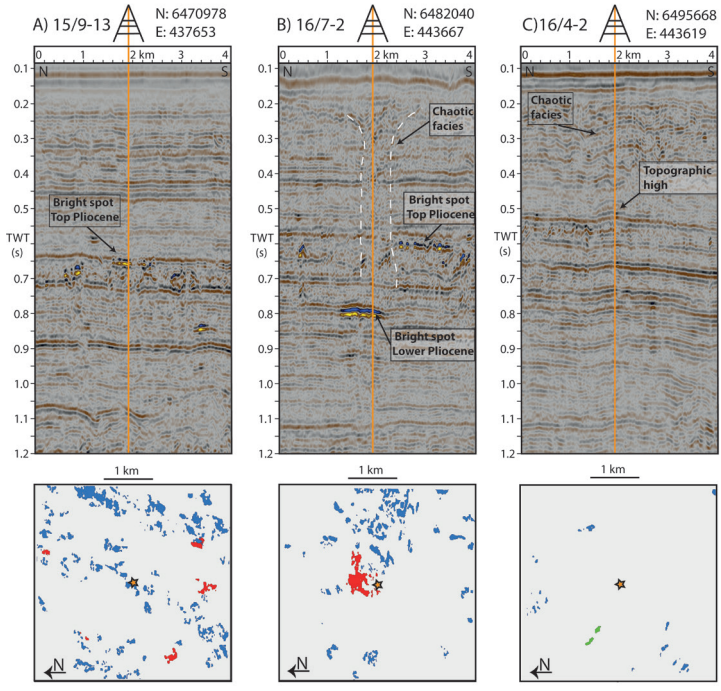

Figure II.5: (Top panel) Seismic profiles indicating shallow gas pockets in the subsurface and the well paths of the 3 abandoned wells (orange line). At well 16/7-2 the outline of the seismic chimney and chaotic reflections is depicted. (Bottom pane) Areal distribution of shallow gas pockets (green= Pleistocene, blue = Top Pliocene, and red= Lower Pliocene) above the deep hydrocarbon reservoirs (orange stars: seafloor location of the abandoned wells).

Thus, leakage problems often are compounded by geotechnical fracturing of sediment around the wellbore and by insufficient filling of these fractures with cement, resulting in a fracture system along the well (Gurevich et al., 1993). The upward migration of gas can occur along any of several pathways associated with the abandoned well: a) between casing and cement; b) between cement plug and casing; c) through the cement pore space as a result of cement degradation; d) through the casing as a result of corrosion; e) through fractures in the cement; and f) between cement and sediment (Gasda et al., 2004). Because all investigated wells have plugs and casing, each of these possible migration conduits is conceivable and would be associated to enhanced effective permeability providing the key to the initiation of gas migration, drawing gas from the surrounding sediment because of lower capillary pressure in the fracture (Bethke et al., 1991; Judd and Hovland, 2007). Nordland Group sediments from ~300 mbsf down to the Utsira Formation primarily consist of clay as indicated by high gamma ray values in the well-logs (Fig. II.2). Therefore, they provide an efficient barrier for capillary gas invasion holding gas at a higher pressure than sand. Hence, strata-crossing upward migration of gas should only be possible along secondary, either natural or well-induced, pathways.

II.4.3 Geological control of leakage

Leaky wells showed continuous gas bubble release into the water-column. However, total seabed emissions at the wells were highly variable (ranging from 1 to 19 t yr^{-1} of CH_4), being ultimately controlled by differences in the number of bubble streams per well (2, 8, and 39). In order to understand the mechanisms that might control leakage activity at abandoned wells, we correlate the bubble emissions of the three boreholes with properties of the subsurface sediments. The most remarkable observation is the presence of a seismic chimney at well 16/7-2 (Fig. II.5B), indicated by disturbed and chaotic reflections in Upper Cenozoic sequences, coinciding with the highest leakage activity being observed here. The chimney apparently provides additional pathways and appears to facilitate gas migration towards the seabed. However, it is not obvious from our data if and to what extent the migrating gas appears to separate from the borehole fracture and uses pre-existing conduits created by the chimney sometime in the geological past. Seismic modelling and S-wave experiments conducted on chimneys above the Tommeliten reservoirs proved that seismic chimneys represent gas-filled fracture networks within impermeable bedrock (Granli et al., 1999; Arntsen et al., 2007; Løseth et al., 2009). Hence, the chimney at well 16/7-2 also might represent a potential source and pathway for leaking gas. The seismic feature is also in good agreement with the evidence of carbonates found at the seafloor that may indicate a longer history of gas seepage in the area of the seismic chimney. However, with the current carbonate isotopic data it is not possible to constrain the seepage history for well 16/7-2 any further.

Considering permanent well plugging and abandonment procedures, final (upper) gas migration and bubble formation are controlled by surface sediments unless there are very high gas flows affecting bubble sizes (Dewar et al., 2013). The required sediment depth for cutting of the wellhead and the following casings typically is at least 5 mbsf to minimize the risk of parts of the well protruding the seabed (NORSOK D010, 2004). A comparison of the three wells with natural seepage systems shows that the initial bubble size distribution at leaky wells is in good agreement to bubble diameters found at Tommeliten (Schneider von Deimling et al., 2011) and the Scanner Pockmark field (Judd and Hovland, 2007) (Tab. II.4). Thus, the bubble formation mechanisms are supposed to be quite similar, regardless if seepage is of anthropogenic or natural origin. Analogous to natural seep sites, local changes in lithology (i.e. clays), and biogeochemical boundaries (i.e. carbonate cementation) might cause lateral diversion or re-trapping of migrating gas bubbles along surfaces in the sedimentary overburden (Judd and Hovland, 2007). Clay inter-beddings in retrieved push cores are in good agreement with reduced leakage activity. With increasing amounts of clay in the upper sediment, vertical movement of the gas likely is restricted and lateral movement encouraged, thus favoring diversion of seepage paths, as indicated by the presence of large bacterial mats at

well 15/9-13 and 16/4-2. By contrast, the relatively coarse sediments at well 16/7-2 facilitate gas migration to the sediment-surface, due to higher permeability (Judd and Hovland, 2007). Unfortunately, we were unable to measure any longer temporal variability of seabed gas emissions. Hence, we are unable to report on the dependency of tidal pressure fluctuations or release and re-filling of near-surface gas pockets, which are commonly believed to control the rate of bubble emissions at the seabed (e.g., Leifer and Wilson, 2007; Linke et al., 1994; Tryon et al., 1999; Wiggins et al., 2015).

We conclude that intense gas leakage at well 16/7-2 is related to relatively coarse surface sediments and a gas chimney in the subsurface, which provides additional pathways for gas migration. Thus, sediment properties appear to control bubble emissions at leaky wells, as previously observed at natural seep sites (Judd and Hovland, 2007). Nevertheless, we cannot exclude further mechanisms that may drive gas migration in the subsurface and leakage activity at the seafloor, such as overpressure in the shallow gas reservoir or fluctuations and differences in gas supply.

Table II.4: Comparison of natural and anthropogenic gas emissions in the North Sea.

Location	Nr. of vents	Bubble radius/ mm	Area/ m^2	Q per vent/ kg yr^{-1}	Q per area/ t yr^{-1}	Reference
Scanner Pockmark	3	2.5	–	36	–	Hovland et al., 2012; Judd and Hovland, 2007; Hovland, 1985, Clayton and Dando, 1996
UK Block 15/25	–	–	22,825	–	6.8	Judd, 2004; Clayton and Dando, 1996
Anvil Point, Dorset UK	–	–	–	–	68	Judd, 2004; Hinchcliffe,1978
Torre Bay, Firth of Forth, Scotl.	–	–	2,400	–	1.25-1.8	Judd et al., 2002
Tommeliten	550	2.2		37.1	26	Schneider von Deimling et al., 2011
Gullfaks-Heincke seeps	1-2 every $5m^2$	–	1,00	–	–	Wegener et al., 2008; Hovland et al., 2012
Blowout well 22/4b	176	–	360	–	$1.7\text{-}33{\cdot}10^3$	Leifer et al., 2015
3 abandoned wells	49	2.6[a]	30	490	24	This study

[a] Based on the peak radius of the combined bubble size distribution determined in this study.

II.4.4 Methane emissions in a North Sea context

In order to place the methane release from the three investigated wells in context to other North Sea methane emissions, we compare them with natural seabed methane fluxes. Although many natural seep locations are known, only few North Sea methane flux calculations have been reported in the literature so far: Tommeliten (Schneider von Deimling et al., 2011), the Scanner Pockmark field within UK Block 15/25 (Hovland, 1985; Judd and Hovland, 2007; Clayton and Dando, 1996; Hovland et al., 2012), Anvil Point (UK, Judd, 2004; Hinchcliffe, 1978), Torre Bay (Scotland, Judd et al., 2002) and the Gullfaks seeps (Hovland, 2007; Wegener et al., 2008). All of them occur as long-lasting-macro-seep systems, associated

with continuous gentle methane venting in the central and northern North Sea (Hovland et al., 2012). Due to their large seepage area, these sites are supposed to contribute considerable amounts of methane to North Sea bottom waters (Bange, 2006) (Tab. II.4). Annual methane emissions vary between 1.25, 26 and 68 t at Torre Bay, Tommeliten, and Anvil Point, respectively, demonstrating the high spatial variability of natural seep sites, apparently in response to variations in the geological setting (Judd and Hovland, 2007). Active venting has been reported at Tommeliten, where around 550 bubble streams emanate at the seafloor (Schneider von Deimling et al., 2011). Despite the much smaller source area and smaller number of vents at the three leaky abandoned wells, their emission rates were estimated to be similar to Tommeliten, due to a source strength exceeding that at Tommeliten by one order of magnitude, i.e. the bubble release rate at individual vents was 27 Hz at each abandoned well and 7 Hz at Tommeliten (Schneider von Deimling et al., 2011). Together with a slightly larger bubble peak radius (i.e. 0.4 mm larger), the three abandoned wells are estimated to emit a comparable seabed flow of ~24 t CH_4 yr^{-1}, mainly driven by the large seabed emissions from well 16/7-2.

Compared to the overpressure-driven gas blowout at well 22/4b, which is shown to be a significant source for methane into the seawater (Leifer, 2015) and the atmosphere (Judd, 2015, Rehder et al., 1998), the leakage from the three abandoned wells indicates an additional and potentially significant anthropogenic methane source in the North Sea.

Considering the extensive drilling activity over the past 40 years and given that overall emissions from only three abandoned wells appear to be comparable to natural emissions at Tommeliten, leaky abandoned wells, depending on the overall number and the magnitude of their emissions, should provide a significant input to the North Sea methane budget.

II.4.5 Methane contribution to the atmosphere

To assess the direct release of seabed methane to the atmosphere, we simulated the bubble-driven methane transport towards the sea-surface with a numerical bubble dissolution model. The vertical transport efficiency of bubbles strongly depends on initial/seabed parameters, in particular bubble size and water depth. Hence, the bubble size distribution and the leakage depth are crucial initial parameters to simulate the fate of methane bubbles. Based on the combined bubble size distribution of wells 15/9-13 and 16/4-2, the model results suggest that the three investigated wells contribute less than 2% of seabed methane directly to the atmosphere (Tab. II.3). The transport efficiency thus slightly exceeds that of bubbles released at the blowout well 22/4b (i.e. ~1%; Leifer et al., 2015) where plume-induced turbulences likely enhance the mass transfer at the bubble-water-interface compensating high rise velocities. In the absence of any plume-induced advection, the critical parameter is the release frequency of large bubbles which manage to reach the sea surface and still contain

methane. At the investigated wells, the major volume fraction (60%) consists of bubbles with radii smaller than 2.7 mm, transporting less than 1% of seabed methane to the sea surface. Bubbles with radii smaller than 2 mm completely lose their methane by the time they have reached the sea surface. We conclude that the three wells represent no significant source for direct methane emissions by bubble transport to the atmosphere. However, methane bubble dissolution in the water-column, particularly in the surface mixed layer, could contribute additional methane to the atmosphere via diffusive gas exchange (Wanninkhof, 1992). The seasonal deepening and breakdown of the thermocline during fall to spring (Nauw et al., 2015; Sommer et al., 2015) and even more so, frequent fall and winter storms (Shakhova et al., 2013) will aid the ventilation of the water column and hence, diffusive outgassing of methane to the atmosphere may slightly enhance emission rates.

Possible leaky wells at shallower depths will be more important for direct atmospheric fluxes, underscoring the importance for leaky well surveys in shallower depths. Although our results indicate the potential for a significant impact of these leaking abandoned wells on the regional CH_4 budget of the North Sea, more data on the number of leaking wells, bubble size spectra and longer time-series of leakage rates will be necessary to constrain their actual role.

II.5 Conclusions

A well, analogous to a fracture, provides the key for the initiation of vertical gas migration in the subsurface. Boreholes surrounded by mechanically disturbed and fractured sediments with enhanced permeability, may guide gas directly to the well head, and serve to focus gas migration into a single pathway. To what extent and when gas migration pathways tend to separate from the borehole cannot be clarified in this study, although it seems that sediments which provide additional conduits for migrating gases, such as gas chimneys, tend to facilitate gas migration and increase seepage activity at the seafloor. The generally light isotopic signature of methane and the minor constituents of higher hydrocarbons in seep gases point towards a microbial origin. Shallow gas pockets overlying the deep hydrocarbon reservoirs are likely sources for the gas emanating at the wells, which is supported by bright spots and zones with chaotic signatures in the seismic data. Comparing properties that are equivalent to natural seep sites, such as bubble size, release frequency, and sediment characteristics, we conclude that geology provides the ultimate control for bubble venting at the seafloor, for both anthropogenic and natural seeps. Our first measurements of methane gas fluxes at abandoned wells indicate that numerous leaky wells may contribute significantly to the North Sea methane budget because estimated annual emissions at the studied wells (~24 t CH_4 yr^{-1}) are comparable to those at major natural seepage sites such as Tommeliten. Direct bubble-driven methane fluxes to the atmosphere remain small at the studied wells since more than 98% of the gas released at the seabed is dissolved in the 81 to 93 m deep

water column before reaching the atmosphere. However, the diffusive sea/air gas exchange may provide an additional pathway of methane release to the atmosphere at these sites. Long-term monitoring campaigns are needed to better constrain the total (annual) methane release into the atmosphere derived from abandoned offshore wells.

Acknowledgements

We would like to thank the crew and master of RV Celtic Explorer and RV Alkor as well as the teams of ROV Kiel 6000 and ROV Phoca for their invaluable support during the cruises CE12010 and AL412. We would also like to acknowledge the high-quality support for geochemical analyses by Andrea Bodenbinder and Meike Dibbern as well as Monika Segl at MARUM/University Bremen for the DIC isotope measurements. We thank Statoil ASA for permission to use the 3-D seismic data. Special thanks to Martin Hovland for making us aware of the gas seepage at the three wells. The cruises and scientific work received funding through the European Community's 7th Framework Program (FP7/2007-2013) in the EUROFLEETS program, the ECO2 project (grant agreement no. 265847) and the DFG funded Cluster of Excellence "Future Ocean".

Supplementary Material is provided in Chapter VI Appendix B.

References:

Arntsen, B., Wensaas, L., Løseth, H., Hermanrud, C., 2007. Seismic modeling of gas chimneys. *Geophysics* **72**, SM251–SM259.

Bange, H.W., Bartell, U.H., Rapsomanikis, S., Andreae, M.O., 1994. Methane in the Baltic and North Seas and a reassessment of the marine emissions of methane. *Glob. Biogeochem. Cycles* **8**, 465–480.

Bange, H.W., 2006. Nitrous oxide and methane in European coastal waters. *Est.Coast.Shelf Sci*. **70**, 361-374.

Behtke, C. M., Reed, J.D., Olzt, D.F., 1991. Long –range petroleum migration in the Illinois Basin. *American Association of Petroleum Geologists (Bulletin)*, **75**, 925-45.

Bernard, B.B., Brooks, J.M., Sackett, W.M., 1987. Light hydro-carbons in recent Texas continental shelf and slope sediments. *J. Geophy. Res.* **83**, 4053-4061.

Boudreau, B.P., 1997. *Diagenetic models and their implementation: modelling transport and reactions in aquatic sediments*. Berlin, Heidelberg, New York, London, Paris, Tokyo, Hong Kong: Springer, 414 pp.

Ciais, P., Sabine, et al., 2013. Climate Change 2013: T*he Physical Science Basis. Contribution of Working Group I to the Fifth Assessment Report of the Intergovernmental Panel on Climate Change,* in: Stocker, T.F., Qin, D., Plattner, G.-K., Tignor, M., Allen, S.K., Boschung, J., Nauels, A., Xia, Y., Bex, V., Midgley,

P.M. (Eds.). IPCC, Cambridge, UK, pp. 465-570.

Clayton, C.J., Hay, J., 1994. Gas migration mechanisms from accumulation to surface. *Bull. Geol. Soc. Den.* **41**, 12-23.

Clift, R., Grace, J.R., Weber, M.E., 1978. *Bubbles, Drops, and Particles*. Academic Press, London p. 380.

Crutzen, P.J., Zimmermann, P.H., 1991. The changing photochemistry of the troposphere. *Tellus Ser. A Dyn. Meteorol. Oceanogr.* **43**, 136–151.

Dewar, M., Wei, W., Chen, B., 2013. Small-scale modelling of the physicochemical impacts of CO_2 leaked from sub-seabed reservoirs or pipelines within the North Sea and surrounding waters. *Mar. Pollut. Bull.* **73**, 504-515.

Duan, Z.H., Mao, S., 2006. A thermodynamic model for calculating methane solubility, density and gas phase composition of methane-bearing aqueous fluids from 273 to 523 K and from 1 to 2000 bar. *Geochim. Cosmochim. Acta* **70**, 3369-3386.

Duan, Z., Moller N., Weare, J.H., 1992. An equation of state for the CH_4-CO_2-H_2O system: I. Pure systems from 0-1000°C and from 0 to 8000 bar. *Geochim. Cosmochim. Acta* **56**, 2605-2617.

Eidvin, T., Rundberg, Y., 2007. Post-Eocene strata of the southern Viking Graben, northern North Sea; integrated biostratigraphic, strontium isotopic and lithostratigraphic study. *Nor. J. Geol.* **87**, 391–450.

Etiope, G., Lassey, K.R., Klusmann, R.W., Boschi, E., 2008. Reappraisal of the fossil methane budget and related emissions from geologic sources. *Geophys. Res. Lett.* **35** (9), L09307, doi:10.1029/2008GL033623.

Farreira, T., Rasband, W., 2012. ImageJ User Guide IJ 1.46r. 185p. http://imagej.nih.gov/ij/docs/guide/index.html.

Galloway, W.E., 2001. Seismic expressions of deep-shelf depositional and erosional morphologies, Miocene Utsira Formation, North Sea Basin. *Mar. Geophys.Res.* **22**, 309–321.

Galloway, W.E., 2002. Paleogeographic setting and depositional architecture of a sand-dominated shelf depositional system, Miocene Utsira Formation, North Sea Basin. *J. Sediment. Res.* **72**, 476–490.

Gasda, S.E., Bachu, S., Celia, M.A., 2004. Spatial characterization of the location of potentially leaky wells penetrating a deep saline aquifer in a mature sedimentary basin. *Environ. Geol.* **46**, 707-720.

Geng, M., Duan, Z.H., 2010. Prediction of oxygen solubility in pure water and brines up to high temperatures and pressures. *Geochim. Cosmochim. Acta* **74**, 5631-5640.

Granli, J.R., Arntsen, B., Sollid, A., Hilde, E., 1999. Imaging through gas-filled sediments using marine shear-wave data. *Geophysics* **64**, 668–677.

Gurevich, A.E., Endres, B.L., Robertson Jr, J.O., Chilingar, G.V., 1993. Gas migration from oil and gas fields and associated hazards. *J. Petr. Sci. Eng.* **9**, 233-238.

Hartmann, D.L., et al., 2013: *Observations: Atmosphere and Surface*. In: Climate Change 2013: The Physical Science Basis. Contribution of Working Group I to the Fifth Assessment Report of the Intergovernmental Panel on Climate Change [Stocker, T.F., D. Qin, G.-K. Plattner, M. Tignor, S.K. Allen, J. Boschung, A. Nauels, Y. Xia, V. Bex and P.M. Midgley (eds.)]. Cambridge University Press, Cambridge, United Kingdom and New York, NY, USA.

Hinchcliffe, J.C., 1978. Death stalks the secret coast. *Triton* **23**, 56–57.

Horvig, S., 1982. WDSS 40 01 16 7 2: Geological Completion Report Well 16/7-2. Esso Exploration and production Norway Inc. http://www.npd.no/engelsk/cwi/pbl/wellbore_documents/40_01_16_7_2_Completion_Report_Geological.pdf.

Hovland, M. ,2007. Discovery of prolific natural methane seeps at Gullfaks, northern North Sea. *Geo. Mar. Lett.* **27** (2-4), 197-201.

Hovland, M., Judd, A.G., 1988. *Seabed Pockmarks and Seepages. Impact on Geology, Biology and Marine Environment.* Kluwer, London, Dordrecht, Boston: Graham & Trotman, 293 pp.

Hovland, M., Sommerville, J.H., 1985. Characteristics of two natural gas seepages in the North Sea. *Mar. Petrol. Geol.* **2**, 319–326.

Hovland, M., Judd, A.G., Burke Jr., R.A., 1993. The global flux of methane from shallow submarine sediments. *Chemosphere* **26** (1–4), 559–578.

Hovland, M., Jensen, S., Fichler, C., 2012. Methane and minor oil macro-seep systems- Their complexity and environmental significance. *Mar. Geol.* **332-334**, 163-173.

Hydro, 1990. WDSS 1560 01: General Information Well 16/4-2. http://www.npd.no/engelsk/cwi/pbl/wdss_old/1560_01_WDSS_General_Information.pdf .

James, A.T., 1990. Correlation of reservoired gases using the carbon isotopic compositions of wet gas Components. *Am. Assoc. Petr. Geol. B.* **74**, 1441-1458.

Jones, R.D., 1991. Carbon-monoxide and methane distribution and consumption in the Photic Zone of the Sargasso Sea. *Deep Sea Res. Part A Oceanogr. Res. Pap.* **38**, 625–635.

Judd, A.G., 2004. Natural seabed gas seeps as sources of atmospheric methane. *Environ. Geol.* **46**, 988-996.

Judd, A.G., Hovland, M., 1992. The evidence of shallow gas in marine sediments. *Cont. Shelf Res.* **12**, 1081-1095.

Judd, A.G., Sim, R., Kingston, P., McNally, J., 2002. Gas seepage on an intertidal site: Torry Bay, Firth of Forth, Scotland. *Cont. Shelf Res*. **22**, 2317–2331

Judd, A.G.,Hovland, M., 2007. *Seabed Fluid Flow- The impact on geology, biology and marine environment*. Cambridge University Press, 475 pp.

Judd, A.G., 2015. The significance of the 22/4b blow-out site methane emissions in the context of the North Sea. *J. Mar. Petrol. Geol.* **68**, Part B, 836–847.

Justwan, H., Dahl, B., 2005. Quantitative hydrocarbon potential mapping and organofacies study in the Greater Balder Area. *Nor. North Sea* **6**, 1317–1329.

Karstens, J., and Berndt, C., 2015. Seismic chimneys in the Southern Viking Graben - Implications for palaeo fluid migration and overpressure evolution. *Earth Planet. Sci. Lett.* **412**, pp. 88-100.

Kvenvolden, K.A., Rogers, B.W., 2005. Gaia's breath-global methane exhalations. *Mar. Petrol. Geol.* **22**, 579-590.

Leifer, I., and Patro, R.K., 2002. The bubble mechanism for methane transport from the shallow sea bed to the surface: A review and sensitivity study. *Cont. Shelf Res.* **22**, 2409–2428, doi:10.1016/S0278-4343(02) 00065-1.

Leifer, I., MacDonald, I.R., 2003. Dynamics of the gas flux from shallow gas hydrate deposits: Interaction between oily hydrate bubbles and the oceanic environment. *Earth Planet. Sci. Lett.* **210**, 411-424.

Leifer, I., Boles, J.R., Luyendyk, B.P., Clark, J.F., 2004. Transient discharges from marine hydrocarbon seeps: Spatial and temporal variability. *Environ. Geol.* **46**, 1038-1052.

Leifer, I., Wilson, K., 2007. The tidal influence on oil and gas emissions from an abandoned oil well: Nearshore Summerland, California. *Mar. Pollut. Bull.* **54** (9), 1495-1506.

Leifer, I., Culling, D., 2010. Formation of seep bubble plumes in the Coal Oil Point seep field. *Geo Mar. Lett.* **30**, 339-353, DOI 10.1007/s00367-010-0187-x.

Leifer, I., 2015. Seabed bubble flux estimation by calibrated video survey for a large blowout seep in the North Sea. *J. Mar. Petrol. Geol.* **68**, Part B, 743–752.

Leifer, I., Solomon, E., Schneider von Deimling, J., Rehder, G., Coffin, R., Linke, P, 2015. The fate of bubbles in a large, intense megaplume for stratified and unstratified water: Numerical simulations of 22/4b expedition field data. *J. Mar. Petrol. Geol.* **68**, Part B, 806–823.

Lelieveld, J., Crutzen, P.J., Bruhl, C., 1993. Climate effects of atmospheric methane. *Chemosphere* **26**, 739–768.

Linke, P., Suess, E., Torres, M., Martens, V., Rugh, W. D., Ziebis, W., and Kulm, L. D., 1994. In situ measurement of fluid flow from cold seeps at active continental margins. *Deep Sea Res. I* **41**, 721-739.

Løseth, H., Gading, M., Wensaas, L., 2009. Hydrocarbon leakage interpreted on seismic data. *J. Mar. Petrol. Geol.* **26**, 1304–1319.

Mao, S., Duan, Z.H., 2006. A thermodynamic model for calculating nitrogen solubility, gas phase composition and density of the N_2-H_2O-NaCl system. *Fluid Phase Equilib.* **248**, 103-114.

McGinnis, D. F., Greinert, J., Artemov, Y., Beaubien, S.E., Wüest, A., 2006. Fate of rising methane bubbles in stratified waters: How much methane reaches the atmosphere? *J. Geophys. Res.* **111**, C09007, doi:10.1029/2005JC003183.

McGinnis, D. F., Little J.C., 2002. Predicting diffused-bubble oxygen transfer rate using the discrete-bubble model. *Water Res.* **36**, 4627–4635, doi:10.1016/S0043-1354(02)00175-6.

Nauuw, J., de Haas, H., Leifer, I., Rehder, G., 2015. A review of oceanographic and meteorologic controls on the fate of North Sea methane from a seabed source. *J. Mar. Petrol. Geol.* (in press).

Normann, T.A., Østby, J.M., 1982. WDSS 45 15 9 13: Completion Report Well 15/9-13 PL 046. Statoil, Esso, Norsk Hydro. http://www.npd.no/engelsk/cwi/pbl/wellbore_documents/45_15_9_13_Completion_report_and_log.pdf .

NORSOK Standard D-010, 2004. http://www.standard.no/PageFiles/1315/D-010r3.pdf.

Pape, T., Bahr, A., Rethemeyer, J., Kessler, J.D., Sahling, H., Hinrichs, K.U., Klapp, S.A., Reeburgh, W.S., Bohrmann, G., 2010. Molecular and isotopic partitioning of low-molecular-weight hydrocarbons during migration and gas hydrate precipitation in deposits of a high-flux seepage site. *Chem. Geol.* **269**, 350–363.

Rehder, G., Schneider von Deimling, J., 2008. RV Sonne Cruise Report SO 196, SUMSUN 2008, Suva Guam Okinawa Trough Manila. February 19- March 26 2008. PANGAEA, hdl: 10013/epic.35734.

Rice D.D., 1992. *Controls, habitat, and resource potential of ancient bacterial gas*. Vially R (Ed.) Bacterial Gas, Editions Technip, Paris, pp. 91–118.

Römer, M., Sahling, H., Pape, T., Bohrmann, G., Spieß, V., 2012. Quantification of gas bubble emissions from submarine hydrocarbon seeps at the Makran continental margin (offshore Pakistan). *J. Geophys. Res. Oceans* **117**, C10015.

Sauter, E.J., Muyakshin, S.I., Charlou, J.-L., Schlüter, M., Boetius, A., Jerosch, K., Damm, E., Foucher, J.-P., Klages, M., 2006. Methane discharge from a deep-sea submarine mud volcano into the upper water column by gas hydrate-coated methane bubbles. *Earth Planet. Sci. Lett.* **243**, 354-365.

Schneider v. Deimling J, Brockhoff J, Greinert J., 2007. Flare imaging with multibeam systems: Data processing for bubble detection at seeps. *Geochem. Geophys. Geosystems* **8**.

Schneider von Deimling, J., Rehder, G., Greinert, J., McGinnis, D.F., Boetius, A., Linke, P., 2011. Quantification of seep-related methane gas emissions at Tommeliten, North Sea. *Cont. Shelf Res.* **31**, 867-878.

Schneider von Deimling, J., Linke, P., Schmidt, M., Rehder. G., 2015. Ongoing methane discharge at well site 22/4b (North Sea) and discovery of a spiral vortex bubble plume motion. *J. Mar. Petrol. Geol.* **68**, Part B, 718–730.

Scranton, M.I., McShane, K., 1991. Methane fluxes in the southern North-Sea – the role of European rivers. *Cont. Shelf Res.* **11**, 37–52.

Shakhova, N., Semiletov Igor P., Leifer, I., Sergienko, V., Salyuk, A., Kosmach, D., Chernikh, D., Stubbs, C., Nicolsky, D., Tumskoy, V., Alexeev, V., Gustafsson, O., 2013. Ebullition and storm-induced methane release from the East Siberian Arctic Shelf. *Nat. Geosci.* **7**, 64-70.

Sofroniou, M., Knapp, R., 2008. Wolfram Mathematica Tutorial Collection- Advanced numerical differential equation solving in Mathematica. Wolfram Research, Inc. http://www.wolfram.com/learningcenter/tutorialcollection/AdvancedNumericalDifferentialEquationSolvingInMathematica/AdvancedNumericalDifferentialEquationSolvingInMathematica.pdf

Sommer, S., Schmidt, M., Linke, P., 2015. Continuous inline mapping of a dissolved methane plume at a blowout site in the North Sea UK using a membrane inlet mass spectrometer – Water column stratification impedes immediate methane release into the atmosphere. *J. Mar. Petrol. Geol.* 68, Part B, 766–775.

Tryon, M. D., Brown, K. M., Torres, M. E., Trehu, A. M., McManus, J., and Collier, R. W., 1999. Measurements of transience and downward fluid flow near episodic gas vents, Hydrate Ridge, Cascadia. *Geology 27*, 1075-1078.

UNESCO. 1981a. The Practical Salinity Scale 1978 and the International Equation of State of Seawater 1980. *UNESCO Tech. Pap. Mar. Sci.* **36**, 25 pp.

Vignes, B., Andreassen, J., Tonning, S.A., 2006. PSA Well Integrity Survey, Phase 1 summary report. Petroleum Safety Authority. http://www.ptil.no/getfile.php/z%20Konvertert/Helse,%20miljø%20og%20sikkerhet/Sikkerhet%20og%20arbeidsmiljø/Dokumenter/nettpsawellintegritysurveyphase1reportrevision3006.pdf.

Wanninkhof, R., 1992. Relationship between wind speed and gas exchange over the ocean. *J. Geophys. Res.* **97**. doi: 10.1029/92JC00188.

Ward, B.B., Kilpatrick, K.A., Novelli, P.C., Scranton, M.I., 1987. Methane oxidation and methane fluxes in the ocean surface-layer and deep anoxic waters. *Nature* **327**, 226–229.

Wegener, G., Shovitri, M., Niemann, H., Hovland, M., Boetius, A., 2008. Biogeochemical processes and microbial diversity of the Gullfaks and Tommeliten methane seeps (Northern North Sea). *Biogeoscience* **5**, 1127-1144.

Wheeler, S.J., Sham, W.K., Thomas, S.D., 1990. Gas pressure in undersaturated offshore soils. *Can. Geotechnical J.* **27**, 79-89.

Wiggins, S., Hildebrand, J., Leifer, I., 2015. Long-term acoustic monitoring at North Sea well site 22/4b. *J. Mar. Petrol. Geol.* **68**, Part B, 776–788.

Wojtanowicz, A.K., Nishikiwa, S., Rong, X., 2001. Diagnosis and Remediation of sustained casing pressure in wells. Mineral Manag. Serv. http://www.wellintegrity.net/Documents/MMS%20-%20Diagnosis%20of%20SCP%20-%202001-07-31.pdf.

Wüest, A., N. H. Brooks, and D. M. Imboden (1992), Bubble plume modeling for lake restoration, *Water Resour. Res.* **28** (12), 3235–3250, doi:10.1029/92WR01681.

Zheng, L., Yapa, P.D., 2002. Modeling gas dissolution in deepwater oil/gas spills. *J. Mar. Sytems* **31**, 299-309.

Leaky wells: An unconsidered source for biogenic methane in the North Sea

Lisa Vielstädte [a,*], Matthias Haeckel [a], Jens Karstens [a], Peter Linke [a], Mark Schmidt [a], Lea Steinle [a,b], Klaus Wallmann [a]

[a] *GEOMAR Helmholtz Centre for Ocean Reserach, Kiel, Germany*

[b] *Department of Environmental Sciences, University of Basel, Switzerland*

Supmitted to the Journal of *Nature*, *Nature Climate Change*, and *Nature Geosciences* without success.

Now in preparation for *Proc. Natl. Acad. Sci. U.S.A.*

Introductory Paragraph

Gas leakage from hydrocarbon infrastructure is a major concern because the primary fugitive component of petroleum and natural gas is methane (CH_4), which has a significant global warming potential[1]. However, regular monitoring of wells is only mandatory during the active life time of the well and is solely targeted at the leakage of thermogenic gas and formation fluids from the deep hydrocarbon reservoir[2-4]. Here, we present geochemical and seismic data of CH_4 emissions from abandoned wells in the Central North Sea (CNS) showing that boreholes constitute unrecognized, but important conduits for the release of biogenic CH_4 originating from shallow gas accumulations (<1,000 m sediment depth) in the overburden of deep reservoirs. Seismic identification of numerous wells poking through shallow gas pockets in the study area of the CNS further indicates that about one third of the wells may emit CH_4. Extrapolating our findings (i.e. the likelihood for leakage and the measured emission rates) to the North Sea scale, we hypothesize that the large number of drilled wells could release a total of 19±10 kt of CH_4 per year into the North Sea. This poses a significant contribution to the North Sea CH_4 budget. A large fraction of this gas (~42%) may reach the atmosphere via direct bubble transport (~2 kt yr^{-1}) and via diffusive exchange of CH_4 dissolving in the surface mixed layer (~6 kt yr^{-1}), as indicated by numerical modeling. These unexpected findings clearly advance our understanding of greenhouse gas emissions from petroleum infrastructure that impact regional CH_4 budgets in hydrocarbon provinces around the world, and indicate that conventional monitoring of well integrity only may need to be extended.

* Corresponding Author. *E-mail address*: lvielstaedte@geomar.de (L. Vielstädte).

III.1 Letter

There is growing evidence for increased CH_4 emissions in hydrocarbon production areas[5-10]. These are generally attributed to leakage of the produced fossil fuel from the infrastructure and equipment during various operation steps[5]. In addition, the petroleum industry considers the potential failure of well material (e.g. casing steel, cement), leading to uncontrolled gas migration from the reservoir, typically identified by sustained casing pressure[4,11]. Available data on such well integrity issues provides an uncertain estimate of 2-75% of all wells[2] being compromised and potentially at risk for leakage. Here, we report the so far unrecognized migration of biogenic CH_4 along the borehole originating from shallow gas accumulations that are penetrated when drilling into the underlying deep hydrocarbon reservoirs. Drilling disturbs and fractures the sediment around the wellbore mechanically, thereby creating highly permeable pathways for the migration of the gas. Thus, anthropogenic CH_4 emissions consist of one more facet, adding uncontrolled, but potentially significant amounts of CH_4 to regional oceanic and global atmospheric greenhouse gas budgets.

In the North Sea, Pleistocene and Pliocene organic-rich sediments are the most prominent stratigraphic units containing biogenic gas accumulations that are widespread in 300-750 m sediment depth[12-13]. Here, we identify these units as potential source areas for the CH_4 emitted from three leaky, abandoned wells investigated in the Norwegian Sector of the CNS. CH_4 in the seep gas is isotopically light ($\partial^{13}C_{CH4}$ < -70‰ VPDB) and contains only minor amounts of higher hydrocarbons ($C_1/\sum C_{2+}$ > 1,000), clearly pointing towards a biogenic origin (Tab. III.1, Chapter II Fig. II.3). The shallow origin is supported by bright spots (e.g. reverse polarity high amplitude anomalies) and zones of chaotic signatures in the seismic data surrounding the well paths of the three wells (Fig. III.1b).

Table III.1: Summary of data from the leaky abandoned wells. Stable carbon isotope signature ($\partial^{13}C_{CH4}$) and hydrocarbon composition ($C_1/\sum C_{2+}$) of the free gas, CH_4 oxidation rates (r_{MOx}) and peak concentrations of dissolved CH_4 (CH_{4max}) in the bottom water, as well as results of video- analysis of active gas bubble venting, i.e. the peak radius of the bubble size distribution (*peak* r_e), the number of bubble streams per well (seeps), and the per-well leakage rate from the seabed (Q_{SF}).

Well ID	$\delta^{13}C_{CH4}$/ ‰ VPDB	$C_1/\Sigma C_{2+}$ / 1	r_{MOx}/ nM d^{-1}	CH_{4max}/ nM	Peak r_e / mm	No. of Seeps	Q_{SF}[c] / t yr^{-1} $well^{-1}$ of CH_4
15/9-13	-75.9	11,131	b.d.[a]	1,014[a]	2.4	2	1
16/4-2	-71.2	7,254	n.d.	n.d.	2.7	8	4
16/7-2	-73.1	2,320	0.19-1.4[b]	10,579-17,294[b]	5.7*	39	19

* At well 16/7-2 bubbles with significantly larger radii were expelled into the water-column, where gas accumulated below a carbonate rock, compared to direct release from the sandy sediments.
[a] Data from CE12010 1-ROV1 and 31-CTD7
[b] Data from CE12010 20-ROV6
[c] based on an average gas flow of 1.4 l min^{-1} $seep^{-1}$at STP (25°C, 1 bar)
b.d.= below detection limit; n.d.= not determined

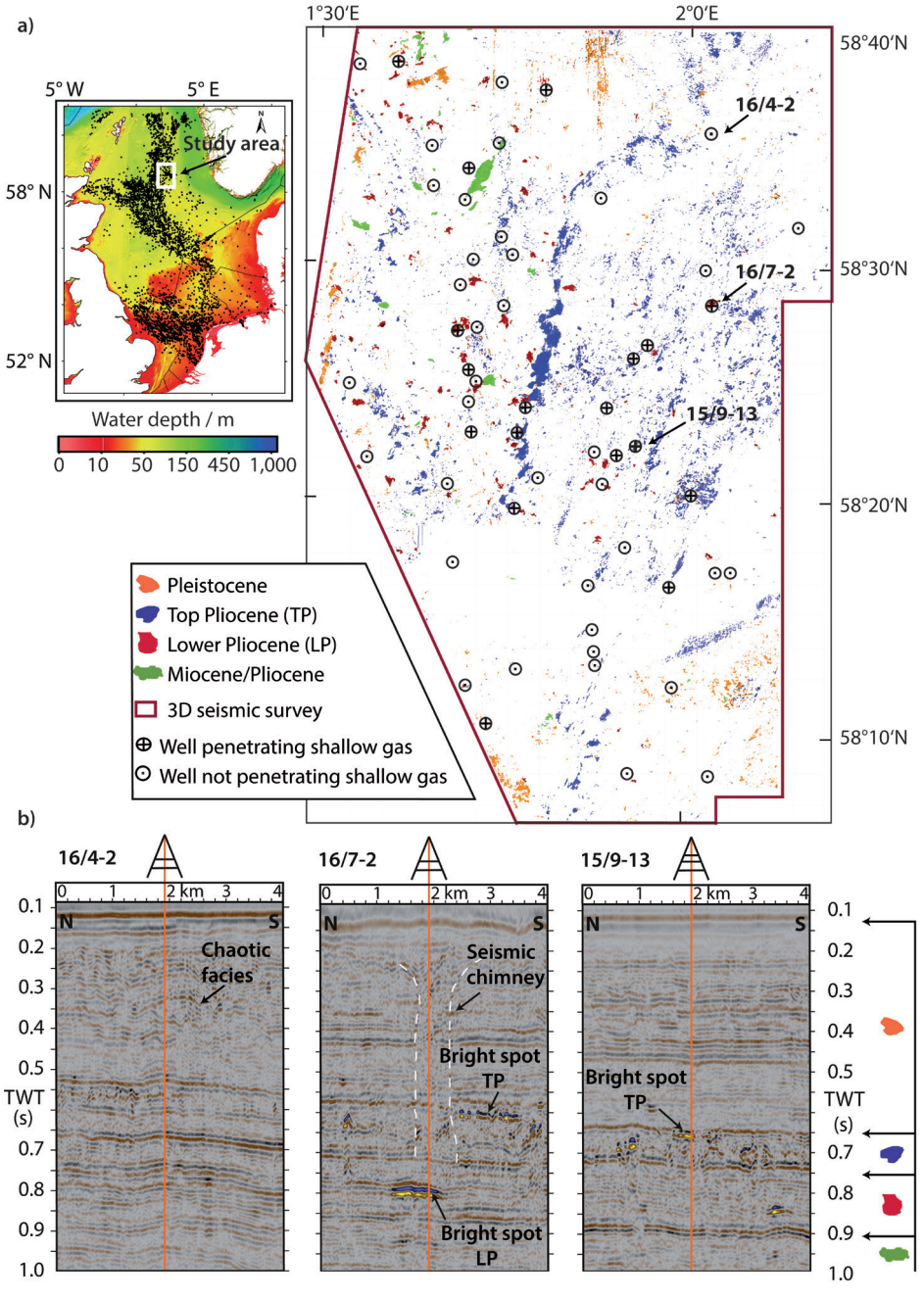

Figure III.1: Distribution of wells and shallow gas in the North Sea. a) Areal distribution of shallow gas pockets that have been mapped by high amplitude anomalies in industrial 3-D seismic data (ST98M3, Statoil ASA) and the seafloor location of wells in the Norwegian CNS. The seismic correlation of 55 well paths revealed that one third of the wells were drilled through shallow gas accumulations in Miocene/Pliocene (green), Lower Pliocene (red), Top Pliocene (blue), and Pleistocene (orange) stratigraphic units. Upper left corner: Bathymetric map of the North Sea showing the location of the study area (white rectangle) and the distribution of wells (black dots). **b**) Seismic profiles indicating shallow gas pockets in the subsurface around the well paths of three investigated leaky abandoned wells (orange line). At well 16/7-2 chaotic reflections indicate the presence of a seismic chimney (dashed white lines).

We further hypothesize that leakage from existing wells in the North Sea is likely to constitute an important part of the respective regional CH_4 budget due to the large number of wells (i.e. ~11,122, discounting extra sidetracked wellbores) and ubiquitous gas accumulations in the shallow subsurface[12,14-15] (Fig. III.1, Supp. Tab. III.3). In the following, we will thus, assess CH_4 leakage from wells into the North Sea and estimate the resulting emission into the atmosphere. Tracking the subsurface well paths of 55 wells in an area of ~2,000 km^2 in the Norwegian Sector of the CNS, where shallow gas accumulations have been identified by bright spots in industrial 3-D seismic data, we examine the likelihood of wells to leak shallow gas: 18 out of 55 wells in this area (about 33%) were drilled through shallow gas accumulations and are thus prone to leak CH_4 (Fig. III.1). Individual leakage rates of three wells (15/9-13, 16/4-2, and 16/7-2) in this area were highly variable (1, 4, and 19 t yr^{-1} of CH_4, respectively)[16]. The highest release rate was measured at well 16/7-2, which was drilled through a seismic chimney (Fig. III.1b), typically believed to be more permeable than the surrounding sediment. Further uncertainty in our quantification is related to the unknown temporal variability of the ebullition. To address these uncertainties in the North Sea wide CH_4 release assignment we distinguish between a conservative (2.5±1.5 t yr^{-1} $well^{-1}$) and a maximum (8±7.9 t yr^{-1} $well^{-1}$) leakage rate taking either, the average of wells 15/9-13 and 16/4-2 only, or also including the high emissions of well 16/7-2, respectively.

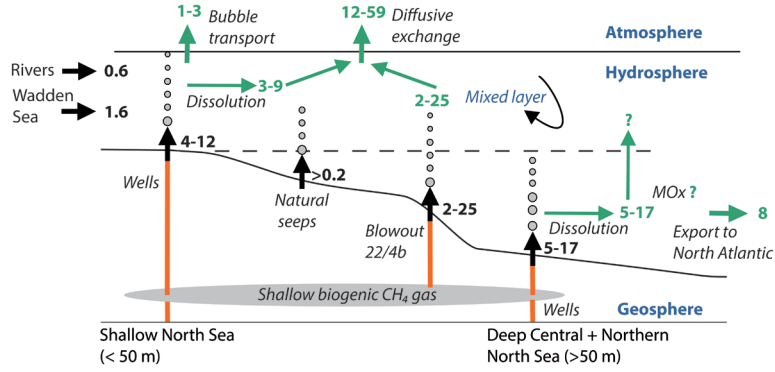

Figure III.2: Sketch of the CH_4 budget of the North Sea. CH_4 sources (black arrows) and sinks (green arrows) are expressed in kt of CH_4 per year. Atmospheric CH_4 emissions comprise direct emissions from leaky wells via bubble transport, predominantly in the shallower coastal and southern regions and the diffusive outgassing of CH_4 from the surface mixed layer. Leaky hydrocarbon wells (orange line) may constitute up to 60% of the total diffusive emissions, comprising the release of shallow buried gas (grey ellipse) investigated in this study and from the single blowout well 22/4b[21]. Note, the imbalance of the North Sea CH_4 budget suggests that an additional input of CH_4 (~10 kt yr^{-1}) is required, either by natural or anthropogenic sources. Details on the numbers and recalculation of the budget are provided in Supplementary Section III.2.2.5.

Using publicly available wellbore data and extrapolating our results to the North Sea scale, we, thus, estimate that leaky wells may release around 19±10 kt of CH_4 from the North Sea seafloor per year, assuming that only 33% of the 11,122 wells in the North Sea leak. In comparison to other major sources for CH_4 in the North Sea, i.e. rivers[17-20] (0.5 kt yr^{-1}), the Wadden Sea area[17] (1.6±0.5 kt yr^{-1}), and known natural seep sites[21-24] (0.2 kt yr^{-1}), leaky wells may constitute a significant input to the CH_4 budget of the North Sea (Fig. III.2 and Supp. Tab. III.4). It should, however, be noted that also numerous additional natural gas seeps have been observed at the seabed of the North Sea[21]. Their abundance and contribution to the CH_4 budget are poorly constrained, indicating that their emissions may have been underestimated[12]. Despite the poor characterization of the North Sea CH_4 sources, the patchiness and high spatial variability of CH_4 super-saturations with respect to atmospheric partial pressure in the surface mixed layer (SML) of the open North Sea, i.e. 103-50,000%[17,20,25], indicate that ubiquitous point sources at the seabed (wells and natural seeps) dominate the regional CH_4 budget. This high super-saturation of the North Sea surface waters constitutes the major sink in the CH_4 budget, a diffusive CH_4 loss to the atmosphere of 12-59 kt yr^{-1} (Fig. III.2).

To examine the extent to which emissions from leaky wells may contribute to this sink, we apply a numerical bubble dissolution model to the North Sea scale. Each of the three key fates of leaking CH_4 is considered: 1) dissolution in the deep stratified layer (>50 m water depth)[26], 2) dissolution in the surface mixed layer (SML, <50 m water depth)[26] contributing to the outgassing to the atmosphere, and 3) direct gas bubble transport into the atmosphere. Leakage depths and initial bubble sizes play a critical role in transporting CH_4 from the seafloor to the atmosphere, thus defining the magnitudes of diffusive exchange and direct ebullition into the atmosphere. Mean initial bubble sizes measured at the leaky wells (r_e=2.6 mm, for details see Chapter II Fig. II.4) were comparable to those observed at natural seeps in the North Sea (i.e. r_e=2.2 mm at Tommeliten[22] and r_e=2.5 mm at the Scanner Pockmark field[21]). This comparability, together with the North Sea wide dominance of fine to medium grained clayey sand[15], suggest that initial bubble sizes are similar across the North Sea, because their formation is believed to be controlled by the mechanical properties of the surface sediments[27].

Hence, applying the average bubble size spectrum of the investigated wells and extrapolating numerical results to the North Sea scale, we estimate that leaky wells could emit a total of 4-12 kt yr^{-1} of CH_4 into the atmosphere (Figs. III.2, III.3). This is a significant proportion (20-30%) of the total CH_4 flux from the North Sea into the atmosphere (13-62 kt yr^{-1}, for details see Supp. Tab. III.4). Leakage from the wells into the atmosphere is dominated by diffusive outgassing of CH_4 dissolved in the SML (i.e. 6±3 kt yr^{-1}), rather than by direct bubble transport (i.e. 2±1 kt yr^{-1}), because of the principally large water depths at which the

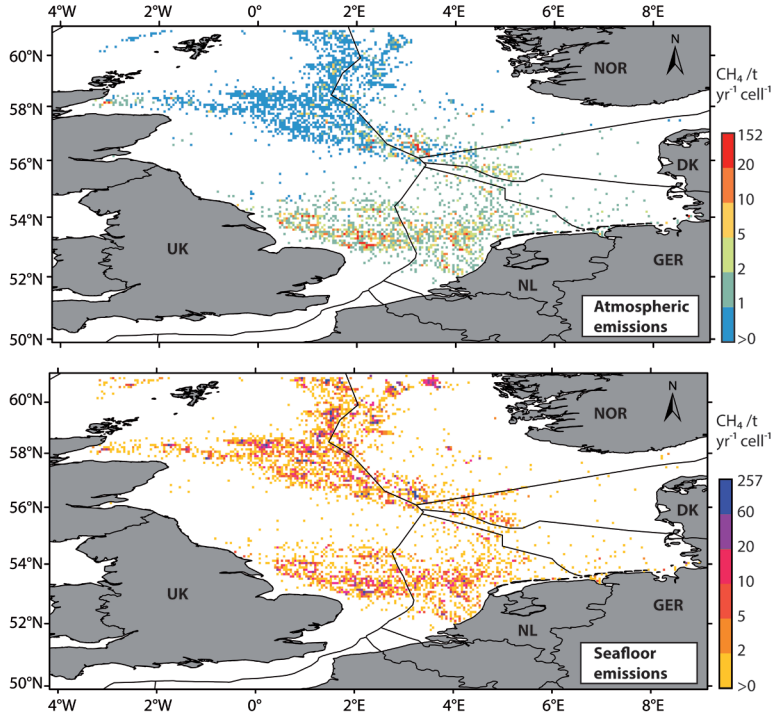

Figure III.3: CH_4 emissions from leaky wells into the North Sea and into the atmosphere. CH_4 emissions were calculated for 5x5 km^2 cells and assuming that 33 % of the 11,122 wells leak CH_4 at a rate of 5.3 (±2.8) t yr^{-1} $well^{-1}$. Emission rates are expressed in tonnes of CH_4 per year per cell. A total annual seabed release of 19±10 kt of CH_4 is estimated for the North Sea (bottom), of which ~8±4 kt may reach the atmosphere (top). Highest CH_4 emissions into the atmosphere occur in the Southern North Sea, where the water depths are shallower (mean water depth <40 m). The map's geographic coordinate system refers to WGS84 and is displayed in Cylindrical Equal Area Projection.

bubbles are released (Fig. III.1, Supp. Fig. III.4). The microbial sink for CH_4 in the water column is expected to be negligible because CH_4 oxidation rates at the investigated leaky wells were very low (<1.4 nM day^{-1}, Tab. III.1) compared to the fast ventilation of CH_4 in the SML (i.e. days to weeks)[25] and the turnover time of North Sea water masses (0.75 years)[26]. Overall, this suggests that essentially all of the CH_4 reaching the SML will be transferred into the atmosphere. A larger proportion of the CH_4 will, however, dissolve in the deep water of the North Sea, below the SML, i.e. 11±6 kt yr^{-1}. While some unknown fraction of this deeply dissolved CH_4 may be mixed into the SML during frequent fall and winter storms and seasonal or inter-annual deepening and breakdown of the thermocline[20,22,26], the deep water CH_4 input is expected to contribute to the export of CH_4 into the North Atlantic Ocean (8 kt yr^{-1})[20]. Thus, drilling-induced CH_4 emissions from shallow biogenic gas accumulations may constitute a significant source for CH_4 in the regional budget of the North Sea, particularly contributing to the observed high diffusive outgassing into the

atmosphere (Fig. III.2). Adding the other anthropogenic CH_4 sources, the blowout well 22/4b in the British Sector[20] and wells with reported integrity issues[2], emissions from oil and gas infrastructure likely determine the North Sea CH_4 budget.

Our extrapolation from the investigated CNS area to the North Sea scale is further corroborated by the spatial correlation of boreholes (Fig. III.1) with areas of frequent shallow gas accumulations and reported hydroacoustic gas flares[12,21]. In addition, it should be noted that the leakage at well 16/4-2 could not be traced seismically to the presence of free gas, thus clearly drawing gas from larger lateral distances. Surveying for leaky wells and quantifying their ebullition rates is clearly needed to better constrain the North Sea CH_4 budget.

The findings presented here show – in line with other recent studies[5-10] – that the conventional focus on well integrity is insufficient. Regulatory frameworks need to be adapted and, hopefully, this study is able to provide some incentives for improved operation and monitoring of oil and gas infrastructure. In the North Sea – as in other hydrocarbon-prolific areas of the world – shallow gas pockets are very frequently observed in the sedimentary overburden above the deep hydrocarbon reservoirs. CH_4 released via this pathway is likely affecting the CH_4 budgets of hydrocarbon provinces in general and contributing significantly to greenhouse gas emissions into the atmosphere. Nevertheless, it should be noted that while it is relatively easy to detect and quantify CH_4 emission rates as low as the reported ones in the marine realm, this may pose a considerable challenge to monitoring technologies presently available for onshore environments, and fixing such leaks may prove difficult.

III.2 Methods summary

Data analysis in the Central North Sea (CNS). On research cruises with RV Celtic Explorer (CE12010, July-August 2012) and RV Alkor (AL412, March 2013) three leaky abandoned wells (15/9-13, 16/4-2, and 16/7-2) located in water depth of 81-93 m were investigated in the CNS by characterizing the origin of the emanating gases, leakage rates, CH_4 oxidation rates in the water column, and initial gas bubble size distributions. Details and additional data are provided in the Supplementary Material (Appendix C S.III.2.1).

Extrapolation of CH_4 leakage to the North Sea scale. CH_4 leakage from wells into the North Sea and the atmosphere, was calculated by applying results of a numerical bubble dissolution model to the EMODnet North Sea bathymetry (available at http://www.emodnet-bathymetry.eu) and combining publicly available data on drilled wells (see Supp. Tab. III.2 for details) using the geographical information system software ArcGIS 10.1. In total, 11,122 active and inactive wells were selected for the CH_4 flux quantification excluding sidetracks of wells (see Supp. Tab. III.3). The North Sea was subdivided into equal area polygons of 25 km^2 using a Cylindric Equal Area projection and the seabed CH_4 flow (Q_{SF}) was calculated for each of these polygons multiplying the leakage probability of 33% for the wells, the number

of wells located inside each polygon, and the per-well CH_4 leakage rate of 2.5 and 8 t yr^{-1} for the conservative and maximum estimate, respectively. For each polygon, the resulting CH_4 flow from the surface water into the atmosphere was then estimated applying a transfer function describing the methane bubble transport efficiency to the sea surface and to the SML of the North Sea as a function of the seabed CH_4 flow and water depth (Supp. Section S.III.2.2.2). All determined flow estimates were added to calculate lower and upper bounds of the total CH_4 ebullition from the seafloor and into the atmosphere. Full methodology is provided in the Supplementary Material (Chapter VI Appendix C).

Acknowledgements

We thank the Captains and crews of RV Celtic Explorer and RV Alkor as well as the teams of ROV Kiel 6000 and ROV Phoca for their invaluable support during the cruises CE12010 and AL412. We thank Andrea Bodenbinder and Meike Dibbern at GEOMAR for conducting geochemical analyses and Monika Segl at MARUM/University Bremen for DIC isotope measurements. We thank Statoil ASA for permission to use the 3-D seismic data and the Norwegian Petroleum Directorate for providing the well path data. Special thanks to Martin Hovland for making us aware of the gas seepage at the three wells. Figures were created with ArcGIS, Petrel, Mathematica, and Adobe Illustrator. The cruises and scientific work received funding through the European Community's 7th Framework Program (FP7/2007-2013) in the EUROFLEETS program, the ECO2 project (grant agreement no. 265847) and the DFG funded Cluster of Excellence "Future Ocean".

References:

1. Ciais, P., et al. *Climate Change 2013: The Physical Science Basis. Contribution of Working Group I to the Fifth Assessment Report of the Intergovernmental Panel on Climate Change*, in: Stocker, T.F., Qin, D., Plattner, G.-K., Tignor, M., Allen, S.K., Boschung, J., Nauels, A., Xia, Y., Bex, V., Midgley, P.M. (Eds.). IPCC, Cambridge, UK, pp. 465-570 (2013).

2. Davies, R.J., et al. Oil and gas wells and their integrity: Implications for shale and unconventional resource exploitation. *Mar. Petrol. Geol.* **56**, 239-154 (2014).

3. NORSOK Standard D-010, 2004. http://www.standard.no/PageFiles/1315/D-010r3.pdf

4. Gurevich A.E., Endres, B.L., Robertson, J.O., Chilingar, G.V. Gas migration from oil and gas fields and associated hazards. *J. Petrol. Sci. Eng.* **9**, 223-238 (1993).

5. Allen, D.T., et al. Measurements of methane emissions at natural gas production sites in the United States. *Proc. Natl. Acad. Sci. U.S.A.* **110**, 17768-17773 (2013).

6. Alvarez, R.A., Pacala, S.W., Winebrake, J.J., Chameides, W.L., Hamburg, S.P. Greater focus needed on methane leakage from natural gas infrastructure. *Proc. Natl. Acad. Sci. U.S.A.* **109**, 6435-6440

(2012).

7. Caulton, D.R., et al. Toward a better understanding and quantification of methane emissions from shale gas development. *Proc. Natl. Acad. Sci. U.S.A.* **111**, 6237-6242 (2014).

8. Miller, S.M., et al. Anthropogenic emissions of methane in the United States. *Proc. Natl. Acad. Sci. U.S.A.* **110**, 20018-20022 (2013).

9. Schneising, O., et al. Remote sensing of fugitive methane emissions from oil and gas production in North American tight geologic formations. *Earth's Future* **2**, 548-558 (2014).

10. Zhang, Y., Zhao, H., Zhai, W., Zang, K., Wang, J. Enhanced methane emissions from oil and gas exploration areas to the atmosphere – The central Bohai Sea. Mar. Pollut. Bull. 81, 157-165 (2014).

11. Brufatto, C., et al. From mud to cement - Building gas wells. *Oilfield Rev.* **15**, 62-76 (2003).

12.Judd, A., et al. Contributions to atmospheric methane by natural seepage on the U.K. continental shelf. *Mar. Geol.* **140**, 427-455 (1997).

13. Karstens, J., Berndt, C. Seismic chimneys in the Southern Viking Graben- Implications for paleo fluid migration and overpressure evolution. *Earth Planet. Sci. Lett.* **412**, 88-100 (2015).

14. Schroot, B.M., Klaver, G.T., Schüttenhelm, R.T.E. Surface and subsurface expressions of gas seepage to the seabed- examples from the Southern North Sea. *Mar. Petrol. Geol.* **22**, 499-515 (2005).

15. Schlüter, M., Jerosch, K. Digital Atlas of the North Sea, version 0.9. Alfred Wegener Institute for Polar and Marine Research et al. hdl:10012/epic.34893.d001 (2009).

16. Vielstädte, L., et al. Quantification of methane emissions at abandoned gas wells in the Central North Sea. *Mar. Petrol. Geol.* (2015).

17. Upstill-Goddard, R.C., Barnes, J., Frost, T., Punshon, S., Owens, N.J.P. Methane in the southern North Sea: Low-salinity inputs, estuarine removal, and atmospheric flux. *Glob. Biogeochem. Cycles* **14** (4), 1205-1217 (2000).

18. Grunwald, M., et al. Methane in the southern North Sea, spatial distribution and budgets. *Est. Coast. Shelf Sci.* **81**, 445-456 (2009).

19. Scranton, M.I., McShane, K. Methane fluxes in the southern North-Sea – the role of European rivers. *Cont. Shelf Res.* **11**, 37–52 (1991).

20. Rehder, G., Keir, R.S., Suess, E., Pohlmann, T. The multiple sources and patterns of methane in North Sea waters. *Aquat. Geochem.* **4**, 403-427 (1998).

21. Judd, A.G., Hovland, M.. *Seabed Fluid Flow- The Impact on Geology, Biology and Marine Environment* (Cambridge University Press, New York, 475 pp, 2007).

22. Schneider von Deimling, J., et al. Quantification of seep-related methane gas emissions at

Tommeliten, North Sea. *Cont. Shelf Res.* **31**, 867-878 (2011).

23. Judd, A.G. Natural seabed gas seeps as sources of atmospheric methane. *Environ. Geol. 46*, 988-996 (2004).

24. Hovland, M., Jensen, S., Fichler, C. Methane and minor oil macro-seep systems – Their complexity and environmental significance. *Mar. Geol.* **332-334**, 163-173 (2012).

25. Bange, H.W., Bartell, U.H., Rapsomanikis, S., Andreae, M.O. Methane in the Baltic and North Seas and a reassessment of the marine emissions of methane. *Glob. Biogeochem. Cycles* **8**, 465–480 (1994).

26. Thomas, H., et al. The carbon budget of the North Sea. Biogeosciences 2, 87-96 (2005).

27. Dewar, M., Wei, W., Chen, B. Small-scale modelling of the physicochemical impacts of CO_2 leaked from sub-seabed reservoirs or pipelines within the North Sea and surrounding waters. *Mar. Pollut. Bull.* **73**, 504-515 (2013).

Footprint and detectability of a well leaking CO_2 into the North Sea:
Implications from a field experiment and numerical modelling

Lisa Vielstädte [a,*], Peter Linke [a], Mark Schmidt [a], Stefan Sommer [a], Benjamin Tews [b], Matthias Haeckel [a], Klaus Wallmann [a]

[a] *GEOMAR Helmholtz Centre for Ocean Reserach, Kiel, Germany*

[b] *Department of Applied Mathematics, University of Kiel, Germany*

In preparation for the *International Journal of Greenhouse Gas Control*

Abstract

Existing wells pose a risk for the fugitive loss of carbon dioxide (CO_2) from Carbon Capture and Storage (CCS) sites, which might compromise the suitability of CCS as climate change mitigation option. Despite a commonly-held belief that leakage is restricted to wells with integrity issues, leakage may also occur along the outside of wells, where drilling has disturbed and fractured the sediment around the wellbore mechanically. The latter may raise questions about the propensity of wells to leak and the performance of CO_2 storage projects that are operating in areas with a high density of boreholes. Here, we focus on the Sleipner CO_2 storage site showing results of a controlled CO_2 release experiment and experimentally constrained numerical simulations that evaluate the detectability and environmental consequences of a well leaking CO_2 into the Central North Sea (CNS) along the wellpath. Our results demonstrate that the detectability and impact of leakage at low rates (<55 t yr^{-1} of CO_2) would be limited to bottom waters and a small area around the leak, due to rapid CO_2 bubble dissolution in seawater (i.e. within the lower 3 m of the water column) and quick dispersion of the dissolved CO_2 plume by tidal currents (i.e. within less than 120 m around the leak). Although the consequences of a single well leaking CO_2 are found to be insignificant in terms of storage performance, from a viewpoint of environmental impact and climate control, prolonged leakage along numerous wells might compromise the long-term perspective of CCS projects in hydrocarbon provinces around the world. It also indicates that monitoring of well integrity may not be sufficient.

* Corresponding Author. *E-mail address*: lvielstaedte@geomar.de (L. Vielstädte).

IV.1 Introduction

Geological storage of carbon dioxide aims at reducing the amount of anthropogenic CO_2 added annually to the atmospheric carbon budget in order to mitigate global climate warming (e.g. Metz et al., 2005). In Europe, the largest potential to store CO_2 is offshore (~240 Gt of CO_2) mostly in deep saline aquifers and marginally in depleted hydrocarbon reservoirs (e.g. EU GeoCapacity, 2009). More than 80% of the total offshore storage capacity is located in Norwegian waters (EU GeoCapacity, 2009) where Statoil operates the world's first large-scale CO_2 storage project "Sleipner" with an annual injection rate of ~1 Mt of CO_2 since 1996 (Fig. IV.1). Here, CO_2 is injected from natural gas production into a saline aquifer in ~900 m sediment depth, overlying the natural gas reservoir where it is extracted from. As such, Sleipner and many other large-scale CCS projects are located in regions that have already been exploited for hydrocarbon production, which has several benefits as compared to undeveloped sites: 1) they tend to be geologically well-understood with existing wellbore and seismic data helping to characterize the local geology and overburden, and 2) may already have infrastructure in place (Jordan et al., 2015). One downside of storing CO_2 in developed sites is the presence of pre-existing wells (Gasda et al., 2004; Nordbotten et al., 2005) which have been identified for posing a greater risk for gas leakage from CO_2 storage formations than natural geological features, such as faults or fractures (Bachu and Watson, 2009). However, so far, there is no evidence of systematic changes at the seafloor (e.g. pockmarks, gas bubbles) (Eiken et al., 2011) or in the overburden (Chadwick et al., 2009) indicating that CO_2 is safely contained within the storage reservoir at Sleipner.

Concern about CO_2 leakage along pre-existing or "old" wells is widely attributed to well barrier failures (Gasda et al., 2004; Nordbotten et al., 2005; OSPAR Convention, 2007; EU CCS Directive, 2011), where CO_2 may escape from the storage reservoir either due to pre-existing failures in the well material or due to subsequent corrosion of the cement and steel casings that are exposed to the subsurface CO_2 plume (Kutchko et al., 2007; Carey et al., 2010; Carey et al., 2007; Crow et al., 2010), but were originally not designed to withstand CO_2 (Bachu and Watson, 2009). Estimates on CO_2 gas flows associated to this kind of leakage are low: 0.1 kg yr^{-1} for leakage along a well with degraded cement (Jordan et al., 2015), less than 0.1 t yr^{-1} for leakage along a well with sustained casing pressure (Tao and Bryant, 2014), and 0.3-3 t yr^{-1} for poorly cemented wells (Jordan et al., 2015) with a typical wellbore cement permeability below 1 Darcy (Crow et al., 2010). Higher leakage rates, on the order of 3-55 t yr^{-1} of CO_2 (Vielstädte et al., 2015), may arise from gas losses along the outside of wells, where drilling has disturbed and fractured the sediment around the wellbore mechanically thereby creating highly efficient pathways for the upward migration of gas (Gurevich et al., 1993). This kind of leakage has recently been observed at abandoned gas wells in the CNS, where biogenic methane, originating from a shallow (<1,000 mbsf)

gas source in the sedimentary overburden above the deep hydrocarbon reservoirs, leaks into seawater (Vielstädte et al., 2015). Shallow gas leakage is presently not targeted by regulatory frameworks, but may have important implications for CCS projects located in developed hydrocarbon provinces and storing CO_2 in geological formations above deeper hydrocarbon reservoirs. It means that leakage can potentially occur along any type of well (production, exploration, or abandoned), as long as it penetrates the subsurface CO_2 plume.

Here, we focus on the Sleipner CO_2 storage site and investigate hypothetic, but probably realistic leakage of CO_2 along a well that penetrates the subsurface CO_2 plume and leaks into the ~80 m deep water column, using a combination of experimental field data and numerical modelling. The main objectives of this study are to predict the spatial footprint, detectability, and environmental consequences of a well leaking CO_2 at low rates and under real tidal forcing by analyzing an existing bubble dissolution model and a newly developed plume dispersion model against the data collected from an *in situ* CO_2 leakage experiment. Results presented in this study are directly applicable to most global offshore CO_2 storage sites, which are planned for hydrocarbon provinces, where ubiquitous hydrocarbon infrastructure pose the risk for the upward migration of gas. This study further fills a gap in previous CCS hydrodynamic modelling research, which mostly operated at large scales and high rates addressing the release of CO_2 during a highly unlikely blowout scenario (Phelps et al., 2014; Dewar et al., 2013; Hvidevold et al., 2015; Greenwood et al., 2015; Dissanayake et al., 2012) or have investigated leakage at low rates into shallow coastal waters (Dewar et al., 2015), with hydrodynamic properties that are not representative for submarine CCS projects that are operating or are under construction in the open North Sea.

IV.2 Methodology

This section is organized as follows. It begins with a description of the *in situ* CO_2 release experiment conducted in the Sleipner area, including details on the experimental setup (IV.2.1), measurements of the gas discharge in the water column (IV.2.1.1), initial bubble sizes (IV.2.1.2), and local hydrodynamics (IV.2.1.3). Numerical models computing CO_2 bubble dissolution (IV.2.2.1), solute plume dispersion (IV.2.2.2), and carbonate system parameters (IV.2.2.3) are described next. The experimental data are then applied to test the validity of numerical methods and parameters used (IV.2.2.4.1). In the last part (IV.2.2.4.2), the calibrated models are applied to compute three leaky well scenarios covering the range of possible emission rates.

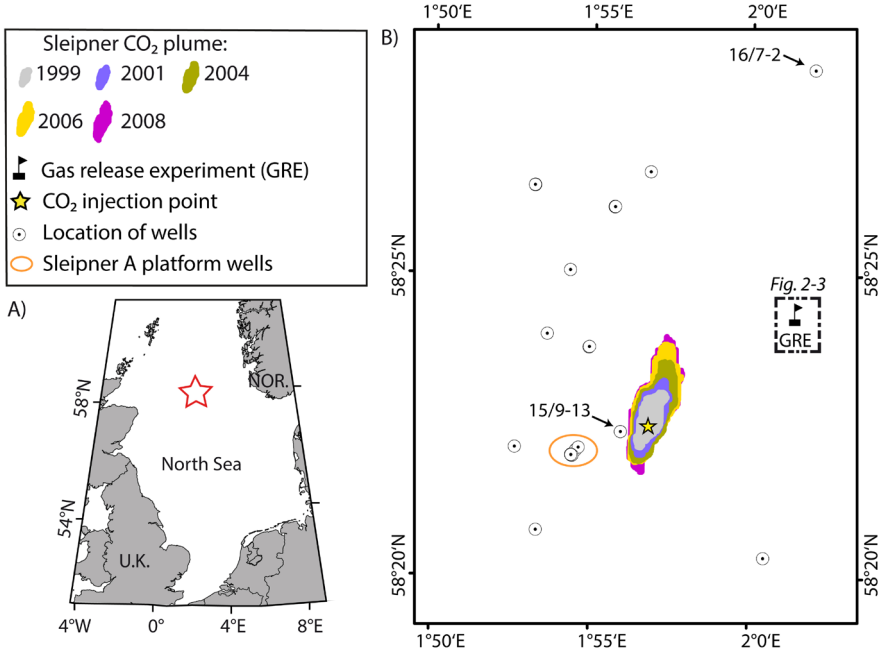

Figure IV.1: A) Overview map showing the location of the study area (red star) in the CNS. **B**) Map of the study area showing the Sleipner CO_2 injection point (yellow star), the predominantly north-eastward growing of the CO_2 plume within the ~900 m deep Utsira sand formation (colored contours), the location of the gas release experiment (black flag), and the location of wells (circles) in that area. Platform wells (orange circle) from which the CO_2 is injected and those which have been identified to leak shallow gas (wells 15/9-13 and 16/7-2, Vielstädte et al., 2015) are highlighted.

IV.2.1 The Gas Release Experiment

During the Celtic Explorer expedition CE12010 (July-August 2012), a controlled gas release experiment (GRE) was conducted in 84 m water depth to replicate small-scale, but realistic, leakage of CO_2 into the North Sea water column in the vicinity of the Sleipner CO_2 storage site (Fig. IV.1b). Three pressure bottles of CO_2 (50 L, 57 bar), one smaller bottle of Krypton (10 L, 250 bar) which was used as a tracer gas, two battery packs, a gas control unit, and release head, were mounted to the Lander system ("Ocean Elevator", Linke et al., 2015) and deployed video-guided at the seafloor (58°24'22.41"N, 2°1'25.54"E) (Fig. IV.2). The control unit included a spiral coil and a heated pressure regulator to reduce the pressure of the outflowing gas from up to 250 bar inside the gas bottle to 11 bar before the gas entered the microcontroller, which regulated the gas flow (Fig. IV.2c). Bubbles were generated on top of the Ocean Elevator by seven 1/8" stainless steel tubes connected by valves and covered by plastic heads which were pierced by three 8 mm holes each (Fig. IV.2b). At a preset gas flow of 30 L min^{-1} at STP (25°C, 1bar), a total of 40 kg of CO_2 was released into the water column over a period of 11.5 hours. This corresponds to an annual leakage rate of 31 t yr^{-1} of CO_2, which is assumed to be in the upper range of possible gas emissions associated to leakage along the outside of a well (Vielstädte et al. 2015).

IV.2.1.1 Monitoring the gas discharge in the water column

The gas discharge was observed *in situ* during a 4 hour dive with the remotely operated vehicle (ROV "Kiel 6000"), equipped with HD camera/video device and a sonar system. The sonar system was used to navigate the ROV downstream of the artificial CO_2 leak by tracking the less soluble and ~27 m high Krypton gas flare.

The spread of the dissolved CO_2 plume was monitored geochemically using the commercial HydroC pCO_2 sensor (S/N 0412-006, CONTROS Systems and Solutions) mounted to the front porch of the ROV. The sensor was calibrated for pCO_2 signals up to 3,000 µatm (accuracy ~1% of reading resolution; resolution: <30 µatm as described by Fietzek et al., 2014) and was programmed to measure in 60 s intervals, which is equal to the sensor's response time (t_{63} ~1 minute; Fiedler et al., 2013). For a better navigation of the ROV in the plume, HydroC sensor data were, in addition to internal data recording, transferred as an analog voltage signal which enabled online reading of the pCO_2 signal during ROV operation. ROV-operated pCO_2 surveying was performed in different vertical heights and distances downstream of the artificial leak (Fig. IV.3c), remaining at each measuring position for at least 10 minutes to ensure a true pCO_2 signal.

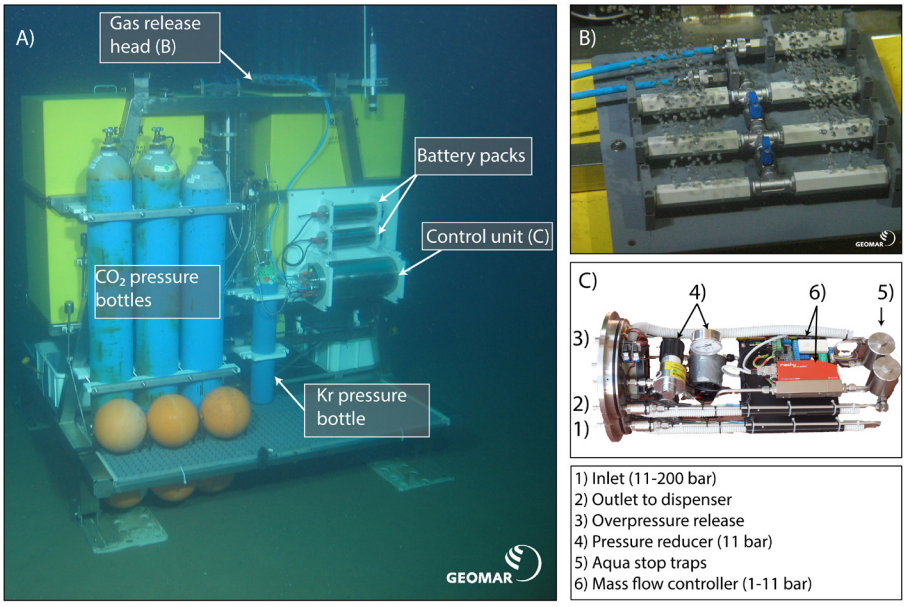

Figure IV.2: A) Picture showing the setup of the gas release experiment (GRE), i.e. the Ocean Elevator (with yellow syntactic foam blocks) and mounted equipment, deployed in ~80 m water depth in the vicinity of the Sleipner CO_2 storage site. **B**) Single CO_2 bubble streams were released from the gas release head on top of the Ocean Elevator (in addition Krypton (Kr), used as a tracer gas, was released from the single tube in the back). **C**) Picture showing the construction of the gas control unit, regulating the pressure and gas flow during the experiment.

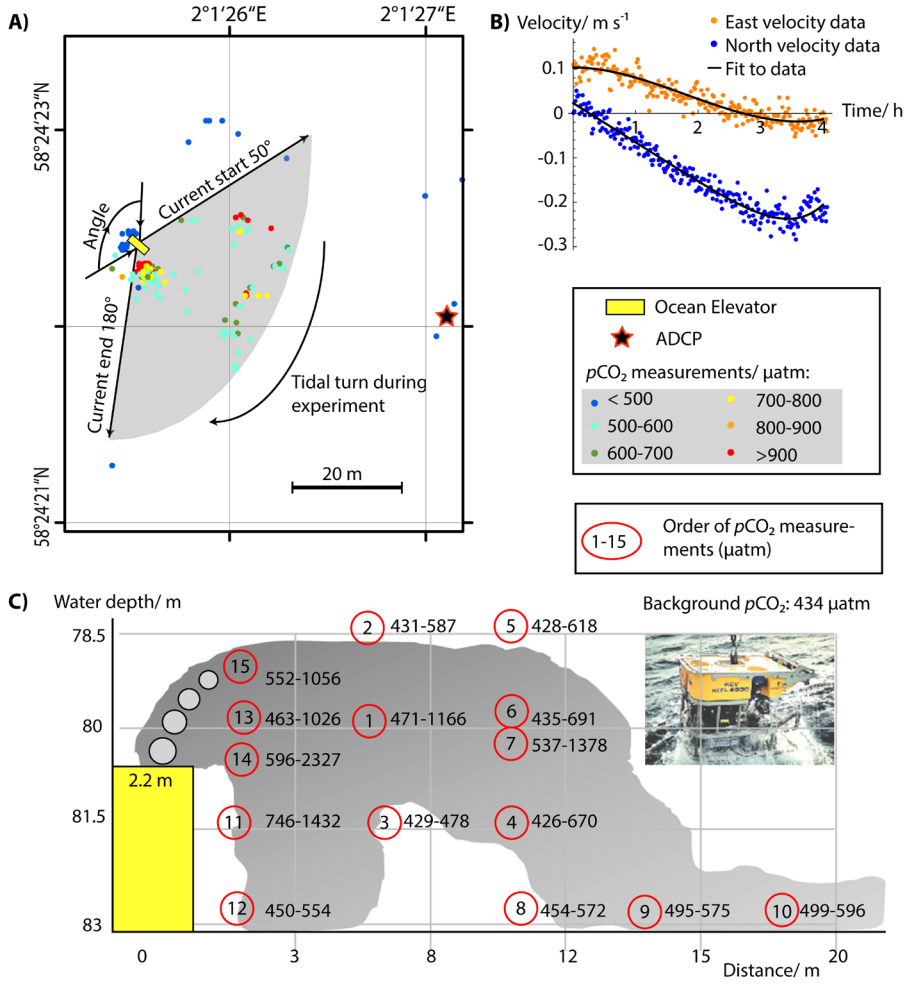

Figure IV.3: **A**) Distribution map of pCO_2 measurements (colored circles) during the 4h ROV observation of the GRE showing the different current flow angles towards the Ocean Elevator (yellow box) when the tide turned and the location of the ADCP (black star) 28 m to the east of the GRE. Background pCO_2 values (blue dots) were measured upstream of the tidal current and before the ROV survey started (background values measured during the ROV survey when the ROV was not downstream of the CO_2 plume have been excluded from the plot). **B**) ADCP measurements of current velocities in eastern (orange dots) and northern (blue dots) directions about 3.2 m above the seafloor (Bin1) and during the 4h ROV observation of the GRE. **C**) Scheme illustrating the order (red circles) and magnitude (black values) of pCO_2 measurements, the quick dispersion, and downwelling of the CO_2 plume as measured downstream of the Ocean Elevator.

IV.2.1.2 Measuring the initial bubble size distribution

The initial bubble size distribution (Ψ), produced during the experiment, was determined from ROV HD images applying the image editing software ImageJ (Farreira and Rasband, 2012). For calibration of bubble sizes, the length of the gas releaser tube (10 cm) was used as scale. Ellipses were manually overlaid to individual bubbles leaving the top of the Ocean Elevator and were marked as overlays. If bubbles had a very irregular shape, they were outlined

manually before using the ellipse fitting object of ImageJ. The corresponding bubble volume, $V_0 = 4/3 \cdot \pi \cdot r_{eq}^2$, was calculated from the equivalent spherical radius, $r_{eq} = (a^2 \cdot b)^{1/3}$ based on the major, a, and the minor half axes, b, of the fitted ellipse. All determined bubble volumes were summarized to calculate the total gas volume (V_ψ) and the volumetric contribution of each bubble size class (i.e. V_0/V_ψ),both required to calculate the CO_2 bubble dissolution rate into seawater during the experiment (Section IV.2.2.1). The accuracy of bubble size measurements was better than 0.2 mm as determined from the HD image resolution of 55.1 pixels cm^{-1} and a measurement precision of 1 pixel.

IV.2.1.3 Measuring local hydrodynamics

Current velocities and directions were recorded during two deployments (OCE1 and OCE2) using an Acoustic Doppler Current Profiler (ADCP) operating at 300 kHz (Tab. IV.1). The vertical resolution of the ADCP was set to 1 m with the first Bin starting 3.2 m above the seafloor (masf). OCE1 was a long-term deployment measuring currents over a few tidal cycles (i.e. 5 days), whereas OCE2 was a short-term deployment recording currents 28 m to the east of the Ocean Elevator during the time of the gas release experiment (Fig. IV.3a,b). Least-squares data fits to ADCP velocity data were used as input parameter for numerical modelling of solute plume dispersion in the water column (Tab. IV.3 and IV.4; Supp. Tab. IV.1-4).

Table IV.1: Location, water depth, and bottom water (BW) temperature of the gas release experiment, ADCP, BIGO and CTD cast 12 during the Celtic Explorer Expedition CE12010.

Site/Gear	Latitude/ °N	Longitude/ °E	Water depth/ m	BW temperature/ °C
Ocean Elevator/ GRE	58.4062	2.0237	84	
11-ADCP OCE1	58.4054	2.0221	77	
43-ADCP OCE2	58.4061	2.0242	76.4	
8-BIGO2-1	58.3727	1.9318	77.2	
45-CTD12	58.406	2.024	80	7.8

IV.2.1.4 Evaluation of field data

The ROV data set including positioning data (longitude, latitude and water depth) was combined with data derived from HydroC-CO_2 and ADCP measurements by correlating their UTC time stamps. The combined dataset was mapped using the geographic information system software ArcGIS v.10.1 (Fig. IV.3a). For comparison with numerical predictions, pCO_2 data was averaged over periods of equal ROV positioning (i.e. 10 minutes).

IV.2.2. Modelling CO_2 leakage

IV.2.2.1 Bubble dissolution

An existing gas bubble dissolution model (BDM; Vielstädte et al., 2015) was applied to calculate the rate of CO_2 dissolution in seawater which is used as input parameter for the plume dispersion model (PDM, Section IV.2.2.2) that is applied subsequently to simulate the dispersion of the dissolved CO_2 in the water column. The BDM calculates the dissolution rate of CO_2 bubbles in seawater with the parameterization for the thermodynamic properties of CO_2, that are the molar volume (Duan et al., 1992), gas compressibility (Duan et al., 1992), and gas solubility in seawater (Duan et al., 2006).

The BDM uses finite difference methods implemented in the NDSolve object of Mathematica (i.e. LSODA, Sofroniou and Knapp, 2008) solving for the shrinkage and expansion of a gas bubble due to a decrease in hydrostatic pressure, dissolution and stripping of gases for each of the relevant gas species (CO_2, N_2, and O_2) and the bubble rise velocity.

Model boundary conditions were obtained from Sea-Bird 9 plus CTD data from July 2012 and run for different initial bubble sizes (r_0) ranging between 1 to 4 mm radius, in accordance to radii observed during the GRE and at wells leaking methane (Vielstädte et al., 2015, Fig. IV.4a), initially containing only CO_2. Simulated water depth was defined as 81.8 m in accordance to that of the GRE and depths important for CO_2 leakage from the seafloor in the Sleipner area. The CO_2 concentration in ambient seawater of 0.021 mM (or 434 µatm) was determined from background HydroC-pCO_2 measurements at the GRE site averaged over 15 minutes (Tab. IV.5), while dissolved O_2 concentrations of 0.235 mM were determined from BIGO-2-1 measurements at well 15/9-13 (Linke et al., 2012; Tab. IV.1). Dissolved N_2 was considered to be in equilibrium with the atmospheric partial pressure due to a lack of water column measurements.

For a given initial bubble radius (r_0), the CO_2 dissolution rate (R in mol s^{-1}) determined numerically by the BDM was normalized to the initial bubble CO_2 content (N_0 in mol) and divided by the bubble rise velocity (v_b in m s^{-1}) to calculate the normalized bubble dissolution rate (BD in m^{-1}) as a function of the bubble distance from the seafloor (z):

$$BD(r_0, z) = \frac{R(r_0, z)/N_0}{v_b(\mathrm{r}, z)} \qquad [\frac{1}{m}] \qquad \text{Eq. IV.1}$$

The combined CO_2 dissolution rate of the initial bubble size distribution ($BD(\Psi,z)$) was then determined by integrating these normalized rates of CO_2 bubble dissolution over the total bubble size distribution weighted by its volumetric contribution (V_0/V_Ψ) to the total gas flow (Vielstädte et al., 2015, Fig. IV.4a):

$$BD(\psi, z) = \frac{1}{MI} \int_{r(min)}^{r(max)} \mathrm{BD}(r_0, \mathrm{z}) \cdot \frac{V_0}{V_\psi}\, dr \qquad [\frac{1}{m}] \qquad \text{Eq. IV.2}$$

Where, *r(min)* and *r(max)* are the minimum and maximum bubble sizes of the total spectrum and *MI* is the measurement interval between individual bubble sizes (i.e. 0.1 mm), both determined from image footage of bubble release.

It should be noted that the applied BDM is reasonable for the release of single bubble streams but not necessarily for bubble plumes which involve additional dynamics (i.e. upwelling). Hence, this study is not meant to capture the physics of overpressure-driven leakage of CO_2, such as blowout accidents, which likely involves much larger leakage rates and bubble plume dynamics.

Table IV.2: Parameterization of the bubble dissolution model.

Parameterization	Range	Variance	Reference
[a] Diffusion coeff.: D_i / m^2 s^{-1}			
$D_{O2}=1.05667\cdot10^{-9}+4.24\cdot10^{-11}\cdot T$	T:0-25°C	$1.00\cdot10^{-21}$	Boudreau, 1997
$D_{N2}=8.73762\cdot10^{-10}+3.92857\cdot10^{-11}\cdot T$	T:0-25°C	$2.94\cdot10^{-23}$	Boudreau, 1997
$D_{CO2}=8.38952\cdot10^{-10}+3.8057\cdot10^{-11}\cdot T$	T:0-25°C	$4.76\cdot10^{-25}$	Boudreau, 1997
Mass transfer coefficient: $K_{L,i}$ / m s^{-1}			
$K_L=0.013(v_b\ 10^2/(0.45+0.4\ r\cdot10^2))^{0.5}\ D_i^{\ 0.5}$	r≤2.5 mm		Zheng and Yapa, 2002
$K_L=0.0694\ D_i^{\ 0.5}$	2.5<r≤6.5 mm		Zheng and Yapa, 2002
$K_L=0.0694\ (2r\cdot10^{-2})^{-0.25}\ D_i^{0.5}$	R<6.5 mm		Zheng and Yapa, 2002
Fit to CTD data as function of z			
$T(z)=8+7/(1+e^{0.375\ (-21.7512+z)})$	Z: 0.100 m	$3.99\cdot10^{-2}$	
$S(z)=35.12-0.67/(1+e^{0.4125\ (-20.1595+z)})$	Z: 0-100 m	$4.97\cdot10^{-4}$	
Density of SW: φ_{SW}/ kg m^{-3}			
$\varphi_{SW}(z)=1027.7-2.150/(1+e^{0.279\ (-21.612+z)})$	Z: 0-100 m	$6.8\cdot10^{-3}$	Unesco,1981
Bubble rise velocity: v_b / m s^{-1}			
$v_b=4474\ r^{1.357}$	r<0.7 mm		Wüest et al., 1992
$v_b=0.23$	0.7≤r<5.1 mm		Wüest et al., 1992
$v_b=4.202\ r^{0.547}$	r≥5.1 mm		Wüest et al., 1992
Gas solubility: c_i / mM			
$cN_2=0.622+0.0721\cdot z$	Z:0-100m	$2.5\cdot10^{-3}$	Mao and Duan, 2006
$cO_2=1.08+0.1428\cdot z$	Z:0-100m	$9.8\cdot10^{-3}$	Geng and Duan, 2010
$cCO_2=(0.041+0.00476\cdot z)^*\ \varphi_{SW}$	Z:0-100 m	$5.7\cdot10^{-5}$	Duan et al., 2006
CO_2 molar volume: $MVCO_2$ / L mol^{-1}			
$MVCO_2=1/(0.04+0.00458\cdot z)$	Z:0-100 m	0.1	Duan et al., 1992
Hydrostatic Pressure: P_{hydro}/ bar			
$P_{hydro}=1.013+\varphi_{SW}\cdot g\cdot z$			

[a] The parameterization of the diffusion coefficients is based on a seawater salinity of 35. Pressure effects have been neglected because at the given water depths (<100 m) the resulting error is less than 1%.

IV.2.2.2 Advection-dispersion of dissolved CO_2

A fine-scale 3-D flow and transport model was developed to simulate the spread of CO_2 released at a point source and the resulting acidification of seawater in an advection dominated marine environment applying the commercial finite element (FEM) software COMSOL Multiphysics ® v.5.0. The model uses the pre-build package "Transport of Diluted Species" (tds) assuming chemical species transport through diffusion and advection in a turbulent flow (i.e. Re> 2,000 for the North Sea) as implemented in the mass balance equation (COMSOL User Guide):

$$\frac{\partial C}{\partial t} = \nabla \cdot ([D_M + D_T]\,\nabla C - u\,C) + S \qquad [\frac{mol}{m^3\,s}] \qquad \text{Eq. IV.3}$$

Where, C is the concentration of the dissolved species (here dissolved inorganic carbon (DIC) in mol m^{-3}), t is the time (s), ∇ is the Nabla Operator of the spatial coordinates x,y, and z , u is the current velocity vector (m s^{-1}), D denotes the diffusion coefficient including a molecular (D_M) and turbulent diffusion component (D_T) (m^2 s^{-1}), and S is the source term of DIC production (mol m^{-3} s^{-1}) resulting from CO_2 bubble dissolution expressed as 2-D Gaussian distribution:

$$S = \frac{1}{\pi\, w} e^{-(\frac{x^2+y^2}{w})} \cdot R_{CO2} \cdot BD(\psi, z) \qquad [\frac{mol}{m^3\,s}] \qquad \text{Eq. IV.4}$$

where, w denotes the area (m^2) of the Gaussian pulse in x and y direction, R_{CO2} is the rate of CO_2 gas bubble release (mol s^{-1}) from the seafloor, and $BD(\Psi,z)$ is the normalized rate of CO_2 bubble dissolution as determined from the BDM (Eq. IV.2, Fig. IV.4b).

The horizontal advective flow (u) in x and y direction is parameterized according to least-squares data fits to ADCP velocity data measured at 3.2 masf and application of the Kármán–Prandtl "Law of the Wall" (LOW) describing the current velocity vector as a function of time (t) and distance from the seabed (z) (Prandtl and Tietjens, 1975):

$$u_x(t,z) = \frac{u_x^*(t)}{k}\ln(\frac{z}{z_0}), \quad u_y(t,z) = \frac{u_y^*(t)}{k}\ln(\frac{z}{z_0}) \qquad [\frac{m}{s}] \qquad \text{Eq. IV.5}$$

Where, u^* denotes the shear velocity in x and y direction determined from the fitting routine, z_0 is the roughness length ($1.4 \cdot 10^{-4}$ m for the North Sea; McGinnis et al., 2014) defining the height at which the current velocity tends to zero (Lefebvre et al., 2011), z is the distance to the seafloor, and k is the dimensionless Kármán constant (0.4, Kundu and Cohen, 2008). As such, advective velocities are assumed to be horizontal, but not vertical and temporally uniform. For simplification, the vertical advection component, which is orders of magnitude

smaller than in horizontal direction, has been ignored.

Using least-squares fits to ADCP velocity data small-scale fluctuations (eddies) in the turbulent flow are not explicitly resolved in the model. The convective phenomenon of turbulent mixing is accounted for in the calculation of the species transport by using an added component of diffusion (D_T), which is expressed in dependency to the distance from the seabed and the shear velocity in resultant current direction (u^*_r) (Prandtl and Tietjens, 1975):

$$D_T = k \cdot u_r^* \cdot z \qquad [\frac{m^2}{s}]$$

Eq. IV.6

Molecular diffusion (D_M) is calculated according to Boudreau (1997) as a function of temperature, pressure, and salinity and is on the order of 10^{-9} m^2 s^{-1}. Diffusion is assumed to be isotropic and hence, is the only mechanism transporting dissolved species vertically in the model domain. Implemented equations fitted to data and constant values are provided in Tables IV.3 and IV.4 for the GRE and leaky well simulation settings, respectively.

To avoid numerical oscillations of the solution in the advection dominated leakage scenario, the COMSOL Model uses both, streamline-upwind (Galerkin method (SUPG), Do Carmo and Alvarez, 2003) and crosswind (Codina, 1998) stabilizing advection schemes, which add artificial diffusion in streamline and orthogonal direction to the advection-diffusion equation (Eq. IV.3). Numerical diffusivity was limited by defining a lower gradient limit (*glim* in mol m^{-4}) denoting the smallest concentration change across an element that is considered by stabilization. *glim* was defined as 3 mol m^{-3} weighted by the mesh element size and has been determined from sensitivity analysis, i.e. increase of *glim* until the solution remains constant (numerical accuracy) while also ensuring sufficient numerical stability. The combination of using stabilizing advection schemes and a high-resolution non-uniform mesh including a local mesh refinement around the gas release (for details see Section IV.2.2.4.1 and IV.2.2.4.2) where concentration gradients change rapidly, ensured the model is well suited for maintaining sharp concentration gradients while also ensuring sufficient numerical stability.

The time-dependent problem was solved by integration of the partial differential equation (i.e. Eq. IV.3) in time according to the implicit backwards differentiated formula method of COMSOL Multiphysics (Press et al., 2007). The COMSOL Multiphysics solver automatically chooses appropriate numerical time steps which were set to be within a certain relative tolerance (i.e. 0.01) for the accuracy of the integration estimated during runtime (Press et al., 2007). The numerical performance (stability) was controlled after each model run by mass balance error (MBE) calculations, which were overall better than 2%.

Table IV.3: Parameterization of the plume dispersion model for the GRE simulation setting.

GRE Parameter	Data fit/Parameterization	Unit
*Resultant velocity as a function of time (t) in seconds	$u_r(t) = 120 + 0.0062\,t - 36\,Sin(\frac{\pi\,t}{8000})$	mm s^{-1}
Sand roughness height	$k_{seq} = 3.2$	µm
Turbulent intensity	$I_T = 0.05$	1
Turbulent length scale	$L_T = 0.01$	m
*Rate of CO_2 bubble dissolution/	$BD(\psi_{GRE}, 81.2) = IF[z < 2.21, 0, 7.6\,e^{-0.31\,z^2}]$	m^{-1}
Leakage rate	R_{CO2}=31	t yr^{-1}
Width of the Gaussian pulse	w=0.3	m^2

*Details on the accuracy of data fits and the correlation of fit parameters are provided in the Supplementary Material Chapter VI Appendix D (S.IV.1.1)

Table IV.4: Parameterization of the plume dispersion model for the leaky well simulation setting.

Leaky Well Scenario Parameter	Data fit/Parameterization	Unit
*East velocity as a function of time (t) in seconds and depth (z) in m above seafloor	$u_x(t,z) = \frac{\left(0.37-2.21\,Sin\left[\frac{\pi(t+5279)}{22400}\right]\right)}{k} \cdot \ln[\frac{z}{z_0}]$	mm s^{-1}
*North velocity as a function of time (t) in seconds and depth (z) in m above seafloor	$u_y(t,z) = \frac{\left(-2.52-3.94\,Sin\left[\frac{\pi(t-36019)}{22400}\right]\right)}{k} \cdot \ln[\frac{z}{z_0}]$	mm s^{-1}
*Shear velocity at 3.2 masf as a function of time (t) in seconds	$u_r^*(t) = \sqrt{\left(-2.05 + 4.56\frac{Sin[\pi(t+8065)]}{22400}\right)^2 + \left(1.84 + 0.65\frac{Sin[\pi(t+23260)]}{22400}\right)^2}$	mm s^{-1}
Turbulent diffusion coefficient	$D_T(t,z) = k \cdot u_r^*(t) \cdot 10^{-3} \cdot z$	$m^2\,s^{-1}$
Molecular diffusion coefficient	$D_M(t) = 10^{-9}$	$m^2\,s^{-1}$
Roughness length	$z_0 = 1.4 \cdot 10^{-4}$ (e.g. McGinnis et al., 2014)	m
Kármán constant	$k = 0.4$ (Kundu and Cohen, 2008)	1
*Normalized rate of CO_2 bubble dissolution	$BD(z) = 1.16\,e^{-1.06 \cdot z^2}$	1 m^{-1}
Leakage rate / of CO_2	R_{CO2} = 10, 20, 55	t yr^{-1}
Width of the Gaussian pulse	w = 0.5	m^2

*Details on the accuracy of data fits and the correlation of fit parameters are provided in the Supplementary Material Chapter VI Appendix D (S.IV.1.1)

IV.2.2.3 pCO_2 and pH calculation

The computed concentration of DIC, which is the sum of chemical species resulting when CO_2 dissolves in seawater ($[CO_2]+[HCO_3^-]+[CO_3^{2-}]$), is converted into carbonate system parameters of interest, i.e. pCO_2 and pH, applying an analytical solution (Zeebe and Wolf-Gladrow, 2001) assuming constant TA and primary physical parameters (temperature, salinity, and pressure) delivered by CTD casts (Seabird 9 Plus) of July 2012 (Tab. IV.5). Total alkalinity of seawater was determined by titration with 0.02 N HCl using a mixture of methyl red and methylene blue as indicator. The titration vessel was bubbled with argon to strip any CO_2 and H_2S produced during the titration. The IAPSO seawater standard was used for calibration; analytical precision and accuracy are both ~2%. TA is assumed to be constant during the GRE.

Table IV.5: Parameterization of the carbonate system.

Carbonate system parameters	Parameterization	Source
Total alkalinity (TA) / mM	2.333	CE12010 45-CTD12
Background pCO_2*/ µatm	434	CE12010 44-HydroC
Background DIC (DIC0)/ mM	2.174	Calculated from TA&pCO_2*
Background pH*	8.0	Calculated from TA&pCO_2*
Seawater temperature/ °C	7.8	CE12010 45-CTD12
Seawater salinity	35.18	CE12010 45-CTD12
Water depth/ m	81.8	CE12010 44-ROV
Total sulfide/ mM	0	
Total boron/ mM	0.42	
Dissolved Ca ions/ mM	11.4	
Spatial DIC heterogeneity/ µM	16 or 0.7g/m³ excess CO_2	DIC bottom water concentrations in Tommeliten seepage area (Supp. Fig. IV.7)
Seasonal DIC variability/ µM	60 or 2.64 g/m³ excess CO_2	Variability based on upper DIC bound given in Bozec (2006) and lower bound measured in the Sleipner area (DIC0)
[a]Conversion of excess DIC (µM) in pCO_2 (µatm)	$\frac{1}{1+e^{DIC_{ex}-50}} \cdot (430 + 4DIC_{ex} - 0.03\,DIC_{ex}^2) + \frac{1}{1+e^{50-DIC_{ex}}} \cdot (480 + 2.1DIC_{ex} + 0.03DIC_{ex}^2 - 1.6 \cdot 10^{-5} DIC_{ex}^3)$	Fit to model-derived data (valid up to DIC_{ex} of 1,000 µM)

[a]Details on the accuracy of the data fit and the correlation of fit parameters are provided in the Supplementary Material Chapter VI Appendix D (Supp. Tab. IV.5)

IV.2.2.4 Input data and simulation settings

IV.2.2.4.1 Simulating the Gas Release Experiment

The first modelling case is designed to simulate the GRE over the 4h period of ROV observation, for which the effects of the tidal turn on CO_2 dispersion are examined and compared to *in situ* pCO_2 measurements. The computational domain is set to be

50 x 50 x 20 m^3, with a smaller rectangle (2.2 x 0.7 x 2.2 m^3) in its center, which represents the geometry of the Ocean Elevator from which the CO_2 bubbles are released. The non-uniform finite element mesh has a spatial resolution of 0.075-1.75 m, with a finer element distribution of maximal 0.2 m in size around the gas release spot (Supp. Tab. IV.11).

The DIC source rate (*S*), resulting from vertical CO_2 bubble dissolution, is parameterized according to the preset gas flow (R_{CO2}) of 85 kg day^{-1} of CO_2 and the calculated bubble dissolution rate (*BD*) of the initial bubble size distribution (Ψ with a peak radius of 2.1 mm) at the given water depth of 81.8 m and seawater conditions found at the location of the experiment (Tab. IV.3, Fig. IV.4b).

In contrast to the PDM setup described above (Section IV.2.2.2), where the current velocity is parameterized in the model domain according to ADCP measurements and the LOW towards the seabed, current velocities (and other convective parameters) around the Ocean Elevator were calculated numerically because the ADCP, which was deployed 28 m away from the experiment, could not observe modifications in the turbulent flow that the obstacle of the Ocean Elevator induced. Generally, the flow field behind an obstacle is suppressed and forms periodically swirling vortices. These effects were resolved by using a k-ε turbulence model (i.e. the spf physics interface) implemented in COMSOL Multiphysics which calculates the turbulent fluid flow numerically by solving the Reynolds-Averaged-Navier-Stokes-Equation (RANS, for details see Supplementary Section S.IV.1.2).

Using the k-ε turbulence model, the advective flow acts in the direction of the Reynolds-averaged velocity and not in the real instantaneous velocity of the fluid in the field. As a result, small eddies of the turbulent flow are not explicitly resolved, having however, a pronounced effect on the species transport, as they cause additional mixing. The advective phenomenon of turbulent mixing is accounted for in the calculation of the species transport by using an added component of diffusion (D_T in addition to molecular diffusion) that is equal to the ratio of the turbulent kinematic viscosity ν_T ($m^2\ s^{-1}$) to the dimensionless turbulent Schmidt number Sc_T:

$$D_T = \frac{\nu_T}{Sc_T} \qquad [\frac{m^s}{s}] \qquad \text{Eq. IV.7}$$

Where Sc_T is a model constant with a typical value of 0.71 (COMSOL User Guide), and ν_T is calculated numerically based on the turbulent kinetic energy (*k* in $m^2\ s^{-2}$) and the dissipation rate of turbulent kinetic energy (ε in $m^2\ s^{-3}$) determined by the k-ε turbulence model:

$$\nu_T = c_\mu \frac{k^2}{\varepsilon} \qquad [\frac{m^2}{s}] \qquad \text{Eq. IV.8}$$

where $c\mu$ is a dimensionless model constant (i.e. 0.09; COMSOL User Guide).

Using the k-ε turbulence model, turbulent velocities (u), viscosities (v_T) and diffusivities (D_T) are calculated numerically, based on a transfer function of the measured current velocity magnitude (i.e. least-scares data fit to the resultant velocity at 3.2 masf, during OCE2) and algebraically specified mixing length (L_T) and turbulent intensity (I_T) defined as inlet boundary condition (for implemented values see Tab. IV.3). By defining an equivalent sand roughness height (k_{seq}) of 3.2 µm at the seafloor, which is related to the roughness length (z_0) by $z_0=k_{seq}/30$ (Lefebvre et al., 2011), the non-slip boundary condition at the bottom of the model domain accounts for friction at the seabed and the average flow velocity is related to the distance from the wall (i.e. seabed).

The spread of dissolved CO_2 during the experiment was obtained from coupling the physics interface of mass transport (tds) to the k-ε turbulence model (i.e. the spf physics interface) thus, accounting for modifications in the advective and diffusive phenomena that the obstacle of the Ocean Elevator induced.

To significantly lower the computational requirements when solving for the turbulent flow and mass transport during the experiment tidal turn (e.g. avoiding too many open boundaries that are weakly constrained), the effect of the tidal currents passing the Ocean Elevator geometry was simulated by rotating the Lander in the model domain relative to a constant flow direction (defined as normal velocity condition at the inlet boundary). The outflow boundary in streamline direction is set as a zero-gradient condition, which accounts for advective mass transfer but neglects any diffusive fluxes across the boundary. The remaining boundaries are defined as slip, no-flow boundary conditions with no-friction, no-viscous forces, and no-mass transfer for seawater or dissolved species. The angles between the current flow and the Ocean Elevator during the tidal turn were calculated by correlating UTC times stamps of ADCP data (i.e. resultant current direction), and ROV positioning and heading during pCO_2 measurements. Based on the spatial orientation of the Ocean Elevator, whose long side was heading 40° to the north-east, two rotation angles of 40° and 70° were determined, in which most of the HydroC measurements occurred and for which the simulations were run.

Initial DIC concentrations and current velocities in the model domain are prescribed to be zero, so that the model calculates excess DIC concentration relative to the background signal observed in the field (Tab. IV.5). After proving sufficient model stability by mass balance error calculations, model results were evaluated against averaged pCO_2 measurements in order to fit the turbulent parameters (turbulent length scale and turbulent intensity) and validate the model for further application of the leaky well scenarios (Fig. IV.5).

IV.2.2.4.2 Simulating CO_2 leakage from a well

The second modelling case is designed to simulate a range of hypothetic, but realistic release scenarios of CO_2 along an abandoned well from the Sleipner CO_2 storage site into the North Sea, using site-specific current velocity data (Fig. IV.6) as well as initial bubble sizes (Fig. IV.4a) and gas flows found at methane-leaking wells in that area (Vielstädte et al., 2015). The computational domain is set to be 600 x 600 x 20 m^3 with the point-source (~ 4 m^2) CO_2 leak located at the seafloor in the model center. The non-uniform mesh has a spatial resolution of 0.15-3 m with a higher finite element density about 80 m around the gas release spot.

According to highly variable gas emissions measured at the methane-leaking wells (Vielstädte et al., 2015), we examine a range of possible leakage rates (R_{CO2}), i.e. 10, 20, and 55 t yr^{-1} of CO_2. The advective flow (u) is prescribed from least-squares data fits to 12 h time-series data of current velocities in east (x) and north (y) directions (OCE1, Bin1) considering the velocity decrease towards the seabed induced by friction (Eq. IV.5, Tab. IV.4). The chosen 12 h time-series data was found to be representative for a whole tidal cycle because the North Sea has a semi-diurnal tide (Fig. IV.6a). The diffusion coefficient (D) is parameterized as described in Section IV.2.2.2. The model accounts for friction at the seabed, so that the advective flow and the turbulent diffusivity are assumed to be horizontal, but not vertical and temporarily uniform. Full details on implemented equations are given in Table IV.4.

Four open lateral boundaries with a zero-gradient boundary condition allow for convective flow in and out of the model domain, while any diffusive fluxes are neglected. The seafloor and upside boundary towards the sea surface are set as no-flow boundary conditions, i.e. no-mass transfer permitted. Initial DIC concentrations and current velocities in the model domain are prescribed to be zero, so that the model calculates excess DIC concentration relative to the background signal observed in the field. To ensure mass balance, the computational domain is tested to be sufficiently large to avoid that outflowing plumes of dissolved CO_2 may return through the boundaries within the simulated time span.

IV.3 Results and Discussion

IV.3.1 The Gas Release Experiment

ROV video observation revealed moderate gas bubbling on top of the Ocean Elevator (Fig. IV.2b). In total, 18 single CO_2 bubble streams with initial bubble sizes of 1.3 to 2.9 mm in radius (Fig. IV.4a) were emanating from the release head and reached a final rise height of ~2 m. This is consistent with pCO_2 measurements which were ~430 µatm two meters above the release spot, i.e. at general background values in the area (Fig. IV.3c).

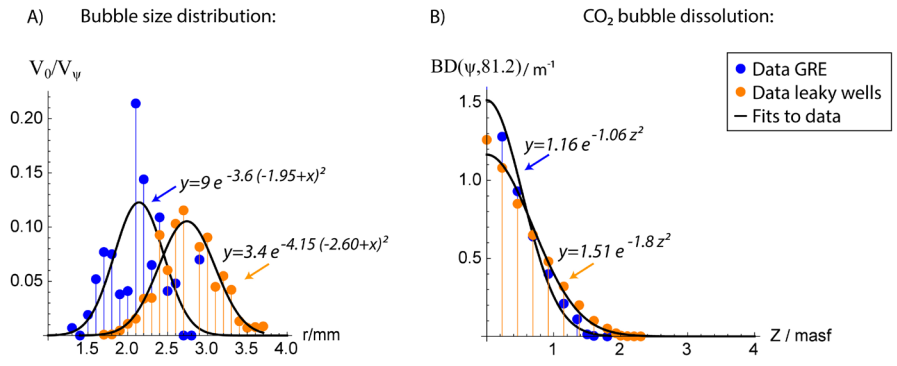

Figure IV.4: A) Bubble size distributions measured during the GRE (blue dots) and at methane leaking wells in the CNS (orange dots, Vielstädte et al., 2015). **B**) Calculated rates of CO_2 bubble dissolution as a function of the distance to the seafloor (z) based on the initial bubble size distributions of the GRE (blue dots) and leaking wells in the CNS (orange dots). CO_2 bubbles dissolve within the lower 3 m of the water column. Details on the accuracy of data fits (black line) are given in the Supplementary Material Chapter VI Appendix D (Section S.IV.1.1.2).

Rapid CO_2 bubble dissolution into seawater significantly increased the bottom water partial pressure of CO_2 close to the release site to values of 2,327 µatm (3 m downstream of the leak, Fig. IV.3c). However, elevated pCO_2 levels sustained only in a very narrow band (< 1 m width) of water mass downstream of the Ocean Elevator. As a result of quick dispersion by ambient bottom currents, background values were attained already ~30 m downstream of the artificial leak, indicating that the impact of the experiment was limited to near-bottom waters and a rather small distance of a few tens of meters downstream of the leak (Fig. IV.3).

Although the experiment successfully simulated CO_2 leakage into the North Sea at low rates, the physical response in the dynamic water column was quite complex. The k-ε turbulence model successfully simulated the suppressed pressure and advective flow downstream of the Ocean Elevator, which induced a downwelling of the solute CO_2 plume (Fig. IV.5a). This effect was particularly strong at the beginning of the experiment, when the turbulent flow was heading towards the long side of the Ocean Elevator (Fig. IV.3a, IV.5a). The density increase of water masses enriched in CO_2 is considered to have no considerable effect on the observed downwelling because the maximum pCO_2 value recorded during the experiment correlates only to an increase in the density of 0.001 kg m^{-3}.

According to numerical results, the turbulent diffusion coefficient (determined from turbulent viscosity and the dimensionless Schmidt number (0.71, Eq. IV.7) ranged on the order of 10^{-4} to 10^{-7} m^2 s^{-1} during the experiment. Low turbulent diffusivities occurred close to the seafloor and downstream of the Ocean Elevator, which coincides with the decrease in the advective flow (Fig. IV.5a). Thus, it is evident that the experimental setup not only significantly decreased the horizontal advective transport, but also suppressed the turbulent

mixing of the artificial CO_2 plume downstream of the Ocean Elevator.

Evaluation of the numerical results against pCO_2 measurements reveals that the applied numerical models accurately describe the rapid CO_2 bubble dissolution in seawater and the spatial and temporal dynamics in excess CO_2 in a tidal flow (Fig. IV.4b, IV.5a). *In situ* measurements of the spatial pCO_2 dispersion correspond well to numerical simulations, showing that the bubble size distribution is depleted in CO_2 1.9 m above its release (Fig. IV.4b) and the added CO_2 is diluted quickly in the bottom waters (Fig. IV.5a). Nonetheless, the model tends to underestimate pCO_2 values measured in the field as the modeled values cluster in the lower range of the pCO_2 measurements (Fig. IV.5b). Possible explanations for this deviation are 1) short-term fluctuations in the real advective flow, which have not been considered in the model, 2) the influence of the ROV and its thrusters in the current flow, also not considered in the model, and 3) some numerical diffusivity introduced to the model.

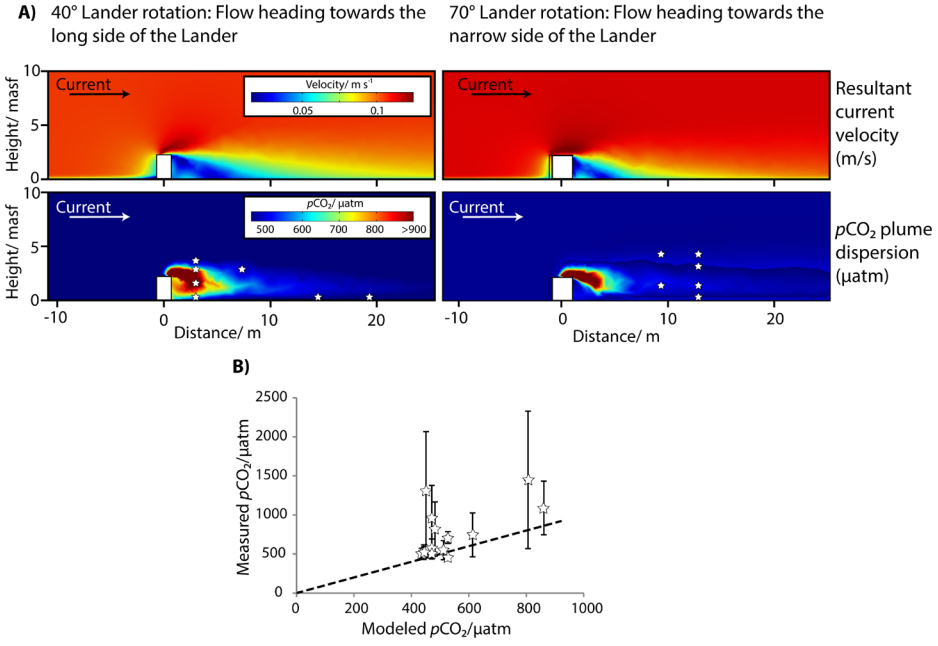

Figure IV.5: COMSOL model results of the GRE simulation showing the modified current velocity field (top) and the dispersion of the solute CO_2 plume (bottom) downstream of the Ocean Elevator/ Lander (white box) for the two simulated rotation angles of the Lander relative to a normal flow vector (black and white arrow). **B**) Comparison of pCO_2 measurements and model-derived pCO_2 values for each ROV measuring position (white stars) indicating that the COMSOL model underestimates measured values but is in the scatter of most measurements (for a discussion see Section IV.3.1). Model-derived pCO_2 values bear an uncertainty of ±124.5 µatm as determined from the standard deviation (1-σ) of the least-squares data fit that was used in the model to covert DIC concentrations into pCO_2 data (see Chapter VI Appendix D Supp.Tab. IV.5). The 1:1 line of model-derived pCO_2 values and HydroC measurements is indicated by the dashed line.

One simplification in the model is that the advective flow acts in the direction of the Reynolds-averaged velocity and not in the real instantaneous velocity of the fluid in the field, where abrupt changes in the flow direction might have resulted in patches of high pCO_2 waters that separated from the main plume, and thus, shortly increased pCO_2 signals measured in the field. The effect of short-term fluctuations is consistent with the large scatter (± 25% on average) in pCO_2 measurements for each measuring position (Fig. IV.5b). Furthermore, as the HydroC sensor was attached to the front porch of the ROV, pCO_2 measurements were likely influenced by the obstacle when the plume hits the ROV (similar to the effect of the Ocean Elevator). Unphysical, numerical diffusivity, which would also result in an underestimation of measured pCO_2 values, has been minimized by tuning the lower concentration gradient limit (*glim*) for artificial diffusion, but cannot be completely excluded to have influenced our simulations.

Despite these simplifications described above, systematic discrepancies cannot be found between the computed plume dispersion and that observed in the field; i.e. both showing rapid bubble dissolution, quick dispersion, and the downwelling of the plume. We therefore argue that the applied models are sufficiently reliable to predict solute plume dispersion of a point-source CO_2 leak on a small spatial scale.

IV.3.2 The Leaky Well Scenarios

The simulated leaky well scenarios with constant and continuous leakage of 10, 20 and 55 t yr^{-1} of CO_2, respectively resulted in dynamic plumes of acidified bottom water that were quickly dispersed from the source location. Generally, within a distance of less than 120 m from the leak background pCO_2 levels are predicted (Fig. IV.7a). As expected, the magnitude of seawater acidification and the spatial extent of detectable CO_2 plumes at the seafloor increased with increasing leakage rate, but were always below -2.1 pH units and 1,400 m^2, respectively (Fig. IV.7 b,c).

The simulated initial bubble size distribution with a peak radius of 2.6 mm (Vielstädte et al., 2015) has lost its CO_2 within the lower 3 m of the water column. 80% of its initial CO_2 content is already dissolved within the first meter above the seafloor (Fig. IV.4b). Such rapid CO_2 bubble dissolution causes leaking CO_2 to remain in the bottom waters and preserves the CO_2 from reaching the atmosphere via direct bubble transport. This is in line with our experimental results and other recent studies (Hvidevold et al., 2015; Dewar et al., 2013; Dissanayake et al., 2012; Phelps et al., 2014). However, once a leak occurs, some of the dissolved CO_2 may reach the atmosphere on the long-term via diffusive sea-air gas exchange, mostly depending on the mixing of the water column and the water depth at which leakage were to occur (Phelps et al., 2014).

In the following, we discuss key drivers controlling the dispersion of CO_2 emitted at a point source leak in a tidally influenced oceanic setting (IV.3.2.1), before discussing modelling-derived estimates on the spatial footprints of detectable (IV.3.2.3) and potentially, biologically harmful CO_2 plumes (IV.3.2.2) in seawater in order to support risk assessments and monitoring strategies of offshore CO_2 storage sites. We distinguish between the spatial footprints of detectable and potentially, biologically harmful CO_2 plumes by referring to two different levels in natural DIC changes: 1) spatial, short-term fluctuations in DIC (here termed spatial heterogeneity), which are important for leak detection, and 2) larger seasonal changes in the carbonate system (here termed seasonal variability), which cause natural changes in pH levels that marine biota should be adapted to. Finally, we discuss the propensity of wells to leak at Sleipner (IV.3.2.4). The robustness of our numerical results is discussed in the Supplementary Material Chapter VI Appendix D (Section S.IV.1.3).

IV.3.2.1 CO_2 Plume dispersion and relationship with tides

Using the tidal velocity data of July 12th for the CNS (Fig. IV.6a), our leaky well simulations show a strong correlation between the dispersion of the dissolved CO_2 plume in the water column and the phase of the semi-diurnal tides (Fig. IV.7). Common temporal and spatial features include (1) the accumulation of DIC near the leak during periods of decelerating flow, (2) thin elongated plumes with low DIC concentrations during periods of strong unidirectional flow, (3) wider plume shapes when the tide turns, and the (4) extensive build-up of DIC peak concentrations during slack water periods with low or stagnant flow (which is in line with other recent studies Greenwood et al. 2015, Fig. IV.7a). These observations indicate that continuous CO_2 leakage into the North Sea would result in a series of plume concentrations and shapes during a tidal cycle, with peak concentrations and largest plumes occurring around slack water periods and close to the seafloor, where advective and diffusive fluxes are low (Fig. IV.6). By contrast, at stronger flow DIC concentrations should be efficiently diluted with ambient seawater quickly reaching background values.

Higher simulated DIC concentrations during low tide (*LT*) as compared to high tide (*HT*) were primarily a consequence of the measured tidal asymmetry, referring to differences in the ebb and flood current velocities (Fig. IV.6a, IV.7c). Tides may not only affect CO_2 dispersion but also the CO_2 emission rate at the seabed since studies at natural gas seeps imply that rates of bubble release at the seafloor respond to tidal pressure fluctuations (e.g. Leifer and Wilson, 2007; Linke et al., 1994; Tryon et al., 1999; Wiggins et al., 2015).

Calculated turbulent diffusion coefficients (D_T) were in agreement to those measured in the benthic boundary layer of permeable sediments in the Central North Sea (McGinnis et al., 2014), suggesting that the applied correlation of D_T and measured current

velocities (Eq. IV.6) obtained reliable results. In our simulations, D_T varied horizontally between 2-9·10^{-3} m^2 s^{-1} at weakest and maximum current flow 3.2 m above the seabed, respectively, and was significantly smaller, that is on the order of 10^{-7} m^2 s^{-1}, close (1 cm asf) to the seafloor throughout the whole tidal cycle (Fig. IV.6d). Despite the wide range of diffusion coefficients, the dimensionless Péclet number (*Pe*), that is the ratio of the rate of advection of a physical quantity by the flow to the rate of diffusion of the same quantity driven by an appropriate gradient, was overall larger than 10 - an indication that diffusive fluxes were overall negligible. This implies that for a North Sea setting and at small scales the lateral diffusive fluxes are low and thus, have only a negligible effect on the dispersion of the dissolved CO_2 plume, whereas the advective transport (i.e. tidal current) is a key parameter. It should however be noted, that diffusion was the only mechanism that controlled the vertical dispersion of the CO_2 plume in our three leaky well simulations, as we neglected any vertical advective transport.

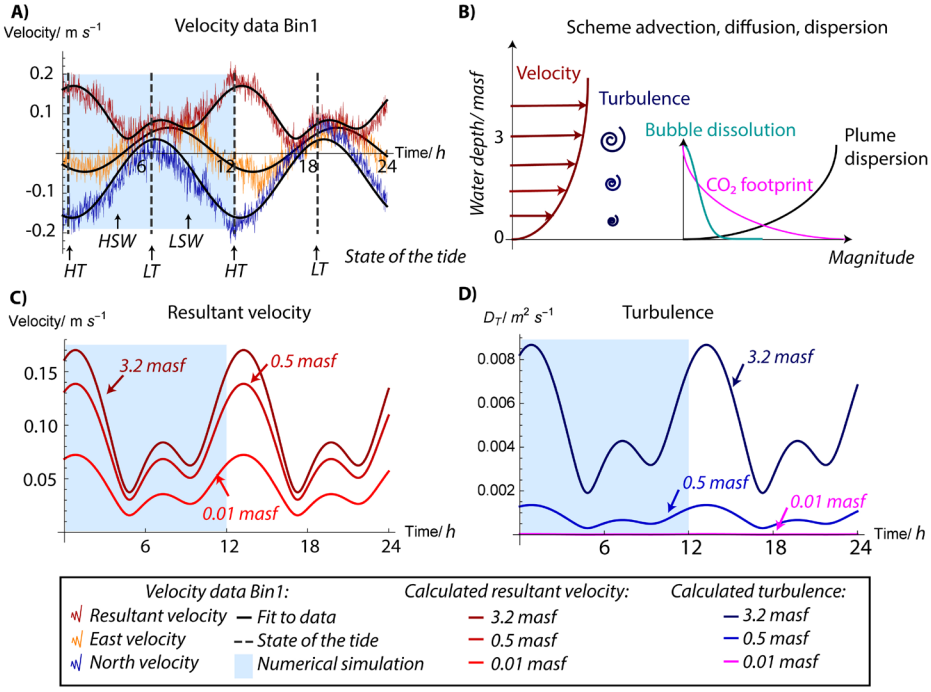

Figure IV.6: A) ADCP velocity data in north (blue), east (orange), and resultant (red) current direction measured 3.2 m above the seafloor during the OCE1 long-term deployment of the ADCP. Data show a tidal asymmetry, referring to differences in the ebb and flood current velocities, i.e. stronger currents during high tide (*HT*) than during low tide (*LT*) and weaker currents during high slack water (*HSW*) than during low slack water (*LSW*). **B**) Scheme illustrating the Law of the Wall (LOW), where the current flow (dark red) and turbulence (dark blue) increase with distance to the seafloor, which results in the weakest dispersion of the CO_2 plume at the seafloor. Together with the declining rate of CO_2 dissolution during bubble ascent, this causes the largest CO_2 footprints (pink line) to occur at the seabed. Figures showing calculated current velocities (**C**) and turbulent diffusivities (**D**) by application of the LOW in the lower 3 m of the water column (this is where CO_2 bubbles dissolve). Least-squares data fits (lines), which were used to force the leaky well scenarios, are highlighted in light blues.

IV.3.2.2 Environmental impact of a well leaking CO_2 in the CNS

The environmental impact of CO_2 leakage into seawater is a critical issue in risk assessment studies and depends on the magnitude of seawater acidification and the spatial and temporal extent of any potentially harmful pH reductions exceeding a site-specific, natural variability which marine biota should be adapted to. In the deeper layers of the Northern and Central North Sea marine DIC concentration varying between 2,110 and 2,175 μmol kg^{-1} have been observed (Bozec et al, 2006). This corresponds to a seasonal variability in pH of 7.85-8.02, assuming a constant TA of 2.333 mM (a simplification due to lacking literature data on seasonal variations in TA in bottom waters of the North Sea) and physicochemical seawater conditions as measured in the Sleipner area in July 2012 (T=7.8°C; S=35.18, P=9.2 bar; Tab. IV.5). As such, effects of CO_2 leakage resulting in pH changes of less than -0.15 units are considered to be indistinguishable from seasonal variability (in line with other North Sea studies; Phelps et al., 2014), and thus, would have no deleterious consequences at Sleipner. Hence, to examine the extent to which marine biota might be affected by a well leaking CO_2, we refer to the seafloor area impacted by pH changes exceeding those of seasonal variability (Tab. IV.6, Fig. IV.7).

Table IV.6: Maximum predicted seafloor areas (m^2), which are considered to be detectable (ΔDIC>16 μM), have significantly harmful impact (ΔpH>1 unit), potentially harmful impact (0.5>ΔpH >0.2 unit), and no impact (0.2>ΔpH>0.15 unit) on marine biota.

Leakage rate/ t yr^{-1} of CO_2	Area with significantly harmful impact (ΔpH>1 unit) / m^2	Area with potentially harmful impact (0.5>ΔpH>0.2 unit) / m^2	Area with no deleterious impact (0.2>ΔpH>0.15 unit) / m^2	Total impacted seafloor area (ΔpH>0.15 unit)/ m^2	Detectable seafloor footprint/ m^2
10	≤1.6	≤13.3	≤8	≤29	≤136
20	≤5	≤25	≤14	≤54	≤292
55	≤27	≤133.8	≤66	≤271	≤1,364

Across all three leakage scenarios, the seafloor area impacted by pH changes exceeding those of seasonal variability increased with increasing leakage rate, but was always below 271 m^2 (Tab. IV.6). This indicates that the impact of a well leaking CO_2 would be extremely localized not exceeding a distance of ~80 m from the leak (Fig. IV.7a at LT, 7.5 h). Note, that the threshold value for leak detection (16 μM of excess DIC) is lower than the seasonal DIC variability (60 μM, dark blue), which marine biota should be adapted to, so that detectable CO_2 plumes are larger (i.e. <1,400 m^2) than the environmentally impacted seafloor area (Fig. IV.7b).

The largest simulated reduction of seawater pH occurred in bottom waters in the direct vicinity of the leak and during high slack water (HSW), where the advective and diffusive

fluxes were weakest (Fig. IV.7c). Here, the change in pH was as high as -1.23, -1.54, and -2.10 units for the low, mid and high leakage rate, respectively. To put these values into context to the potential impact to marine biota, we follow the classification suggested by Phelps et al. (2014) and Widdicombe et al. (2013). According to these authors, long-term reductions of pH approaching or exceeding 1.0 unit can be considered as significantly harmful, whereas a reduction of the order of 0.2-0.5 is potentially harmful. Based on this, our three leaky well scenarios indicate that CO_2 leakage, even at the smallest rate (10 t yr^{-1}), would reduce the pH below the critical value that would have a significant negative impact on benthic organisms. However, such harmful conditions would be extremely localized, occurring only in the immediate vicinity of the leak, whereas most of the impacted seafloor area would be exposed to seawater pH conditions that are considered to be potentially harmful (mid and high leakage scenario) or are unlikely to have any impact at all (low leakage scenario) (Tab. IV.6). It should be noted further that these classifications are based on experimental data, where marine organisms have been exposed to reduced pH values for a few weeks (Widdicombe et al., 2013). Futhermore, marine biota may respond different by the on-and-off exposures of acidified seawater as observed in our experiment and numerical

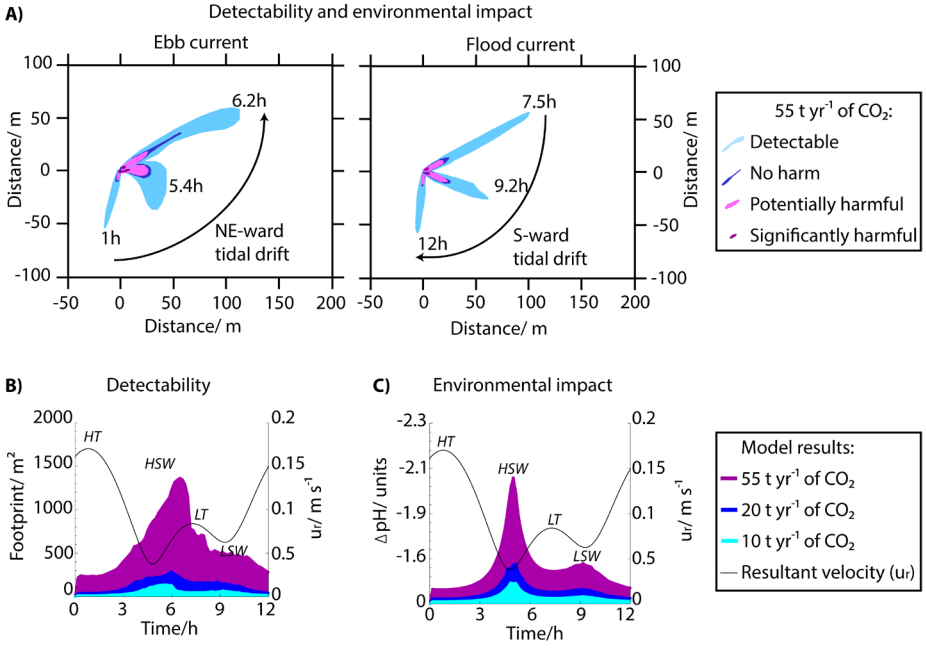

Figure IV.7: **A**) Model-derived CO_2 plume dispersion during half a tidal cycle (12 h) showing the varying footprints of detectable (light blue) and environmentally harmful (light and dark magenta) CO_2 plumes at the seafloor. Because the threshold value for leak detection (16 µM of excess DIC) is lower than the seasonal DIC variability (60 µM, dark blue), which marine biota should be adapted to, detectable CO_2 plumes are larger than the environmentally impacted seafloor area. **B**) Simulated footprints of detectable CO_2 plumes and **C**) maximum seawater acidification at the seafloor as a function of time resulting from a leaky well in the CNS that emits 10 (cyan), 20 (blue), and 55 (magenta) t yr^{-1} of CO_2 into the water column.

simulations (Fig. IV.3a, IV.8). Repeated short-term (minutes to hours) exposures to low-pH waters might be less harmful than continuous exposure, suggesting that more research is necessary to examine the effect of oscillating pH changes on marine organisms and different time scales for organisms to adapt.

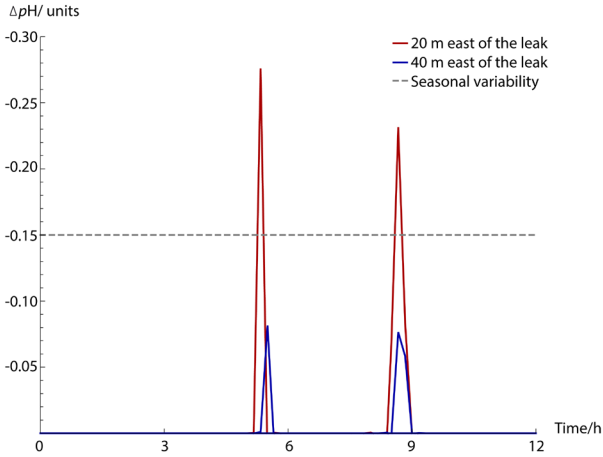

Figure IV.8: Modelled seawater acidification showing the on-and-off exposure of benthic organisms to low pH conditions 20 m (red) and 40 m (blue) east of a leaky well (20 t yr^{-1}). pH reductions exceeding those of natural variability (dashed line) are restricted to the direct vicinity of the well and occur twice in a 12 h period.

IV.3.2.3 Detectability and monitoring of a leaky well

Conventionally leaky wells are determined by an assessment of well integrity, generally identified by sustained casing pressure (Brufatto et al., 2003). However, this approach is unable to detect gas leakage along the outside of wells, where injected CO_2 might escape from the storage reservoir through disturbed and fractured sediments in the surrounding of the wellbore. As such, we recommend to extent the monitoring strategy in order to detect a leaky well by correlating the well paths of boreholes poking through the storage formation with the sub-seafloor location of the CO_2 plume as identified in seismic data (Vielstädte et al., 2015). Wells (apart from the injection well) that were proven to penetrate the subsurface plume or are located in its direct vicinity while also reaching the depth of the storage formation, will pose a higher risk for leakage and will thus, require monitoring. The survey area needs to be adjusted continuously as injection proceeds and the CO_2 plume spreads in the subsurface.

The size of the seafloor area around a "risky well" that would require monitoring is site-specific and will mostly depend on the spatial extent of the CO_2 plume in the water column, which can be geochemically distinguished from any natural heterogeneity in the carbonate chemistry. Therefore, a combination of a thorough baseline study of environmental conditions (i.e. carbonate chemistry, currents), resolving changes over relatively short time scales, and numerical modelling will enable reliable prediction of the spatial and temporal characteristics of the solute CO_2 plume in the water column. Due to the presumably small emission rates

associated to a leaky well, models will need to provide a high spatial resolution to resolve the small footprint of the solute CO_2 plume in seawater.

For monitoring purposes, spatial heterogeneities, caused by short-term fluctuations in background marine DIC concentration, are more relevant than the larger seasonal variability. Nonetheless, long-term baseline studies are needed in order to obtain trends in short-term variations. In the Sleipner case, spatial heterogeneity is assumed to be on the order of 16 µM as determined by DIC measurements along a "nearby" transect in the Tommeliten seepage area (Supp. Fig. IV.7). Due to the similar water depth and physicochemical seawater conditions, a threshold of 16 µM of DIC for detecting leakage was assumed to be also representative for Sleipner. Based on this threshold value, our numerical results suggest monitoring a seafloor area of less than 1,400 m^2 around a "risky well" where CO_2 leakage can be detected (Tab. IV.6). Hence, geochemical monitoring surveys need to be performed at a very high spatial resolution to capture leaky wells. Moreover, instruments (pCO_2 or pH sensors) should be deployed <3 m above the seafloor to reliably detect CO_2 leakage since rapid CO_2 bubble dissolution limits detectable concentration anomalies to bottom waters in close contact with the seabed (Fig. IV.6b).

As natural, spatial heterogeneity in the carbonate chemistry at Sleipner (i.e. ±16 µM of DIC, corresponding to ±45 µatm of pCO_2, and ±0.04 pH units) appears to be larger than the accuracy of most available sensors (i.e. ± 1 µmol kg^{-1} of DIC (Dickson et al., 2007), ±30 µatm of pCO^2 at sensor calibration up to 3,000 µatm (Fietzek et al., 2014), and ±0.005 pH units (Shitashima et al., 2013)), the probability for detecting a leaky well tends to be rather independent from the sensors applied but will likely increase with the number of *in situ* instruments available (Hvideveld et al., 2015) and the time period of continuous in situ monitoring. Due to a lack of temporal coverage and low spatial resolution distinct water sampling of DIC appears insufficient to capture CO_2 leakage, while continuous *in situ* monitoring over a few tidal cycles (days-weeks) is promising, which is in agreement with the final conclusions of the QICS CO_2 injection experiment (Atamanchuk et al., 2015). Finally, once a leak has been identified, long-term investigations of the environmental consequences will be necessary because fixing such emissions will be challenging.

IV.3.2.4 Propensity of wells to leak at Sleipner

In contrast to the conventional approach of assessing the risk of wells to leak by well integrity, we evaluate the risk of CO_2 leakage along the outside of wells, currently not considered in regulatory frameworks such as the EU CCS Directive (2011) and the OSPAR Convention. The larger Sleipner area hosts 80 adjacent wells, of which 39 belong to the Sleipner A platform from which CO_2 is being injected into the ~900 m deep Utsira sandstone formation

(Fig. IV.1b). According to the latest publically available 3-D seismic time-lapse data of 2008, none of these wells penetrates the subsurface plume of injected CO_2 (Fig. IV.1b) and thus, constitutes a risk for CO_2 leakage from the storage reservoir. The closest well 15/9-13, which is located around 500 m to the west of the CO_2 injection point, was ~350 m away from the outer rim of the 2008er subsurface plume and has been identified to emit shallow (~600 mbsf), biogenic methane into the CNS (Vielstädte et al., 2015). Despite its vicinity to the subsurface CO_2 plume and its demonstrated leakage for gas, the slow and predominantly north-eastward migration of the injected CO_2 in the storage reservoir (Eiken et al., 2011) may prevent that well 15/9-13 will pose a future risk for CO_2 leakage (Fig. IV.1b). However, newer time-lapse data and more sophisticated models evaluating the spreading of injected CO_2 in the storage reservoir are needed to assess if and when the injected CO_2 might reach well 15/9-13. Due to the large distance of the other wells (> 1.5 km) and the slow movement of the injected CO_2 in the storage reservoir (Eiken et al., 2011; Chadwick et al., 2009), it is unlikely that the Sleipner CO_2 plume will ever reach wells other than 15/9-13 during the operation's lifetime (i.e. 30 years).

From a climate control point of view a single leaky well with CO_2 emission rates of < 55 t yr^{-1} has insignificant impact on storage performance. In the Sleipner case, CO_2 injection at 1 Mt yr^{-1} and leakage of 55 t yr^{-1} would mean losses of 0.006% per year, which falls below 0.01% per year, being considered as a threshold value to retain the long-term (millennium) suitability of CCS as a climate change mitigation option (Haugan and Joos, 2004). Considering the long-term suitability of CCS is important because leakage along a well (similar to natural conduits, such as faults and fractures) may persist for a long time, far beyond the active period of CO_2 injection, due to the slow dissolution of the injected CO_2 in the formation waters, the buoyancy-driven leakage, and the challenge to fix such leaks. At Sleipner, reservoir simulations have indicated that the injected CO_2 will completely dissolve within around 4,000 years (Torp and Gale, 2004), determining the timespan for which the fugitive loss of CO_2 (if present) could theoretically continue. However, CO_2 dissolution and the associated loss of buoyancy starts immediately after injection and may become efficient in shorter timespans (i.e. around 500-1,000 years), thereby reducing the amount of CO_2 that could be lost from the reservoir (Kempka et al., 2014). As such, only prolonged leakage (>1,000 years) along numerous (>2) wells may pose risk for a non-tolerable leakage rate above 0.01% at Sleipner. Note, that the prospective implementation of CCS at a scale that would have significant impact on reducing anthropogenic CO_2 emissions requires much larger CO_2 injection rates than those currently realized at Sleipner. In this case, the tolerable number of leaky wells, in terms of retaining a meaningful climate change mitigation option, should increase, particularly offshore, where emissions are not directly released into the atmosphere.

IV. 4. Conclusions

This study highlights that the impact of a well leaking CO_2 would be very localized, i.e. a few tens to one hundred meter around the gas release spot, which is arguably not significant on a regional scale. Strong tidal currents and cycles, both prominent in the North Sea, significantly diminish the spreading of low-pH water masses into the far field of a leak by efficiently diluting elevated pCO_2 levels with background concentrations. Nonetheless, even small CO_2 leakage may have significant negative impact on benthic marine organisms, primarily in the direct vicinity of the gas release and during periods of low or stagnant flow. These effects might be mitigated by the recurrently short (minutes to hours) exposure to low pH conditions in a tidally oscillating flow. However, leakage along the outside of a well may persist for a long time (several hundreds to thousands of years) because fixing such emissions proves to be challenging. Prolonged leakage along numerous wells may compromise the long-term suitability of CCS in terms of retaining a meaningful climate change mitigation option (particularly onshore where emissions are directly released into the atmosphere) and environmental sustainability. This stresses the importance of leak detection and emphasizes that the conventional focus on well integrity needs to be extended because it neglects the potential escape of injected CO_2 through drilling-induced fractures along the outside of wells. As such, regulatory frameworks need to be adapted and, hopefully, this study is able to provide some incentives for improved risk assessment and monitoring of hydrocarbon infrastructure in CCS storage areas.

Acknowledgements

We would like to thank the crew and master of RV Celtic Explorer and the team of ROV Kiel 6000 for their invaluable support during the cruise CE12010. Special thanks to Sergiy Cherednichenko for his invaluable technical support in designing and conducting the gas release experiment. We would also like to thank Statoil ASA for permission to use the 3-D seismic time-lapse data. The cruises and scientific work received funding through the European Union Community's 7th Framework Program (FP7/2007-2013) in the EUROFLEETS program, the ECO2 project (grant agreement no. 265847) and the DFG-funded Cluster of Excellence "Future Ocean".

Supplementary Material is provided in Chapter VI Appendix D.

References:

Atamanchuk et al., 2015. Detection of CO_2 leakage from a simulated sub-seabed storage site using three different types of pCO_2 sensor. *Int. J. Greenh. Gas Control* **38**, 121-134. Doi:10.1016/j.ijggc.2014.10.021.

Bachu, S., and Watson, T.L., 2009. Review of failures for wells used for CO_2 and acid gas injection in Alberta, Canada. *Energy Procedia* **1**, 3531-3537. Doi:10.1016/j.egypro.2009.02.146.

Boudreau, B.P., 1997. *Diagenetic models and their implementation: modelling transport and reactions in aquatic sediments*. Berlin, Heidelberg, New York, London, Paris, Tokyo, Hong Kong: Springer, 414 pp.

Blackford, J., et al., 2014. Detection and impacts of leakage from sub-seafloor deep geological carbon dioxide storage. *Nat. Clim. Change* **4**, 1011-1016. Doi:10.1038/NCLIMATE2381.

Bozec, Y., et al., 2006. Assessment of the processes controlling seasonal variations of dissolved inorganic carbon in the North Sea. *Limnol. Oceanogr.* **51** (6), 2746-2762.

Brooks, A.N., Hughes, T.J.R, 1982. Streamline upwind/Petrov-Galerkin formulations for convection dominated flows with particular emphasis on the incompressible Navier-Stokes equations. *Comput. Methods Appl. Mech. Engrg.* **32**, 199-259.

Brufatto, C., et al., 2003. From mud to cement - Building gas wells. *Oilfield Rev.* **15**, 62-76.

Carey, J.W., et al., 2007. Analysis and performance of oil well cement with 30 years of CO_2 exposure from the SACROC Unit, West Texas, USA. *Int. J. Greenh. Gas Control* **1**, 75–85.

Carey, J.W., Svec, R., Grigg, R., Zhang, J., Crow, W., 2010. Experimental investigation of wellbore integrity and CO_2-brine flow along the casing-cement microannulus. *Int. J. Greenh. Gas Control* **4**, 272–282.

Chadwick, R.A., Noy, D., Arts, R.J., Eiken, O., 2009. Latest time-lapse seismic data from Sleipner yield new insights into CO_2 plume development. *Energy Procedia* **1**, 2103–2110. doi:10.1016/j.egypro.2009.01.274

Codina, R., 1998. Comparison of some finite element methods for solving the diffusion-convection-reaction equation. *Comput. Methods Appl. Mech. Engrg.* **156**, 185-210.

COMSOL User Guide. http://nf.nci.org.au/facilities/software/COMSOL/4.3/doc/pdf/mph/COMSOLMultiphysicsUsersGuide.pdf

Crow, W.J., Carey, J.W., Gasda, S.E., Williams, D.B., Celia, M., 2010. Wellbore integrity analysis of a natural CO_2 producer. *Int. J. Greenh. Gas Control* **4** (2), 186-197.

Dewar, M., Wei, W., McNeil, D., Chen, B., 2013. Small-scale modelling of the physicochemical impacts of CO_2 leaked from sub-seabed reservoirs or pipelines within the North Sea and surrounding waters. *Mar. Pollut. Bull.* **73** (August(2)), 504–515.

Dewar, M., Sellami, N., Chen, B., 2015. Dynamics of rising CO_2 bubble plumes in the QICS field experiment Part 2- Modelling. *Int. J. Greenh. Gas Control* **38**, 52-63.

Dickson, A., Sabine, C., Christian, J.E., 2007. Guide to best practices for ocean CO_2 measurements. PICES Spec. Publ. 3.

Dissanayake, A.L., et al., 2012. Modeling the impact of CO_2 releases in Kagoshima Bay, Japan. *J. Hydro-environ. Res.* **6**, 195-208.

Do Carmo, E.G., Alvarez, G.B., 2003. A new stabilized finite element formulation for scalar convection-diffusion problems. *Comput. Methods Appl. Mech. Engrg.* DOI: 10.1016/S0045-7825(03)00292-5.

Duan, Z., Sun, R., Zhu, C., Chou, I.M., 2006. An improved model for the calculation of CO_2 solubility in aqueous solutions containing Na^+, K^+, Ca^{2+}, Mg_{2+}, Cl^-, and SO_4^{2-}. *Mar. Chem.* **98**, 131-139.

Duan, Z., MØller, N., Weare, J.H., 1992. An equation of state for the CH_4-CO_2-H_2O system: 1. Pure systems from 0 to 1000°C and 0 t0 8000 bar. *Geochim. Cosmochim. Ac.* **56** (14), 2605-2617.

Eiken, O., et al., 2011. Lessons Learned from 14 years of CCS Operations: Sleipner, In Salah and Snøhvit. *Energy Procedia* **4**, 5541-5548.

EU CCS Directive GD1, 2011. Implementation of Directive 2009/31/EC on the Geological Storage of Carbon Dioxide. Guidance Document 1, CO_2 Storage Life Cycle Risk Management Framework. 60 pp.

EU GeoCapacity, 2009. Assessing Europe Capacity for Geological Storage of Carbon Dioxide. D16 WP2 Storage Capacity, 170 pp.

Farreira, T., Rasband, W., 2012. ImageJ User Guide IJ 1.46r. 185p. http://imagej.nih.gov/ij/docs/guide/index.html.

Fiedler, B., et al., 2013. In situ CO_2 and O_2 measurements on a profiling float. *J Atmos Ocean Tech.* **30**, 112-26. Doi:10.1175/JTECH-D-12-00043.1.

Fietzek, P., Fiedler, B., Steinhoff, T., Körzinger, A., 2014. In situ quality assessment of a novel underwater pCO_2 sensor based on membrane equilibration and NDIR spectrometry. *J Atmos Ocean Tech.* **31**, 181-96. Doi:10.1175/JTECH-D-13-00083.1.

Gascoigne. High Performance Adaptive Finite Element Toolkit. URL http://www.gascoigne.uni-hd.de

Gasda S, Bachu S, Celia M., 2004. The potential for CO_2 leakage from storage sites in geological media: analysis of well distribution in mature sedimentary basins. *Environ. Geol.* **46** (67), 707–20.

Geng, M., Duan, Z.H., 2010. Prediction of oxygen solubility in pure water and brines up to high temperatures and pressures. *Geochim. Cosmochim. Ac.* **74**, 5631-5640.

Global CCS Institute, 2014. The Global Status of CCS: 2014, Melbourne, Australia. 199 pp.

Greenwood, J., Craig, P., Hardman-Mountford, N., 2015. Coastal monitoring strategy for geochemical detection of fugitive CO_2 seeps from the seabed. *Int. J. Greenh. Gas Control* **39**, 74-78. Doi: 10.1016/j.ijggc.2015.05.010.

Gurevich, A.E., Endres, B.L., Robertson Jr, J.O., Chilingar, G.V., 1993. Gas migration from oil and gas fields and associated hazards. *J. Petr. Sci. Eng.* **9**, 233-238.

Hvideveld, H.K., et al., 2015. Layout of CCS monitoring infrastructure with highest probability of detecting a footprint of a CO_2 leak in a varying marine environment. *Int. J. Greenh. Gas Control* **37**, 274-279. Doi:10.1016/j.ijggc.2015.03.013.

Jordan, A.B., Stauffer, P.H., Harp, D., Carey, J.W., Pawar, R.J., 2015. A response surface model to predict CO_2 and brine leakage along cemented wellbores. *Int. J. Greenh. Gas Control* **33**, 27-39. Doi:10.1016/j.ijggc.2014.12.002.

Kempka, T., De Lucia, M., Kühn, M., 2014. Geomechanical integrity verification and mineral trapping quantification for the Ketzin CO_2 storage pilot site by coupled numerical solutions. *Energy Procedia* **63**, 3330-3338.

Kundu, P.K., Cohen, I.M., 2008. *Fluid Mechanics*, 4th ed., Elsevier.

Kutchko, B.G., Strazisar, B.R., Dzombak, D.A., Lowry, G.V., Thaulow, N., 2007. Degradation of wellbore cement by CO_2 under geologic sequestration conditions. *Environ. Sci. Technol.* **41**, 4787–4792.

Lefebvre, A., Ernstsen, V.B., Winter, C., 2011. Influence of compound bedforms on hydraulic roughness in a tidal environment. *Ocean Dyn.* **61** (12), 2201-2210.

Leifer, I., Wilson, K., 2007. The tidal influence on oil and gas emissions from an abandoned oil well: Nearshore Summerland, California. *Mar. Pol. Bull.* **54** (9), 1495-1506.

Linke, P., Schmidt, M., Rohleder, M., Al-Barakati, A., Al-Farawati, R., 2015. Novel online digital video and high-speed data broadcasting via standard coaxial cable onboard marine operating vessels. *Mar. Technol. Soc. J.* **49** (1), 7-18.

Linke, Peter, ed .,2012. RV Celtic Explorer EUROFLEETS cruise report CE12010 - ECO2@NorthSea : 20.07. – 06.08.2012, Bremerhaven - Hamburg . GEOMAR Report, N. Ser. 004 . GEOMAR, Kiel, Germany, 60 pp. Doi:10.3289/GEOMAR_REP_NS_4_2012.

Linke, P., et al., 1994. In situ measurement of fluid flow from cold seeps at active continental margins. *Deep-Sea Res. Pt.* I **41**, 721-739.

Mao, S., Duan, Z.H., 2006. A thermodynamic model for calculating nitrogen solubility, gas phase composition and density of the N_2-H_2O-NaCl-system. *Fluid Phase Equilibr.* **248**, 103-114.

McGinnis, D.F., Sommer, S., Lorke, A., Glud, R.N., Linke, P., 2014. Quantifying tidally driven benthic

oxygen exchange across permeable sediments: An aquatic eddy correlation study. *J. Geophys. Res. Oceans* **119**, 6918-6932. Doi:10.1016/2014JC010303

Metz, B., Davidson, O., De Coninck, H.C., Loos, M., 2005. IPCC special report on carbon dioxide capture and storage. Prepared by Working Group III of the Intergovernmental Panel on Climate Change. IPCC.

Nordbotten, J.M., Celia, M.A., Bachu, S., Dahle, H.K., 2005. Semianalytical Solution for CO_2 Leakage through an Abandoned Well. *Environ. Sci. Technol.* **39**, 602-611.

OSPAR Convention, 2007. OSPAR guidelines for risk assessment and management of storage of CO_2 streams in geological formations. Reference number 07-12. 32 pp.

Phelps, J.J.C., Blackford, J.C., Holt, J.T., Polton, J.A., 2014. Modelling large-scale CO_2 leakages in the North Sea. *Int. J. Greenh. Gas Control.* Doi:10.1016/j.ijggc.2014.10.013.

Prandtl, L., Tietjens, O.G., 1957. *Fundamentals of Hydro- and Aerodynamics*. New York: Dover Publications Inc, 270 pp.

Press, W.H., Teukolsky, S.A., Vetterling, W.T., Flannery, B.P., 2007. *Numerical Recipes: The Art of Scientific Computing (third ed.)* Cambridge University Press, Cambridge.

Shitashima, K., Maeda, Y., Ohsumi, T., 2013. Strategies for detection and monitoring of CO_2 leakage in sub-seabed CCS. *Energy Procedia* **37**, 4283-4290. Doi:10.1016/j.egypro.2013.06.331.

Sofroniou, M., Knapp, R., 2008. Wolfram Mathematica Tutorial Collection- Advanced numerical differential equation solving in Mathematica. Wolfram Research, Inc. http://www.wolfram.com/learningcenter/tutorialcollection/AdvancedNumericalDifferentialEquationSolvingInMathematica/AdvancedNumericalDifferentialEquationSolvingInMathematica.pdf.

Tao, Q., Bryant, S.L., 2014. Well permeability estimation and CO_2 leakage rates. *Int. J. Greenh. Gas Control* **22**, 77-87. Doi:10.1016/j.ijggc.2013.12.022.

Torp, T.A., Gale, J., 2004. Demonstrating storage of CO_2 in geological reservoirs: The Sleipner and SACS projects. *Energy* **29**, 1361-1369.

Tryon, M. D., et al., 1999. Measurements of transience and downward fluid flow near episodic gas vents, Hydrate Ridge, Cascadia. *Geology* **27**, 1075-1078.

UNFCCC (United Nations Framework Convention on Climate Change), 2006. http://unfccc.int/resource/docs/publications/handbook.pdf.

UNESCO, 1981. The Practical Salinity Scale 1978 and the International Equation of State of Seawater 1980. *Tech. Pap. Mar. Sci.* **36**, 25 pp.

Van der Zwaan, B., Smekens, K., 2007. CO_2 Capture and Storage with Leakage in an Energy-Climate Model. *Environ Model Assess.* Doi:10.1007/s10666-007-9-125-3.

Vielstädte et al., 2015. Quantification of methane emissions at abandoned gas wells in the Central North Sea. *Mar. Petrol. Geol.* **68**, Part B, 848–860. Doi:10.1016/j.marpetgeo.2015.07.030.

Widdicombe, S., Blackford, J.C., Spicer, J.I., 2013. Assessing the environmental consequences of CO_2 leakage from geological CCS: generating evidence to support environmental risk assessment. *Mar. Pollut. Bull.* **73** (2), 399-401.

Wiggins, S., Hildebrand, J., Leifer, I., 2015. Long-term acoustic monitoring at North Sea well site 22/4b. *Mar. Petrol. Geol.* **68**, Part B, 776–788.

Wüest, A., Brooks, N. H., Imboden, D. M., 1992. Bubble plume modeling for lake restoration. *Water Resour. Res.* **28** (12), 3235–3250, doi:10.1029/92WR01681.

Zheng, L., Yapa, P.D., 2002. Modeling gas dissolution in deepwater oil/gas spills. *J. Marine Syst.* **31**, 299-309.

Zeebe, R. E. and Wolf-Gladrow, 2001. *CO_2 in Seawater: Equilibrium, Kinetics, Isotopes.* Elsevier Oceanography Series, 65, pp. 346, Amsterdam.

V. Synthesis

An integrated approach of geochemical, seismic, and numerical analysis was adopted in this thesis to investigate the so far unconsidered leakage of shallow gas (CH_4 and potentially CO_2) along the outside of hydrocarbon wells. Leaky wells presented in Chapter II and III provided new seismic and geochemical evidence for a shallow, biogenic gas emission source in the Central North Sea. Light $\partial^{13}C$-signatures in the emanating gas together with a gas flow that correlates with the local geology, i.e. largest rates at the seafloor were found at well 16/7-2 that was drilled through a seismic chimney, give clear hints that leakage is related to gas migration along the wellpath, and not to well integrity issues as conventionally assumed. These findings manifest a new "facet" of anthropogenic methane emissions with source strengths being comparable to natural major seep sites in that region. Basin-wide extrapolation of our data revealed that the methane input into the entire North Sea from this leakage could be almost 10-times larger than the other known methane sources (rivers, Wadden Sea, and natural seeps). Shallow gas leakage was thus concluded to likely constitute one of the so far unknown contributors to the methane release from the North Sea (atmospheric degassing and export into the North Atlantic), which are ~20-times larger than the known sources. Together with the large emissions from the blowout well 22/4b in the British Sector of the North Sea, anthropogenic emissions of shallow gas likely determine and close the CH_4 budget of the North Sea. However, additional measurements are required to constrain our conclusion on the importance of leaky wells by determining the distribution and persistence of CH_4 flows from this kind of leakage.

In Chapter IV particular emphasis was given to the Sleipner CO_2 storage project for which the hypothetic, but realistic loss of CO_2 along a well was simulated using a combination of experimental field data and numerical modelling. The findings give evidence that the impact and detectability of such leakage at low rates (<55 t yr^{-1} of CO_2) would be very localized, i.e. a few tens to one hundred meter around the gas release spot which is arguably not significant on a regional scale. Strong tidal currents and cycles, both prominent in the North Sea, were found to significantly diminish the spreading of low-pH water masses into the far field of a leak by efficiently diluting elevated pCO_2 levels with background concentrations. This important finding implies that high-energetic oceanic environments are preferable sites for the geological storage of CO_2 since rapid dilution reduces potential negative environmental consequences. As leakages along wellpaths will be challenging to fix (similar to natural conduits) prolonged leakage along numerous wells may compromise storage safety. This gives hints to avoid areas with a high density of wells in order to reduce the propensity of leakages and associated potential costs for compensation actions. If avoiding wells is not possible they need to be carefully monitored. Results presented in this thesis suggest that a combination

of a thorough baseline study of environmental conditions (i.e. carbonate chemistry, currents) and numerical modelling can be employed to predict the spatial and temporal characteristics of the solute CO_2 plume in the water column. This approach can also be used to improve monitoring strategies and their ability to reliably locate and detect leakage. Due to the presumably small emission rates associated to a leaky well, it was highlighted that models will need to provide a high spatial resolution to resolve the small footprint of the solute CO_2 plume in seawater.

Leaky wells presented in this thesis advance our present understanding of gas leakages from the hydrocarbon industry manifesting an important, but unconsidered source for anthropogenic GHG emissions (CH_4 and potentially CO_2) along the outside of the well. In the North Sea – as in other hydrocarbon-prolific areas of the world – shallow gas pockets containing CH_4 are very frequently observed in the sedimentary overburden above the deep hydrocarbon reservoirs. In addition, large amounts of CO_2 are prospectively stored in depleted oil and gas reservoirs if CCS is implemented at a scale that would have a significant impact on reducing anthropogenic CO_2 emissions. Considering the millions of oil and gas wells drilled world-wide, the leakage of shallow gas along hydrocarbon wells is apparently a widespread phenomenon and not restricted to the marine environment (Kang et al., 2014). As such, shallow gas leakage is likely to pose a significant contribution to methane (and prospectively CO_2) emissions from oil and gas infrastructure, particularly onshore where gas is directly emitted into the atmosphere. Comparing our CH_4 emissions to those measured from surface installations in the U.S. (Allen et al., 2013; Brandt et al., 2014; Miller et al., 2013) gives a similar value of ~2 t of CH_4 per year per well. These and other recent studies (Schneising et al., 2014; Zhang et al., 2014,) clearly document strongly increased methane emissions in areas with oil and gas operations, which may counteract our efforts to reduce GHG emissions by switching energy supply from coal to gas.

Further manifestations of such leakages are likely to be discovered in other oil and gas producing provinces if these areas are investigated using suitable geophysical and geochemical techniques. An improved understanding of shallow gas leakage may help to bridge the current gaps in local, regional, and global CH_4 budgets. Moreover, it may contribute to enhance current monitoring and risk assessment strategies for CCS storage sites. Exploration of these largely disregarded emissions is essential for a sound understanding of anthropogenic GHG emission sources and hopefully this study is able to provide impetus to consider leakage of shallow gas along hydrocarbon wells in the legal framework regulating oil and gas exploration and production.

References:

Allen, D.T., et al., 2013. Measurements of methane emissions at natural gas production sites in the United States. *Proc. Natl. Acad. Sci. U.S.A.* **110**, 17768-17773.

Brandt et al., 2014. Methane Leaks from North American Natural Gas Systems. *Science* **343**, 733-735.

Kang et al., 2014. Direct measurements of methane emissions from abandoned oil and gas wells in Pennsylvania. *Proc. Natl. Acad. Sci. U.S.A.* **111**, 18173–18177.

Miller, S.M., et al., 2013. Anthropogenic emissions of methane in the United States. *Proc. Natl. Acad. Sci. U.S.A.* **110**, 20018-20022.

Schneising, O., et al., 2014. Remote sensing of fugitive methane emissions from oil and gas production in North American tight geologic formations. *Earth's Future* **2**, 548-558.

Zhang, Y., Zhao, H., Zhai, W., Zang, K., Wang, J., 2014. Enhanced methane emissions from oil and gas exploration areas to the atmosphere – The central Bohai Sea. *Mar. Pollut. Bull.* **81**, 157-165.

Appendix A: Additional work I contributed to during the period of my PhD

Simultaneous quantification of methane and carbon dioxide fluxes reveals that a shallow arctic methane seep is a net sink for greenhouse gases

J.W. Pohlman, J. Greinert, C. Ruppel, A. Silyakova, ***L. Vielstädte****, C. Magen, M. Casso, S. Bünz, J. Meinert*

In preparation for the Journal of *Science*

Abstract

Warming of high-latitude continental-margin oceans has the potential to release large quantities of carbon from gas hydrate and other sedimentary reservoirs. To assess how carbon mobilized from the seafloor might amplify global warming or alter ocean chemistry, a robust analysis of the concentrations and isotopic content of methane and carbon dioxide (CO_2) in the water column and atmosphere is required. To this effect, a gas analysis system consisting of three cavity ring-down spectrometers was developed to obtain a real-time, three-dimensional characterization of the distribution and isotopic variability of methane and CO_2 at a shallow (<100 m water depth) bubbling methane seep offshore of western Svalbard. Surface water methane concentrations from the continuous-flow CRDS system agreed remarkably well with discrete samples analyzed by the GC-based headspace analysis technique and with a CRDS-based discrete sample analysis module. Reliable carbon isotope data were also obtained from the CRDSs once an isotopic calibration routine was applied.

The resulting data revealed that CO_2 uptake from the atmosphere within the surface water methane plume overlying the gas seep was elevated by 36-45% relative to surrounding waters. In comparison to the positive radiative forcing effect expected from the methane emissions, the negative radiative forcing potential from CO_2 uptake was 32-43 times greater. Lower water temperatures, elevated chlorophyll-fluorescence and ^{13}C-enriched CO_2 within the surface methane plume suggest that bubble-driven upwelling of cold, nutrient-rich water stimulated CO_2 uptake by phytoplankton. The observation that a shallow methane seep has a net negative radiative forcing effect challenges the widely-held perception that methane seeps contribute to the global atmospheric greenhouse gas burden.

Effects of climate change on methane emissions from seafloor sediments in the Arctic Ocean: A review

Rachael H. James, Phillippe Bousquet, Ingeborg Bussmann, Matthias Haeckel, Rolf Kipfer, Ira Leifer, Ilia Ostrosky, Helge Niemann, Jacek Piskozub, Gregor Rehder, Tina Treude, ***Lisa Vielstädte****, and Jens Greinert*

Submitted to the Journal of *Limnology and Oceanography*

Abstract

Large quantities of methane are stored in hydrates and permafrost within shallow marine sediments in Arctic and sub-Arctic regions. These reservoirs are highly sensitive to climate warming, potentially injecting methane to the atmosphere. This feedback accelerates climate change, but the fate of methane released into sediments is uncertain. Here we review the principal physical and biogeochemical processes that regulate methane distributions in Arctic seafloor sediments, its fate if it is transferred into the water column, and the controls on subsequent release of methane to the atmosphere. We find that the fluxes of dissolved methane are significantly moderated by anaerobic and aerobic oxidation of methane, but the response of the microbial community to putative increased fluxes in the future may be insufficient to prevent release to the atmosphere. Increased stratification in Arctic shelf seas due to higher freshwater discharges may, on the other hand, inhibit transfer of methane gas to surface waters. Loss of sea-ice is likely to increase wind speeds and sea-air exchange of methane will consequently increase. We find that studies of the distribution and cycling of methane beneath and within sea ice are very limited, but it seems likely that sea ice acts to modulate methane sea-air fluxes in seasonally ice-covered regions. Our review reveals that there are numerous linkages and feedback pathways between climate warming and release of methane from marine sediments, and there is a need to develop process-based models for methane. Increased observations around especially the anaerobic and aerobic oxidation of methane, bubble transport, and the effects of ice cover, are required to support this.

Appendix B: Supporting Material to Chapter II

Quantification of methane emissions at abandoned oil and gas wells in the Central North Sea

Lisa Vielstädte, Jens Karstens, Matthias Haeckel, Mark Schmidt, Peter Linke, Susan Reimann, Volker Liebetrau, Daniel F. McGinnis, Klaus Wallmann

Spplementary Table II.1: Quantification of gas emissions from funnel measurements based on video material. Left columns: gas volume estimations; Right columns: funnel volume estimation. The optically derived funnel volume was compared to the known funnel volume to calculate a correction factor, F_{corr}, and corrected gas flows, Q_{corr}. The error of the gas flows is estimated from the uncertainty in fill time of 1 s.

Gas Volume				**Funnel Volume**			
Measures	15/9-13	16/4-2	16/4-2	True funnel dimensions	15/9-13	16/4-2	16/4-2
m / mm	98.30	52.23	15.01	125	120.3	124.47	125.5
r_T / mm	18.85	16.61	42.65	15	18.85	16.61	13.9
r_B / mm	71.33	43.46	48.23	75	83.4	77.81	64.95
h / mm	83.12	44.80	13.93	109.66	101.5	108.39	114.7
V /l	0.59	0.14	0.09	0.8	0.9	0.87	0.6
Gas Flow				**Correction**			
Start Time	00:00:43	00:01:08	00:00:00	Offset/ L	0.14	0.006	-0.16
End Time	00:05:14	00:01:59	00:00:42	F_{corr},	0.88	0.92	1.33
Fill time/s	331	51	42				
Q /l min^{-1}	0.11	0.16	0.13				
Q_{corr}/l min^{-1}	0.09	0.15	0.17				
Error /cm^3 s^{-1}	0.01	0.05	0.05				

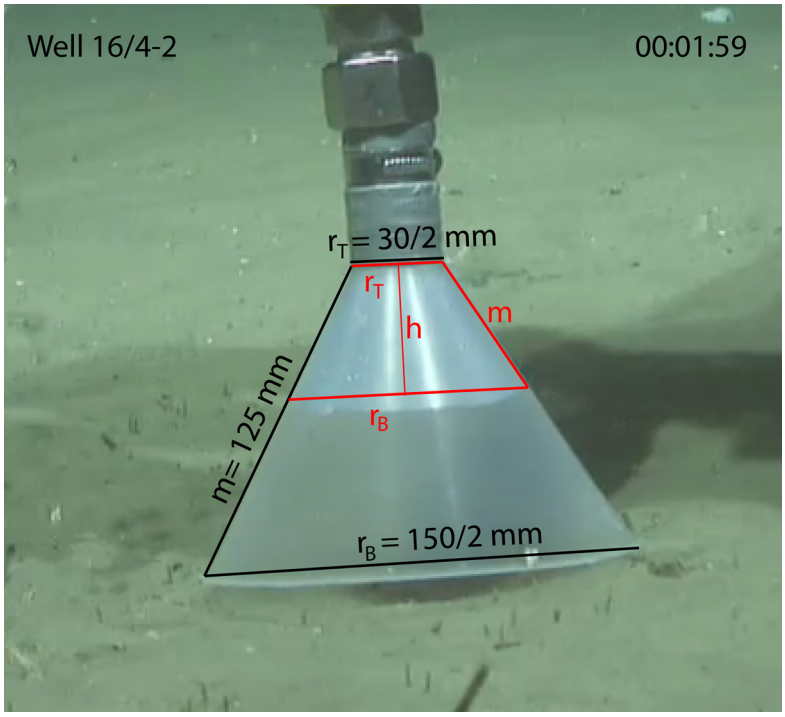

Spplementary Figure II.1: Exemplary visualization of optically derived gas flow measurement at well 16/4-2 using the funnel attached to the gas sampler. The known dimensions of the funnel are given in black: lateral funnel height, *m*, and radii of the top plane, r_T, and bottom plane, r_B, respectively. The gas volume was determined by measuring the corresponding dimensions of the gas filled frustum of a cone and calculating the height, *h* (red letters). See Supplementary Table II.1 for the results.

Appendix C: Supporting Material to Chapter III:

Leaky wells – An unconsidered source for biogenic methane into the North Sea

Lisa Vielstädte, Matthias Haeckel, Jens Karstens, Peter Linke, Mark Schmidt, Lea Steinle, and Klaus Wallmann

S.III.1. Definitions and nomenclature

Leakage: In this paper leakage is defined as "fugitive", or unintended emission of shallow gas. It is sourced from gas accumulations in the overburden of the deep hydrocarbon reservoir (i.e. in the upper 1,000 m of sediment), through which the well has been drilled. To the best of our knowledge, leakage of shallow gas can be induced by any type of well (production, injection, dry, or abandoned).

Well integrity: There is no common global definition of well integrity, but the NORSOK D-010[3] definition is widely used for the North Sea. It defines well integrity as an application of technical, operational and organizational solution to reduce the risk of uncontrolled release of formation fluids throughout the life cycle of the well. Based on this definition, operators and governmental agencies perform well integrity surveys, targeting the leakage of formation fluids through the cement, casing and completion equipment, having a focus mostly on active wells, as monitoring is not mandatory after well abandonment[3].

Well: According to the Norwegian Petroleum Directorate (NPD) guidelines for designation of wells and wellbores[28], a well is defined as a borehole which is drilled in order to discover or delimit a petroleum deposit and/ or to produce petroleum or water for injection purposes, to inject gas, water or other media, or to map or monitor well parameters[28]. A well may consist of one or several wellbores (well paths) and may have one or several termination points[28].

Wellbore (well path): A wellbore/well-path designates the location of the well from one termination point to the wellhead and may consist of one or more well tracks[28].

Well track: The well track is the part of a wellbore (well path) which extends from a point of drilling out on the existing wellbore (kick-off point) to a new termination point for the well[28].

Multilateral wells: Multilateral wells have more than one wellbore radiating from the main wellbore[28]. In contrast to sidetracked wells, where the first bottom section is plugged back before a sidetrack is drilled, multilateral wellbores have more than one wellbore open at the same time[28].

Active wells: Operating-/active wells are defined as production or injection wells that are currently producing or injecting[28].

Abandoned wells: Inactive wells may be temporarily or permanently abandoned. According to the regulations of the NORSOK D-010 standard[3], temporarily abandoned wells are defined as all wells/ wellbores except all active wells and wells that are permanently plugged and abandoned (P&A). Temporarily abandoned wells can be sealed with a mechanical plug, whereas permanently plugged and abandoned wells, whose casings and wellhead need to be cut-off at least 5 mbsf, are sealed with cement[3].

S.III.2. Supplementary Material and Methods

S.III.2.1 Geochemical and seismic data analysis of CH_4 leakage at abandoned gas wells in the Central North Sea

The following section provides details and additional data on the geochemical and seismic analysis of three leaky abandoned wells (15/9-13, 16/4-2, and 16/7-2) located in water depth of 81-93 m in the Norwegian CNS (Supp. Fig. III.1). The data were used to characterize the origin of the emanating gases (S.III.2.1.1), leakage rates (S.III.2.1.2), CH_4 oxidation rates in the water column (S.III.2.1.4), and initial gas bubble size distribution (S.III.2.1.3).

S.III.2.1.1 Determining the origin of leaking gases. The origin of the leaking gases was analyzed by a combination of geochemical and seismic investigations at the three leaky abandoned wells (15/9-13, 16/4-2, and 16/7-2) in the Norwegian Sector of the CNS investigated in Chapter II. Full methodological details on the collection and geochemical analysis of the surface sediments and emanating gases at the three wells are provided in Chapter II Section II.2.1. Results of stable carbon isotope- and hydrocarbon composition at the three wells are given in Supplementary Table III.1 and Figure II.3 in Chapter II.

In addition to geochemical analysis, industrial 3-D seismic data (ST98M3, Statoil ASA) were analyzed for shallow gas pockets in the area around the three wells by mapping high amplitude anomalies[33] in the upper 1,000 m of sediment using Petrel (Schlumberger). The locations of identified gas pockets were assigned to stratigraphic units[13] and correlated with the well-paths of the three leaky wells. Two of the wells (i.e. 15/9-13 and 16/7-2) have been drilled through shallow gas in Lower Pliocene (LP) and Top Pliocene (TP) stratigraphic units (Fig. III.1b). For well 16/4-2, the seismic data do not reveal prominent bright spots (i.e. reverse polarity high amplitude anomalies) in the direct vicinity of the well-path, indicating that leakage at well 16/4-2 draws gas from larger distances (spatial resolution of the seismic data is ~10m). Additionally, seismic turbidity in near-surface sediments (Fig. III.1b, 0.1 – 0.4 s two-way-travel time TWT) might indicate an unfocussed distribution of gas[34].

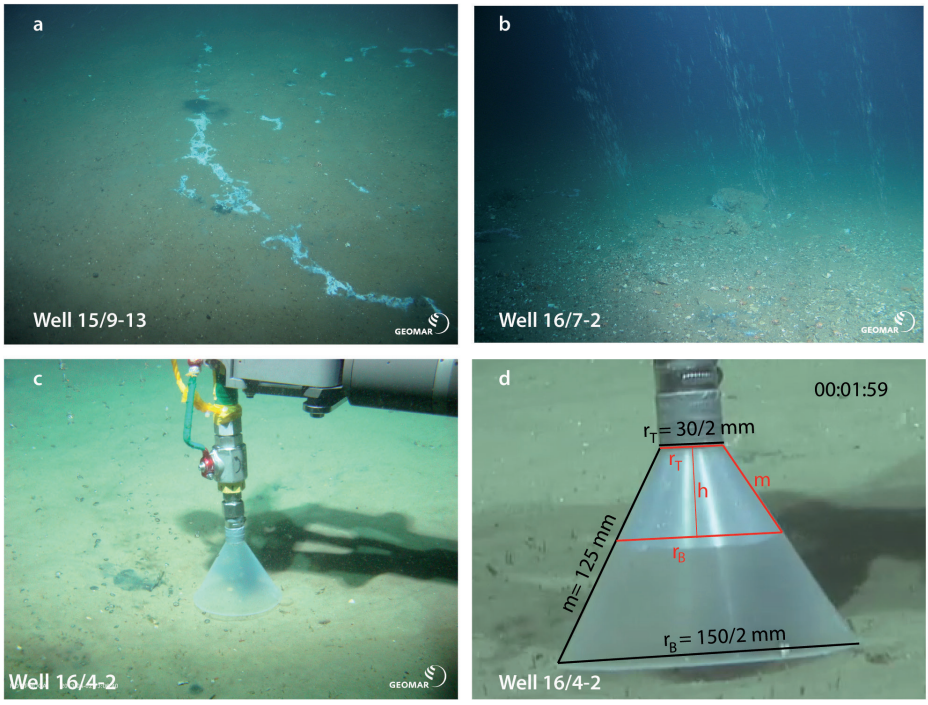

Spplementary Figure III.1: Gas leakage and gas flow measurements at the three wells. Pictures showing **a**) bacterial mats related to CH_4 leakage at well 15/9-13, **b**) the most intense leakage at well 16/7-2, **c**) gas flow measurement at well 16/4-2, and **d**) exemplary visualization of optically derived gas flow measurement at well 16/4-2 using the funnel attached to the gas sampler. Dimensions of the funnel are: m = lateral funnel height, r_T = radius of the top plane, and r_B = radius of the bottom plane. The gas volume was determined by measuring the corresponding dimensions of the gas filled frustum of a cone and calculating the height, h (red letters).

S.III.2.1.2 Quantifying per-well leakage rates. The *in situ* gas flow was quantified at single bubble streams of wells 16/4-2 and 15/9-13 using the ROV-operated gas sampler with attached funnel (Supp. Fig. III.1c,d). Full methodological details are provided in Chapter II Section II.2.2.1. At well 16/7-2, the *in situ* gas flow was derived from bubble size measurements described in Chapter II Section II.2.2.2. Results of gas flow measurements are summarized in Supplementary Table III.1.

To allow comparison of the gas emissions, measured at different locations (i.e. 58.373° N and 1.932° E; 58.473° N and 2.033° E; and 58.596° N and 2.028° E) and at variable water-depths (i.e. 81, 83, and 93 m at well 15/9-13, 16/7-2, and 16/4-2, respectively), *in situ* gas flows measured at 7.8 °C and 5.1 °C were expressed for standard pressure and temperature conditions (STP: P = 1 bar; T = 298.15 K). The standard gas flow, *Q*, ranged from 0.9 to 1.8 L min^{-1} (STP) with an average gas flow of 1.4 (±0.4) L min^{-1} (STP) at the sampled bubble streams (Supp. Tab. III.1). This corresponds to a relative variability of 27%, which was (due to lack of information) also assumed to be equivalent to the spatial variability at a single well. Thus, based on the average *Q* and the number of individual bubble streams at the wells,

the total seabed CH_4 gas flow was estimated to range between 2.8 L min^{-1} and 55 L min^{-1} (STP), corresponding to an annual CH_4 release of 1-19 t yr^{-1} $well^{-1}$ assuming no larger variability over prolonged times (Supp. Tab. III.1). The highest release rate was measured at well 16/7-2, which was drilled through a seismic chimney (Fig. III.1b), typically believed to be more permeable than the surrounding sediment. The gas flow measurements at the three wells are required for the quantification of the North Sea-wide release assignment, where we distinguish between a conservative (2.5±1.5 t yr^{-1} $well^{-1}$ of CH_4) and a maximum (8±7.9 t yr^{-1} $well^{-1}$ of CH_4) leakage rate taking either, the average of wells 15/9-13 and 16/4-2 only, or also include the high emissions of well 16/7-2, respectively (Supp. Tab. III.1).

Spplementary Table III.1: Quantification of seabed gas emissions the three abandoned wells in the Central North Sea.

Well (Water depth)	Q_{SF} (in situ)/ L min^{-1} $seep^{-1}$ of CH_4	Q_{SF} (STP)/ L min^{-1} $seep^{-1}$ of CH_4	No. of seeps	Q_{SF}[a]/ t yr^{-1} $well^{-1}$ of CH_4
15/9-13 (81 mbsl)	0.09	0.9[f]	2	1
16/4-2 (93 mbsl)	0.15/0.17[b]	1.6/1.8[b,d]	8	4
16/7-2 (83 mbsl)	0.15[c]	1.4[e]	39	19

[a] based on the average gas flow of 1.4 L min^{-1} $seep^{-1}$ at STP (25°C, 1 bar)
[b] based on replicate gas flux measurements at well 16/4-2
[c] derived from bubble size, due to lack of direct funnel measurements
[d] measured at high tide
[e] measured at low tide
[f] measured 2 h after low tide

S.III.2.1.3 Measuring initial bubble sizes. Initial bubble size spectra at the three wells were analysed applying the image editing software ImageJ[35] as described in Chapter II Section II.2.2.2. These size spectra are required to calculate the fate of leaking CH_4 from the seafloor to the atmosphere using a numerical bubble dissolution model (Supp. Section S.III.2.2.2).

Determined bubble sizes at well 15/9-13 and 16/4-2 were combined into a common bubble size distribution (Ψ) (for details see Chapter II Fig. II.4). Given that the gas flow at individual seeps of the wells was low such that initial bubble formation processes are primarily controlled by the mechanical properties of the surface sediments[27], Ψ is proposed to be representative for bubbles released from the fine to medium-grained clayey sand found at the investigated wells and in wide areas of the North Sea[15]. The combined bubble size distribution (Chapter II Fig. II.4) was thus, used for further extrapolation of CH_4 leakage to the North Sea scale. Measurements at well 16/7-2 were excluded for the determination of the combined bubble

size distribution because bubbles escaped from below a carbonate rock, thereby expelling significantly larger bubbles into the water column than bubbles directly released from the sandy sediments (i.e. at well 15/9-13 and 16/4-2, Chapter II, Fig. II.4).

S.III.2.1.4 Quantifying dissolved CH_4 and CH_4 oxidation rates in the water column. During cruise CE12010 (July-August 2012), seawater samples were taken with Niskin bottles attached to a video-guided CTD or operated by ROV Kiel 6000[37]. At wells 15/9-13 and 16/7-2 seawater was sampled near the seafloor and additionally through the water column at well 15/9-13. No water samples were recovered at well 16/4-2. For dissolved gas analysis, subsamples were transferred bubble-free into 100 ml headspace vials immediately after recovery of the Niskin Water Sampler Rosette. Dissolved gases were released from the seawater samples by headspace technique (headspace of 10 ml of Ar 4.5). After adding 50µl of saturated $HgCl_2$- solution the vials were stored at 4°C. Concentration determination of CH_4 released into the headspace was conducted by using onboard gas chromatography (Shimadzu 2010, for results see Chapter III, Tab. III.1 and Supp. Fig. III.2).

To assess CH_4 oxidation rates (r_{MOx}) in the water column, subsamples were transferred bubble-free into ~23 ml headspace vials and closed with grey bromo-butyl stoppers (Helvoet Pharma, Belgium), immediately after recovery of the Niskin bottles. Shortly after sampling, a 6 µl gas bubble of ^{14}C-CH_4:N_2 gas (0.25 kBq) was added to the subsamples, which were then incubated for 2 days in the dark at *in situ* temperature (~8°C). After 2 days, samples were fixed in 4 pellets of NaOH and stored at 4°C until rate measurements were performed in the home laboratory. Radioactive substrate and product pools were quantified as described by Blees and colleagues[38-39] to determine the rate constant. Assuming sufficient oxygen supply during incubation, CH_4 oxidation rates were then calculated according to:

$$r_{MOx} = k \cdot [CH_4] \qquad \text{Supp. Eq. III.1}$$

where k is the first-order rate constant and $[CH_4]$ denotes the concentration of CH_4 in seawater (for results see Tab. III.1). All rates were determined in quadruplicates. Killed controls (addition of 200 µl saturated $HgCl_2$ at the start of the incubation) were analyzed for each incubation period. Recovery of the radioactive tracer was >95%. The detection limit of the rate depends on the amount of radioactive CH_4 added and the initial CH_4 concentration and varied between 0.01 and 6.45 nM day^{-1} depending on the sample. Above well 15/9-13, all rates were below detection limit. Above well 16/7-2, one out of three sampling locations showed rates below detection limit. For the other two locations above well 16/7-2, rates were 0.19±0.07 and 1.40±0.83 nM day^{-1} (σ_n/SE, n=4).

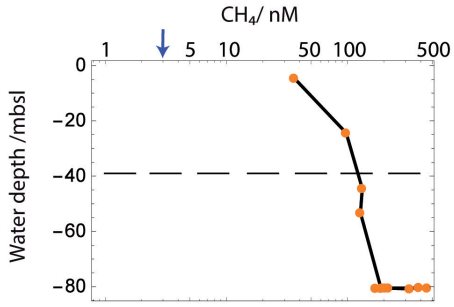

Spplementary Figure III.2: Dissolved CH_4 concentrations in the water column. Depth profile showing the concentration of dissolved CH_4 in the water column (orange bullets) based on measurements during CE12010 31-CTD7 at well 15/9-13. The dashed line indicates the depth of the thermocline and the blue arrow represents the equilibrium concentration of CH_4 in the surface mixed layer (i.e. 3 nM)[21] with respect to the atmospheric partial pressure of CH_4.

S.III.2.2 Extrapolation of drilling-induced CH_4 leakage to the North Sea scale

S.III.2.2.1 Seismic mapping of shallow gas and the probability of wells to leak. The examination of the probability of wells to leak shallow gas is based on the analysis of an industrial 3-D seismic data set ST98M3, which is the result of merging seven independently acquired and processed sub-datasets. Detailed information regarding processing parameters of the specific subsets are not available, while the processing sequence for merging the data included resampling, filtering, phase rotation and amplitude adjustments. The final 3-D seismic cube shows positive acoustic impedance contrasts as positive amplitude (blue) followed by negative amplitude (yellow). The bin-size is 12.5 m and the vertical resolution is ~10 m (dominant frequency 45 Hz, seismic velocity of ~1,800 m/s for the upper 400 m and ~2,000 m/s below). The dataset extends 62 km from north to south and 46 km from east to west covering an area of more than 2,000 km² (Chapter III, Fig. III.1a).

Shallow gas pockets in the uppermost 1,000 m of sediment, identified by high amplitude anomalies in the seismic data[33], were mapped and assigned to stratigraphic units[13] using the seismic analysis software Petrel (Schlumberger). Assuming that leakage of shallow gas can potentially occur along any type of well (producing, injecting, abandoned, dry), as long as there is a shallow gas accumulation in its vicinity, an increased permeability induced by the drilling operation, and a driving force for gas movement, which could be buoyancy or excess pore pressure, we correlated the well paths of a total of 55 wells in the seismic study area with locations of shallow gas pockets. 50 sidetracked and multilateral wells were excluded for the correlation analysis because they separate from the main well in the deeper subsurface, which was not the scope of this study. Further, 55 wells, having platforms at the sea surface, were deselected because no 3-D seismic data of the overburden sediments existed. The probability of wells to leak shallow gas was then determined by the fraction of wells which penetrate high amplitude anomalies in the shallow subsurface (i.e. 18 of 55 selected wells, Chapter III, Fig. III.1) and is required for further extrapolation of CH_4 leakage to the North Sea scale.

S.III.2.2.2 Modeling the fate of leaking CH_4. A numerical bubble dissolution model was used to calculate the bubble-mediated CH_4 flow to the atmosphere by a single rising gas bubble. The simulation of a single rising bubble seems to be justified because only single bubble streams were observed at the investigated wells (Supp. Fig. III.1) with very little to no interaction between the bubbles, or plume dynamics (upwelling). Assuming that the release of single bubble streams is representative for leaky wells in the North Sea, the model simulates the shrinking of a gas bubble due to dissolution in the water column, its expansion due to decreasing hydrostatic pressure in the course of its ascent and gas stripping, and the final gas transport to the atmosphere. A set of coupled ordinary differential equations (ODEs) was solved numerically describing these processes for each of the involved gas species (CH_4, N_2, and O_2; Supp. Eq. III.2) and the bubble rise velocity (Supp. Eq. III.3), thus time being the only independent variable. Thermodynamic and transport properties of the gas components, such as molar volume, gas compressibility, and gas solubility in seawater, were calculated from respective equations of state[40-43], and empirical equations for diffusion coefficients[44], mass transfer coefficients[45], and bubble rise velocities[46], taking into account local pressure, temperature and salinity conditions as measured by CTD casts. Implemented equations and values are provided in Chapter II Tab. II.2. The ODE system is solved using finite difference methods implemented in the NDSolve object of Mathematica (i.e. LSODA)[47].

The mass exchange of gas components across the bubble surface is generally described as[46,48-49]:

$$dN_i / dt = 4\pi r_{eq}^2 \cdot K_{L,i} (C_{a,i} - C_{eq,i}) \qquad \text{Supp. Eq. III.2}$$

where i is the ith gas species, N, is the amount of gas in the bubble, $4\pi \cdot r_{eq}^2$ is the surface area of the equivalent spherical bubble, K_L is the specific mass transfer rate between gas phase and aqueous phase, C_a is the dissolved gas concentration, and C_{eq} is the gas solubility. All of the above variables are functions of the water depth, z, i.e. pressure, temperature and salinity (see Chapter II Tab. II.2 for details and references). The change of the vertical bubble position is related to the bubble rise velocity, v_b (Chapter II Tab. II.2):

$$dz / dt = v_b \qquad \text{Supp. Eq. III.3}$$

Model simulations were performed based on boundary conditions obtained in the CNS from Sea-Bird 9 plus CTD data of August 2012 (Chapter II Tab. II.2) and run for different initial bubble sizes (ranging between 1.0 to 4.0 mm radius, in accordance to radii of the combined bubble size distribution, Supp. Section III.2.1.3), initially containing only CH_4. Simulated water depths ranged between 20 and 150 m in accordance to those important for the CH_4 bubble transport to the SML of the North Sea. Larger water depths were not considered

because additional model runs revealed that the combined bubble size distribution completely loses its initial CH_4 content in the deep layer of the North Sea when released from more than 150 m depth, Supp. Fig. III.3.

The CH_4 emissions from leaky wells to the atmosphere were calculated distinguishing between direct emissions via bubble transport and indirect emissions via the diffusive outgassing of CH_4 dissolving in the surface mixed layer (SML, i.e. the upper 50 m of the North Sea water column)[26]. The direct bubble CH_4 transport to the atmosphere was calculated from the remaining/residual amount of CH_4 in the bubble, when it reaches the sea surface, N_S, i.e.

$$N_S(r,z) = N_0(r,z) - \int_{t=0}^{tmax} dN(r,z)\, dt \qquad \text{Supp. Eq. III.4}$$

,where N_0 is the initial amount of CH_4 in the bubble and *tmax* is the time required by the gas bubble to travel to the sea surface and is determined numerically by the bubble dissolution model. The amount of CH_4 dissolving in the SML of the North Sea (N_{SML}) was calculated by integrating the rate of CH_4 bubble dissolution over the time which is needed by the bubble to travel through the upper 50 m of the water column (i.e. *t50* to *tmax*, both determined numerically by the bubble dissolution model):

$$N_{SML}(r,z) = \int_{t50}^{tmax} dN(r,z)\, dt \qquad \text{Supp. Eq. III.5}$$

Both, the residual CH_4 and the CH_4 dissolving in the SML depend on the initial bubble size (r) and water depth (z) and were normalized to the corresponding N_0. The relative amount of CH_4 at the sea surface and in the SML with respect to the initial bubble CH_4 content, i.e. $\Omega_S(r,z) = N_S(r,z) / N_0(r,z)$ and $\Omega_{SML}(r,z) = N_{SML}(r,z) / N_0(r,z)$, are referred to as the transport efficiencies of a single gas bubble to the sea surface and to the SML, respectively.

A transfer function was fitted to numerical results using the non-linear least-squares fit algorithm. The fit describes the CH_4 transport efficiency of a single bubble to the sea surface as a function of the initial bubble size (r) and the leakage depth (z):

$$\Omega_S(r,z) = e^{-\frac{a}{r^b} z} \qquad \text{Supp. Eq. III.6}$$

	Correlation matrix for parameters		Least squares estimates of parameters	Standard error (1-σ)
	a	b		
a	1	-0.97	-0.156	0.007
b	-0.97	1	1.26	0.04

The variance, s^2 of the residuals is better than 0.00013 and the linear correlation coefficient of the fit-curve to the numerical data is better than 0.99. The fit function is valid for initial

bubble radii ranging between 1 and 4 mm initially containing only CH_4 and for the given physicochemical properties of the water column obtained in the CNS from Sea-Bird 9 plus CTD data of August 2012 (Chapter II Tab. II.2). By applying Supplementary Eq. III.6, the mass transfer of gases other than CH_4, N_2, and O_2, as well as the development of upwelling flows are considered to be negligible for the CH_4 transport to the sea surface.

Because leaky wells expelled a range of initial bubble sizes, the transport efficiencies $\Omega_S(r,z)$ and $\Omega_{SML}(r,z)$ were calculated for each bubble size and weighted by its volumetric contribution, V_0, to the total emitted gas bubble volume, V_Ψ. Integrating this weighted bubble transport efficiencies over the entire bubble size spectrum (Ψ) gives the total CH_4 transport efficiency to the SML (Ω_{SML}) and to the sea surface (Ω_S) with respect to the initial CH_4 release at the seafloor, respectively:

$$\Omega_S(\psi,z) = \frac{1}{MI}\int_{r(min)}^{r(max)} \Omega_S(r,z)\frac{V_0\,(r)}{V_\psi}\,dr \qquad \text{Supp. Eq. III.7}$$

$$\Omega_{SML}(\psi,z) = \frac{1}{MI}\int_{r(min)}^{r(max)} \Omega_{\mathrm{SML}}(r,z)\frac{V_0\,(r)}{V_\psi}\,dr \qquad \text{Supp. Eq. III.8}$$

where, *r(min)*, and *r(max)* are the minimum and maximum radii of the bubble size spectrum Ψ, respectively, and *MI* is the measurement interval between individual bubble sizes (i.e. 0.1 mm). V_0 and V_Ψ refer to optical size measurements at individual gas streams of the investigated wells, which were conducted to determine the combined bubble size spectrum (Chapter II Fig. II.4). Applying Supplementary Eq. III.7 and III.8, we assume that there is no change in the weighted volumetric contribution of each bubble size to the total emitted bubble volume (i.e. $V_0(r) / V_\Psi = const.$), so that the relative distribution of bubble sizes is considered to be constant, although the release frequency of bubbles may change due to a variability of the seabed gas flow. This means that at a constant mass flow (i.e. per-well leakage rate) a decrease in the hydrostatic pressure (i.e. leakage depth) increases the rate of bubble formation but not their size distribution, as generally validated for seeps with a low gas flow[27]. Transfer functions were fitted to numerical results of Supplementary Equation III.7 and III.8, respectively using the non-linear least-squares fitting algorithm "NonlinearModelFit" of Mathematica (Supp. Fig. III.3). The fit-curves describe the transport efficiency of the bubble size distribution to the sea surface (Supp. Eq. III.9) and to the SML (Supp. Eq. III.10) with respect to the seabed CH_4 flow and as a function of the leakage depth (z), respectively:

$$\Omega_S(\psi,z) = e^{-a\ z} \qquad \text{Supp. Eq. III.9}$$

Parameter	Least squares estimates of parameter	Standard error (1-σ)
a	0.0435	0.0007

$$\Omega_{SML}(\psi,z) = \frac{1}{1+e^{z-50}}\ a{\cdot}z^{0.5} + \frac{1}{1+e^{50-z}}\cdot\frac{1}{b+c*z^{4.6}} \qquad \text{Supp. Eq. III.10}$$

	Correlation matrix for parameters			Least squares estimates of parameters	Standard error (1-σ)
	a	b	c		
a	1	0.3	-0.2	0.127	0.003
b	0.3	1	-0.8	0.73	0.04
c	-0.2	-0.8	1	$6.1{\cdot}10^{-9}$	$4{\cdot}10^{-10}$

The variance, s^2, of the fits is 0.0001 and 0.0005 for the transport efficiency to the sea surface and to the SML, respectively. The numerical accuracy of the model, determined from mass balance errors, was overall better than 99.9%. Supplementary Eq. III.9 and III.10 are required for the North Sea-wide extrapolation of drilling-induced CH_4 emissions from the seafloor into the atmosphere (Supplemetary Section III.2.2.4).

S.III.2.2.3 The well inventory and bathymetry of the North Sea. To extrapolate CH_4 leakage to the North Sea scale, all 15,781 offshore wellbore data (including the well identification, location, status, and type) were incorporated into a database created in ArcGIS (v10.1), sourced from online datasets published by governmental energy departments and regulation agencies in 2012 to 2013 (Supp. Tab. III.2, Supp. Fig. III.4). Filters (queries) were applied to categorize and identify the wells for analysis (Supp. Tab. III.3). As leakage of shallow gas can potentially occur along any type of well, whether it is producing hydrocarbons, injecting fluid into a reservoir, was dry, or has been abandoned, we selected all types of wells (i.e. 11,122 wells, see Supp. Tab. III.3), excluding extra sidetracked and multilateral wells which tend to separate from the main well in the deeper subsurface (i.e. < 1,000 m). Sidetracked and multilateral wells were deselected manually from the database following the guidelines for designation of wells and wellbores[30]. In addition, the EMODnet North Sea bathymetry with a spatial resolution of 5 minutes (available at: http://www.emodnet-bathymetry.eu; Supp. Fig. III.4) was incorporated into the ArcGIS database. Bathymetric data were required to estimate CH_4 emissions into the atmosphere, which are depth-dependent.

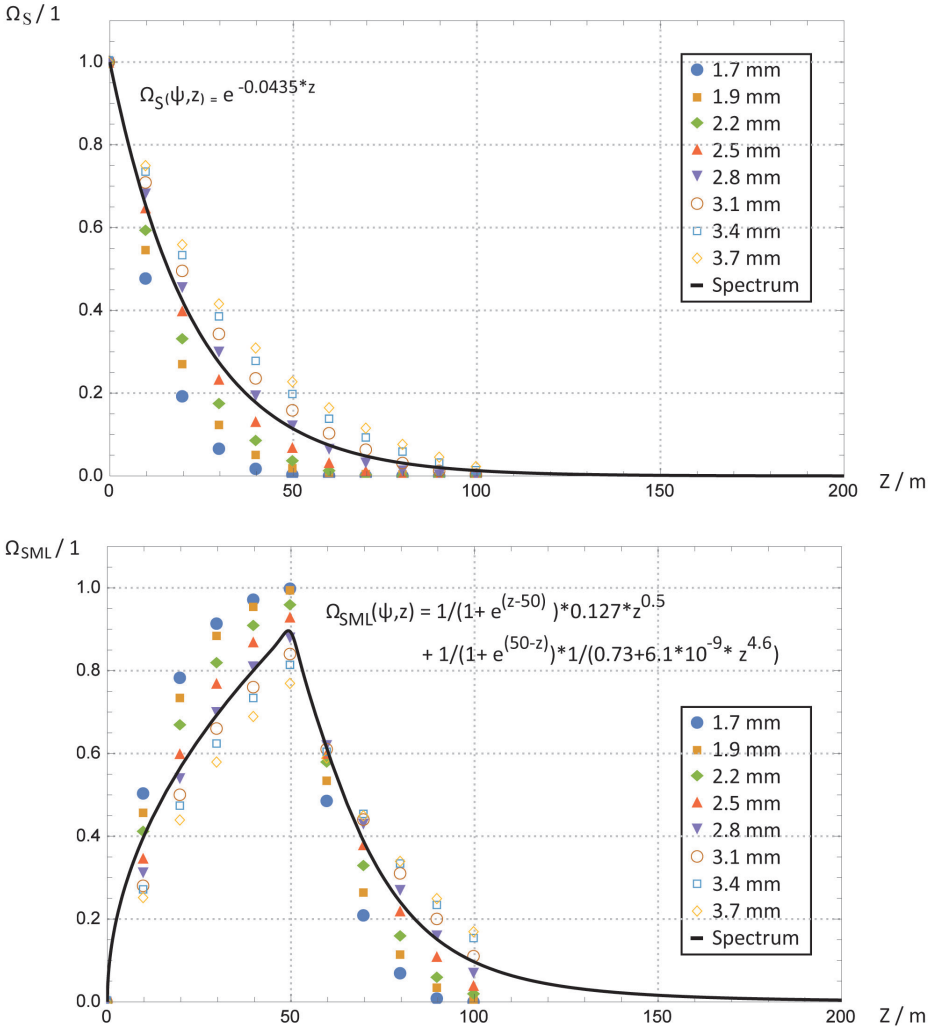

Spplementary Figure III.3: Numerical results of the bubble dissolution model. Model results show the CH_4 bubble transport efficiency to the surface mixed layer (Ω_{SML}) and to the sea surface (Ω_S) of the North Sea, respectively as a function of the leakage depth (z) and for initial bubble radii ranging between 1.7 to 3.7 mm (in accordance to bubble sizes of the combined bubble size distribution, Fig. II.4). The CH_4 transport efficiency of the combined bubble size distribution (black curve;) was determined by fit curves to the data using the non-linear least-squares fitting algorithm "NonlinearModelFit" of Mathematica. The variance, s^2, of the fit-curves is better than 0.001 and 0.005 for $\Omega_S(\Psi,z)$ and $\Omega_{SML}(\Psi,z)$, respectively.

Spplementary Table III.2: Source data of the North Sea well inventory.

Country	Data Source (Date)	Link
Norway	Norwegian Petroleum Directorate (Sept. 2013)	http://factpages.npd.no/ReportServer?/FactPages/geography/geography_all&rs:Command=Render&rc:Toolbar=false&rc:Parameters=f&IpAddress=1&CultureCode=en
United Kingdom	Department of Energy and Climate Change (Aug. 2013)	http://www.gov.uk/oil-and-gas-offshore-maps-and-gis-shapefiles
Germany	Niedersächsisches Landesamt für Bergbau, Energie und Geologie (Jul. 2013)	http://nibis.lbeg.de/cardomap3/?TH=BOHRKW
Denmark	Danish Energy Agency (Jan. 2012)	http://www.ens.dk/en/oil-gas/oil-gas-related-data/wells
Netherland	Netherland Oil and Gas Portal (Jun. 2013)	http://http://www.nlog.nl/en/activity/activity.html

S.III.2.2.4 Extrapolation of drilling-induced CH_4 leakage to the North Sea scale. CH_4 leakage from wells into the North Sea and atmosphere was calculated by extrapolating data obtained in the CNS (leakage rates, initial bubble size distributions, and the likelihood of wells to leak) and results of a numerical bubble dissolution model (Supplementary Section III.2.2.2) on the EMODnet North Sea bathymetry and combining publicly available data on drilled wells (Supplementary Section III.2.2.3) using the geographical information system software ArcGIS v10.1.

In total, 11,122 active and inactive wells were selected for the North Sea-wide CH_4 release quantification excluding sidetracks of wells (Supp. Tab. III.3). The North Sea was subdivided into equal area polygons of 5x5 km^2 using a Cylindric Equal Area projection and the "Fishnet" tool of ArcGIS v.10.1. Spatial joining of the selected wells and bathymetric data gives each polygon a summary of numeric attributes that fall inside it, i.e. the average water depth (z) and a count field showing how many points fall inside it, i.e. the number of wells.

The seabed CH_4 flow (Q_{SF}) was calculated for each of these polygons multiplying the leakage probability (LP) of 33% for the wells (Supplementary Section III.2.2.1), the number of wells located inside each polygon (AF, activity factor), and the per-well CH_4 leakage rate (LR) of 2.5 and 8 t yr^{-1} for the conservative and maximum estimate, respectively:

$$Q_{SF} = AF \cdot LP \cdot LR \qquad \text{Supp. Eq. III.11}$$

For each polygon, the resulting CH_4 flow from the surface water into the atmosphere (Q_{Atm}) was then estimated applying a transfer function describing the CH_4 bubble transport efficiency

Spplementary Table III.3: Classification of wells in the North Sea (as of 2012-2013).

Well Status	Main Wells/Wellhead	Additional sidetracked & multilateral wells	Total number
Active[a]	2,818	1,629	4,447
Inactive[b]	7,498	2,637	10,135
Shut-in[c]	5,636	1,696	7,332
Unknown status[d]	806	393	1,199
Total	11,122[e]	4,659	15,781

[a] including injection, production, and open wells
[b] including temporarily and permanently plugged and abandoned wells
[c] including only permanently plugged and abandoned/ shut-in wells; excluding wells in the Danish Sector because here no well status was reported in the source data
[d] including wells where no well status or type was reported, and Norwegian wells which have been completed to well, or predrilled with no further specification
[e] selected for analysis

to the sea surface and to the SML of the North Sea (Supplementary Section III.2.2.2, Supp. Eq. III.9 and Supp. Eq. III.10) as a function of the seabed CH_4 flow (Q_{SF}) and average water depth of the polygon (z):

$$Q_{Atm,i} = Q_{SF,i} \cdot \Omega_{SML,i/\,S,i}(\psi,z) \qquad \text{Supp. Eq. III.12}$$

, where i is the leakage scenario (the conservative or maximum leakage estimate), and Ψ is the common bubble size distribution (Supplementary Section III.2.1.3). Applying Supplementary Eq. III.12, we assume no variation of initial bubble sizes over the extended area of the North Sea (Supplementary Section III.2.1.3) and that essentially all of the CH_4 reaching the SML will be transferred into the atmosphere.

All determined flow estimates of individual polygons, were added to calculate lower and upper bounds of the total CH_4 ebullition from the seafloor and into the atmosphere. All estimates are reported as arithmetic means of lower and upper bounds and their standard deviation (1σ).

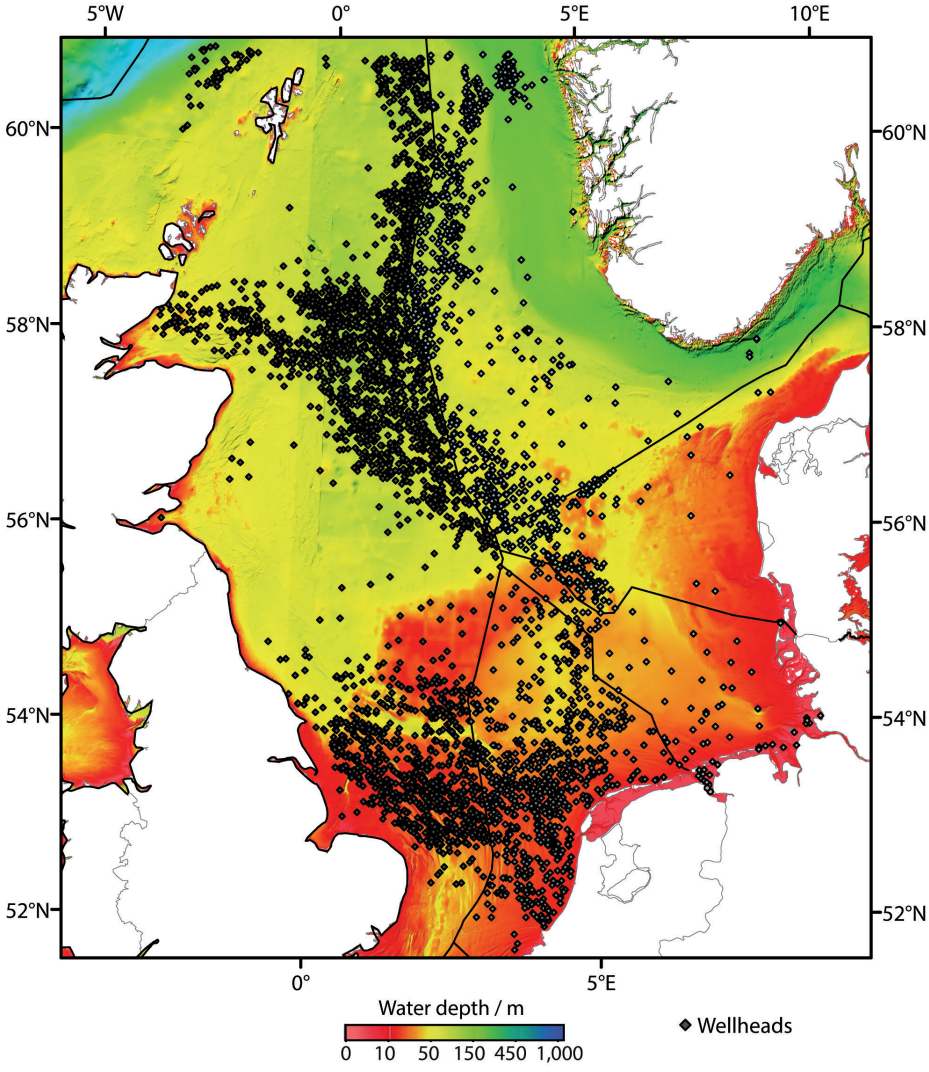

Spplementary Figure III.4: Bathymetric map of the North Sea and the surface location of the 11,122 wells (greyish diamonds). The maps geographic coordinate system refers to WGS84 UTM Zone 31N and is displayed in Mercator Projection.

S.III.2.2.5 Leakage from oil and gas infrastructure in a North Sea CH_4 context. We recalculated the CH_4 budget of the North Sea compiling quantitative literature data on major sources and sinks for CH_4 and adding the so far unrecognized emissions from leaky wells quantified in this study (for results see Chapter III Fig. III.2 and Supp. Tab. III.4).

Existing estimates on North Sea-wide CH_4 emissions into the atmosphere are based on the extrapolation of point measurements of CH_4 concentrations in the near-surface seawater and the atmosphere[17,20,25]. The reported diffusive emissions into the atmosphere range from

10-34 kt yr^{-1} and are believed to already include the diffusive contribution of leaky wells (3-9 kt yr^{-1}), because their CH_4 anomalies are distributed over a broad area of the North Sea (Fig. III.3) and have thus, likely been detected during the measurement campaigns. In contrast, the blowout well 22/4b constitutes a very local, high flow CH_4 source in the British Sector. It was created in 1990, when Exxon Mobile accidently drilled into an over-pressurized shallow gas pocket. Its contribution to the atmospheric CH_4 flow was detected in only one[20] of the three surveys[17,20,25], 3.5 years after the incident occurred. According to the data of Rehder et al. (1998) [20], well 22/4b emitted additional 7-12 kt yr^{-1} of anthropogenic CH_4 into the atmosphere, increasing North Sea-wide atmospheric emissions to up-to 50 kt yr^{-1} [20]. More recent studies suggest that the blowout well releases 2-25 kt yr^{-1} of CH_4 from the seabed[51-52], of which particularly nothing is directly transported into the atmosphere[53]. The lack of direct bubble transport suggests that essentially all of the CH_4 released at the seabed dissolves in the water column and reaches the atmosphere by outgassing on an annual basis. Current atmospheric emissions of well 22/4b are thus, believed to be similar to those quantified by Rehder et al. (1998)[20] in their earlier conservative study. To incorporate these new data of drilling-induced CH_4 emissions, we recalculated the budget. Total emissions from the North Sea into the atmosphere comprise the range of existing quantifications on the diffusive gas exchange (10-34), the additional emissions from well 22/4b (2-25)[51-52], and direct bubble ebullition from leaky wells (1-3 kt yr^{-1} of CH_4) (Supp. Tab. III.4).

The high super-saturation of the North Sea surface waters and the resulting atmospheric degassing of CH_4 constitute the major sink in the CH_4 budget (12 to 59 kt yr^{-1}) (Supp. Tab. III.4). Adding the amount of CH_4, which is exported to the North Atlantic Ocean (8 kt yr^{-1})[20], the sinks for CH_4 are almost 20-times larger than the known natural sources (rivers, the Waddden Sea, and natural seeps). Measured CH_4 oxidation rates in the water column were very low (Chapter III Tab. III.1), such that the microbial sink for CH_4 is expected to be negligible (Supp. Tab. III.4). The North Sea-wide CH_4 input from drilling-induced leakage (leaky wells and blowout well 22/4b), thus likely contributes significantly to the CH_4 sinks, constituting ~60% of the total sinks (see Chapter III Fig. III.2 and Supp. Tab. III.4). It should, however, be noted that emissions from natural seeps are based on only few quantitative measurements (Supp. Tab. III.4). Thus, their contribution to the CH_4 budget is currently poorly constrained. Uncertainties attached to the localization of individual CH_4 sources at the seabed and the quantification of their emissions are in line with Judd et al. (1997)[12], who suggested that emissions from natural seeps on the UK continental shelf have been significantly underestimated. However, their reported values of 120-3,500 kt yr^{-1} of CH_4 are orders of magnitude higher than measurements of other CH_4 sources and sinks in the North Sea suggest. Due to this inconsistency, we disregarded their estimates in our reassessment of the North Sea CH_4 budget.

Spplementary Table III.4: Sources and sinks for CH_4 in the North Sea. Bold values have been taken to recalculate the CH_4 budget of the North Sea.

CH_4 Sources	Input /t yr^{-1} of CH_4	Reference
Natural seeps		
Scanner Pockmark Field*	0.1-13	Judd and Hovland, 2007 and references therein[21]; Hovland et al., 2012 and references therein[24]
UK Block 15/25	7±?	Judd, 2004 and references therein[23]
Anvil Point UK	68±?	Judd, 2004 and references therein[23]
Torre Bay Firth of Fourh	1-2	Judd, 2004 and references therein[23]
Tommeliten	26-42	Schneider von Deimling et al., 2011 (lower bound)[22]; Judd, 2004 (upper bound)[23]
Norwegian Block 1/9 Ekofisk**	52±?	Judd and Hovland, 2007 and references therein[21]; Hovland et al., 2012 and references therein[24]
Total input seeps	**>0.2·10³**	
Rivers		
Rhine	339	Upstill-Goddard et al., 2000[17]
Weser	86	Grunwald et al., 2009[18]
Wash	61	Upstill-Goddard et al., 2000[17]
Elbe	35	Rehder et al., 1998 [20]; Grunwald et al., 2009 and references therein[18]
Humber	5	Upstill-Goddard et al., 2000[17]
Tyne	2	Upstill-Goddard et al., 2000[17]
Sheld	22-34	Scranton and McShane, 1991[19]
Total riverine input	**0.6±? ·10³**	
Wadden Sea		
Spiekeroog Island back barrier area	53	Grunwald et al., 2009[18]
East Frisian back barrier area	125	Grunwald et al., 2009[18]
Entire back barrier tidal flats* **	**1-1.2·10³**	Based on Grunwald et al., 2009 and references therein[18]
Hydrocarbon infrastructure		
Blowout well 22/4b	2-25·10³	Sommer et al., revised (lower bound)[51]; Leifer, revised (upper bound)[52]
Leaky Wells	9-29·10³	This study
Total wells	**11-55·10³**	

CH_4 Sinks	Input /t yr^{-1} of CH_4	Reference	
Atmosphere			
Diffusive gas exchange (excl. 22/4b)	$10\text{-}34{\cdot}10^3$	Bange et al., 1994[25] and Upstill-Goddard et al., 2000 [17](lower bound); Rehder et al., 1998[20] (upper bound)	
Diffusive gas exchange (incl. 22/4b)	$20\text{-}50{\cdot}10^3$	Rehder et al., 1998[20]	
Potential diffusive contribution of leaky wells	$3\text{-}9{\cdot}10^3$	This study	
Potential direct ebullition from leaky wells	$1\text{-}3{\cdot}10^3$	This study	
Total atmospheric emissions	**$13\text{-}62{\cdot}10^3$**	(Range comprising the diff. Gas exchange excl. 22/4b, recent gas emissions of well 22/4b, and direct ebbullition from leaky wells)	
Microbial CH_4 oxidation****	**$0.02{\cdot}10^3\pm?$**	This study	
CH_4 export to the North Atlantic Ocean	**$8{\cdot}10^3$**	Rehder et al., 1998[20]	
Total CH_4 Budget	Total CH_4 sources	Total CH_4 sinks	Imbalance
kt yr^{-1} of CH_4	13-58	21-70	8-12

*Assuming a gas flow of 5.7 L h^{-1}seep^{-1} at STP[21] and 3 active seeps[25], the Scanner Pockmark field emits 0.1 t $yr^{-1}$of CH_4 (lower bound). Assuming a seabed gas flow of 1 m^3 d^{-1} seep^{-1} [25], a molar volume of CH_4 of 1.34 L mol^{-1} at 160 m water depth, and 3 active seeps[24], the Scanner Pockmark field emits ~13 t yr^{-1} of CH_4 (upper bound).
** Based on a seabed emission of ~24 m^3 d^{-1} of CH_4 [21,24] and assuming a molar volume of CH_4 of 2.69 L mol^{-1} at 75 water depth, the Norwegian Block 1/9 emits ~52 t yr^{-1} of CH_4.
*** We extrapolated the CH_4 export of the East Frisian back barrier area (125 t yr^{-1} of CH_4 per 197 km^2)[18] on the entire back barrier tidal flat area from Den Helder to Esbjerg (1,188-3,364 km^2)[18] assuming that the CH_4 concentrations and the water outflow of the Spiekeroog study area[18] are representative.
**** We estimated the loss of CH_4 by methanotrophic communities at leaky wells, based on the maximum measured CH_4 oxidation rate of 1.4 nM d^{-1}(this study), a leakage area of 10 m^2 well^{-1} [16], and an average leakage depth of 80 m (in accordance to the spatial distribution of wells and the North Sea bathymetry).

Overall, the imbalance of the budget suggests that an additional CH_4 input of ~10 kt yr^{-1} is required to close the budget, either by natural or anthropogenic sources. This remains, however, in the range of uncertainty of the total budget.

S.III.2.2.6 Sources of uncertainty in our estimates. The range of uncertainty of shallow gas leakage in the North Sea is substantial, as might be expected from the current state of knowledge of leaky wells, mainly depending on the representativeness of data obtained in the Norwegian CNS. There is a large uncertainty in our estimates related to the temporal and spatial variability of per-well leakage rates that might, in addition to sediment properties

and tidal pressure fluctuations, be driven by overpressure in the shallow gas reservoir, or by differences in the gas supply. Further uncertainty is associated to the probability of wells to leak shallow gas. Our conservative estimate for CH_4 leakage from hydrocarbon wells in the North Sea is based on the lower two measured emission rates and the assumption that wells poking through shallow gas pockets will leak, which is corroborated by observed ebullition of biogenic gas at wells 15/9-13 and 16/7-2 (this study) as well as 15/9-11 and 15/9-16[54]. However, leakage was also found at well 16/4-2, where no presence of free gas could be imaged in the seismic data (Chapter III Fig. III.1b, note that the spatial resolution of the seismic data is ~10 m), thus clearly drawing gas from larger distances. The lower emission estimate is thus definitely conservative, because per-well leakage rates and the number of leaky wells might have been underestimated. Surveying for leaky wells and quantifying their ebullition rates (including longer time-series) is clearly needed in order to better constrain the North Sea CH_4 budget.

Atmospheric emission estimates bear further uncertainty arising from three additional factors: (1) temporal and spatial variability of the bubble chain dynamics (upwelling), (2) variability of initial bubble sizes, and (3) seasonal/ inter-annual changes of seawater conditions. The latter may significantly affect the diffusive outgassing of CH_4 due to the seasonal deepening and breakdown of the thermocline[20,22,26,51] and the efficient ventilation of the entire water column during frequent fall and winter storms, which both should aid annual diffusive CH_4 emissions. No significant inter-annual variability is expected in the rate of direct CH_4 ebullition to the atmosphere because the bubble CH_4 transport is independent of the water column stratification and also nearly temperature-independent. This is because the increase in gas transfer velocity (K_L) compensates the decrease in gas solubility at elevated temperature. The lower atmospheric emission estimate is thus definitely conservative because the gas transport to the atmosphere might has been underestimated due to the seasonal increase in the ventilation of the water column or the evidence of upwelling flows at high-emitting seeps. Uncertainties related to initial bubble sizes remain, which might, in addition to spatial heterogeneities in the sediment properties, be driven by variations in the seabed gas flow, or bottom current intensity, or changes in the hydrostatic pressure[27].

References:

1. Ciais, P., et al. *Climate Change 2013: The Physical Science Basis. Contribution of Working Group I to the Fifth Assessment Report of the Intergovernmental Panel on Climate Change*, in: Stocker, T.F., Qin, D., Plattner, G.-K., Tignor, M., Allen, S.K., Boschung, J., Nauels, A., Xia, Y., Bex, V., Midgley, P.M. (Eds.). IPCC, Cambridge, UK, pp. 465-570 (2013).

2. Davies, R.J., et al. Oil and gas wells and their integrity: Implications for shale and unconventional resource exploitation. *Mar. Petrol. Geol.* **56**, 239-154 (2014).

3. NORSOK Standard D-010, 2004. http://www.standard.no/PageFiles/1315/D-010r3.pdf

4. Gurevich A.E., Endres, B.L., Robertson, J.O., Chilingar, G.V. Gas migration from oil and gas fields and associated hazards. *J. Petrol. Sci. Eng.* **9**, 223-238 (1993).

5. Allen, D.T., et al. Measurements of methane emissions at natural gas production sites in the United States. *Proc. Natl. Acad. Sci. U.S.A.* **110**, 17768-17773 (2013).

6. Alvarez, R.A., Pacala, S.W., Winebrake, J.J., Chameides, W.L., Hamburg, S.P. Greater focus needed on methane leakage from natural gas infrastructure. *Proc. Natl. Acad. Sci. U.S.A.* **109**, 6435-6440 (2012).

7. Caulton, D.R., et al. Toward a better understanding and quantification of methane emissions from shale gas development. *Proc. Natl. Acad. Sci. U.S.A.* **111**, 6237-6242 (2014).

8. Miller, S.M., et al. Anthropogenic emissions of methane in the United States. *Proc. Natl. Acad. Sci. U.S.A.* **110**, 20018-20022 (2013).

9. Schneising, O., et al. Remote sensing of fugitive methane emissions from oil and gas production in North American tight geologic formations. *Earth's Future* **2**, 548-558 (2014).

10. Zhang, Y., Zhao, H., Zhai, W., Zang, K., Wang, J. Enhanced methane emissions from oil and gas exploration areas to the atmosphere – The central Bohai Sea. Mar. Pollut. Bull. 81, 157-165 (2014).

11. Brufatto, C., et al. From mud to cement - Building gas wells. *Oilfield Rev.* **15**, 62-76 (2003).

12.Judd, A., et al. Contributions to atmospheric methane by natural seepage on the U.K. continental shelf. *Mar. Geol.* **140**, 427-455 (1997).

13. Karstens, J., Berndt, C. Seismic chimneys in the Southern Viking Graben- Implications for paleo fluid migration and overpressure evolution. *Earth Planet. Sci. Lett.* **412**, 88-100 (2015).

14. Schroot, B.M., Klaver, G.T., Schüttenhelm, R.T.E. Surface and subsurface expressions of gas seepage to the seabed- examples from the Southern North Sea. *Mar. Petrol. Geol.* **22**, 499-515 (2005).

15. Schlüter, M., Jerosch, K. Digital Atlas of the North Sea, version 0.9. Alfred Wegener Institute for Polar and Marine Research et al. hdl:10012/epic.34893.d001 (2009).

16. Vielstädte, L., et al. Quantification of methane emissions at abandoned gas wells in the Central North Sea. *Mar. Petrol. Geol.* **68**, Part B, 848–860, (2015).

17. Upstill-Goddard, R.C., Barnes, J., Frost, T., Punshon, S., Owens, N.J.P. Methane in the southern North Sea: Low-salinity inputs, estuarine removal, and atmospheric flux. *Glob. Biogeochem. Cycles* **14** (4), 1205-1217 (2000).

18. Grunwald, M., et al. Methane in the southern North Sea, spatial distribution and budgets. *Est. Coast. Shelf Sci.* **81**, 445-456 (2009).

19. Scranton, M.I., McShane, K. Methane fluxes in the southern North-Sea – the role of European rivers. *Cont. Shelf Res.* **11**, 37–52 (1991).

20. Rehder, G., Keir, R.S., Suess, E., Pohlmann, T. The multiple sources and patterns of methane in North Sea waters. *Aquat. Geochem.* **4**, 403-427 (1998).

21. Judd, A.G., Hovland, M.. *Seabed Fluid Flow- The Impact on Geology, Biology and Marine Environment* (Cambridge University Press, New York, 475 pp, 2007).

22. Schneider von Deimling, J., et al. Quantification of seep-related methane gas emissions at Tommeliten, North Sea. *Cont. Shelf Res.* **31**, 867-878 (2011).

23. Judd, A.G. Natural seabed gas seeps as sources of atmospheric methane. *Environ. Geol. 46*, 988-996 (2004).

24. Hovland, M., Jensen, S., Fichler, C. Methane and minor oil macro-seep systems – Their complexity and environmental significance. *Mar. Geol.* **332-334**, 163-173 (2012).

25. Bange, H.W., Bartell, U.H., Rapsomanikis, S., Andreae, M.O. Methane in the Baltic and North Seas and a reassessment of the marine emissions of methane. *Glob. Biogeochem. Cycles* **8**, 465–480 (1994).

26. Thomas, H., et al. The carbon budget of the North Sea. Biogeosciences 2, 87-96 (2005).

27. Dewar, M., Wei, W., Chen, B. Small-scale modelling of the physicochemical impacts of CO_2 leaked from sub-seabed reservoirs or pipelines within the North Sea and surrounding waters. *Mar. Pollut. Bull.* **73**, 504-515 (2013).

28. NPD Guidelines for Designation of Wells and Wellbores, (2014). http://www.npd.no/Global/Norsk/5Regelverk/Tematiskeveiledninger/Bronner_betegnelser_og_klassifisering_e.pdf .

29. Rehder, G., Schneider von Deimling, J. RV Sonne Cruise Report SO 196 SUMSUN. Leibniz Institute for Baltic Sea Research, Warnemünde, 77 p. (2008) , doi: PANGAEA, hdl: 10013/epic.35734.

30. Pape, T., et al. Molecular and isotopic partitioning of low-molecular-weight hydrocarbons during migration and gas hydrate precipitation in deposits of a high-flux seepage site. *Chem. Geol.* **269**, 350–363 (2010).

31. Bernard, B.B., Brooks, J.M., Sackett, W.M. Light hydro-carbons in recent Texas continental shelf and slope sediments. *J. Geophy. Res.* **83**, 4053-4061 (1987).

32. James, A.T. Correlation of reservoired gases using the carbon isotopic compositions of wet gas Components. *Am. Assoc. Petr. Geol. B.* **74**, 1441-1458 (1990).

33. Løseth H., Gading, M., Wensaas, L. Hydrocarbon leakage interpreted on seismic data. *Mar. Petrol. Geol.* **26**, 1304-1319 (2009).

34. Judd, A.G., Hovland, M. The evidence of shallow gas in marine sediments. *Cont. Shelf Res.* **12**, 1081-1095 (1992).

35. Farreira, T., Rasband, W. ImageJ User Guide IJ 1.46r. 185p (2012). http://imagej.nih.gov/ij/docs/guide/index.html.

36. Clift, R., Grace, J.R., Weber, M.E. *Bubbles, Drops, and Particles*. Academic Press, London p. 380 (1978).

37. Linke, P., Schmidt, M., Rohleder, M., Al-Barakati, A., Al-Farawati, R. Novel online digital video and high-speed data broadcasting via standard coaxial cable onboard marine operating vessels. *Mar. Technol. Soc. J.* **49** (1), 7-18 (2015).

38. Blees, J., et al. Micro-aerobic bacterial methane oxidation in the chemocline and anoxic water column of deep south-Alpine Lake Lugano (Switzerland). *Limnol. Oceanogr.* **59** (2), 311–324 (2014).

39. Treude, T., Boetius, A., Knittel, K., Wallmann, K., Jørgensen, B.B. Anaerobic oxidation of methane above gas hydrates at Hydrate Ridge, NE Pacific Ocean. *Mar. Ecol. Prog. Ser.* **264**, 1–14 (2003).

40. Duan, Z., Moller N., Weare, J.H. An equation of state for the CH_4-CO_2-H_2O system: I. Pure systems from 0-1000°C and from 0 to 8000 bar. *Geochim. Cosmochim. Acta* **56**, 2605-2617 (1992).

41. Duan, Z.H., Mao, S. A thermodynamic model for calculating methane solubility, density and gas phase composition of methane-bearing aqueous fluids from 273 to 523 K and from 1 to 2000 bar. *Geochim. Cosmochim. Acta* **70**, 3369-3386 (2006).

42. Geng, M., Duan, Z.H. Prediction of oxygen solubility in pure water and brines up to high temperatures and pressures. *Geochim. Cosmochim. Acta* **74**, 5631-5640 (2010).

43. Mao, S., Duan, Z.H. A thermodynamic model for calculating nitrogen solubility, gas phase composition and density of the N_2-H_2O-NaCl-system. *Fluid Phase Equilibr.* **248**, 103-114 (2006).

44. Boudreau, B.P. *Diagenetic Models and their Implementation: Modelling Transport and Reactions in Aquatic Sediments*. Berlin, Heidelberg, New York, London, Paris, Tokyo, Hong Kong: Springer, 414 pp (1997).

45. Zheng, L., Yapa, P.D., 2002. Modeling gas dissolution in deepwater oil/gas spills. *J. Marine Syst.* **31**, 299-309.

46. Wüest, A., Brooks, N.H., Imboden, D.N. Bubble plume modeling for lake restoration. *Water Resour. Res.* **28** (12), 3235–3250 (1992).

47. Sofroniou, M., Knapp, R. Wolfram Mathematica Tutorial Collection- Advanced numerical differential equation solving in Mathematica. Wolfram Research, Inc. (2008). http://www.wolfram.com/

learningcenter/tutorialcollection/AdvancedNumericalDifferentialEquationSolvingInMathematica/AdvancedNumericalDifferentialEquationSolvingInMathematica.pdf

48. McGinnis, D. F., Little J.C. Predicting diffused-bubble oxygen transfer rate using the discrete-bubble model. *Water Res.* **36**, 4627–4635 (2002).

49. Leifer, I., and Patro, R.K. The bubble mechanism for methane transport from the shallow sea bed to the surface: A review and sensitivity study. *Cont. Shelf Res.* **22**, 2409–2428 (2002).

50. UNESCO, 1981. The Practical Salinity Scale 1978 and the International Equation of State of Seawater 1980. *Tech. Pap. Mar. Sci.* **36**, 25 pp (1981).

51. Sommer, S., Schmidt, M., Linke, P. Continuous inline mapping of a dissolved methane plume at a blowout site in the Central North Sea UK using a membrane inlet mass spectrometer – water column stratification impedes immediate methane release into the atmosphere. *Mar. Petrol. Geol.* **68**, Part B, 766–775, (2015).

52. Leifer, I. Seabed bubble flux estimation by calibrated video survey for a large blowout seep in the North Sea. *Mar. Petrol. Geol.* **68**, Part B, 743–752, (2015).

53. Leifer, I., et al. The fate of bubbles in a large, intense bubble megaplume for stratified and unstratified water: Numerical simulation of 22/4b Expedition field data. *Mar. Petrol. Geol.* **68**, Part B, *806–823,* (2015).

54. Pedersen, R.B., et al. ECO2 Deliverable 1.1: Report of Leakage Assessment. (2013). http://dx.doi.org/10.3289/ECO2_D1.1.

Appendix D: Supporting Material to Chapter IV:

Footprint and detectability of a well leaking CO_2 into the North Sea:
Implications from a field experiment and numerical modelling

Lisa Vielstädte, Peter Linke, Benjamin Tews, Mark Schmidt, Stefan Sommer, Matthias Haeckel, and Klaus Wallmann

S.IV.1. Supplementary Material and Methods

This section provides details on the least-squares fits of data, i.e. accuracy and correlation of fit parameters, used in this study to force numerical models of CO_2 bubble dissolution (Section S.IV.1.1.3-S.IV1.1.4) and solute plume dispersion (Section S.IV.1.1.1) and to convert predicted DIC concentrations into carbonate system parameters of interest, i.e. pH and pCO_2 (Section S.IV.1.1.2). Furthermore, we provide additional data on the setup of the COMSOL model to simulate the GRE, i.e. by the coupling of fluid flow and mass transport physical interfaces (Section S.IV.1.2). In Section S.IV.1.3 we discuss the robustness of numerical results by comparing the results of two numerical codes (i.e. COMSOL Multiphysics and Gascoigne) that have been applyed to simulate the same CO_2 leakage scenario. Finally, we show results of DIC measurements recorded during a transect in the Tommeliten seepage area (Alk374), which data have been used to determine the spatial heterogeneity of DIC concentrations in the Sleipner area (Section S.IV.1.4).

S.IV.1.1 Data fitting

All data-fits were processed using least-scares data fitting tools implemented in the Wolfram Mathematica software. In the following, the accuracy of applied fit equations and the correlation of fit parameters are provided in table form.

S.IV.1.1.1 Fitting velocity data

Supplementary Table IV.1: Fitting velocity data in northern direction (u_y in mm s^{-1}) as a function of time (t/ s) and distance to the seafloor (*z*; here 3.2 m) by application of the law of the wall (with z_0=1.4·10^{-4} m and k=0.4; e.g. McGinnis et al., 2014). This fit has been used to force the horizontal advective transport of DIC in the leaky well simulations.

$$u_y(t,z) = \frac{\left(a - b\,Sin\left[\frac{\pi(t+c)}{22400}\right]\right)}{k} \cdot \ln[\frac{3.2}{z_0}]$$

	Correlation matrix for parameters a	b	c	Least squares estimates of parameters	Standard error (1-σ)
a	1	0.04	0.03	-2.52	0.03
b	0.04	1	0.03	-3.94	0.04
c	0.03	0.03	1	36019	79
	Standard deviation of the fit (1σ)/ mm s^{-1}			29.7	

For data fitting, ADCP velocity data recorded during OCE1 Bin 1 (3.2 masf) have been used.

Supplementary Table IV.2: Fitting velocity data in eastern direction (u_x in mm s^{-1}) as a function of time (t/ s) and distance to the seafloor (*z*; here 3.2 m) by application of the law of the wall (with z_0=1.4·10^{-4} m and k=0.4; e.g. McGinnis et al., 2014). This fit has been used to force the horizontal advective transport of DIC in the leaky well simulations.

$$u_x(t,z) = \frac{\left(a - b\,Sin\left[\frac{\pi(t+c)}{22400}\right]\right)}{k} \cdot \ln[\frac{3.2}{z_0}]$$

	Correlation matrix for parameters a	b	c	Least squares estimates of parameters	Standard error (1-σ)
a	1	0.03	0.05	0.37	0.03
b	0.03	1	0.03	-2.21	0.04
c	0.05	0.03	1	-5279	118
	Standard deviation of the fit (1σ)/ mm s^{-1}			24.5	

For data fitting, ADCP velocity data recorded during OCE1 Bin 1 (3.2 masf) have been used.

Supplementary Table IV.3: Fitting resultant velocity data (u_r in mm s^{-1}) as a function of time (t in s) at 3.2 m distance from the seafloor by application of the law of the wall. The fit has been used to calculate the shear velocity (u_r* in mm s^{-1}) as a function of time (t in s) in order to further determine the water column turbulent diffusivity (D_T), which has been used to force the turbulent diffusive transport of DIC in the leaky well simulations (see Eq. IV.6).

$$u_r(t,z) = \frac{u^*(t)}{k} \cdot ln\left[\frac{3.2}{z_0}\right];\ with$$

$$u_r^*(t) = \sqrt{\left(a + b\frac{Sin[\pi(t-c)]}{22400}\right)^2 + \left(d + e\frac{Sin[\pi(t-f)]}{22400}\right)^2}$$

	Correlation matrix for parameters						Least squares estimates of parameters	Standard error (1-σ)
	a	b	c	d	e	f		
a	1	-0.32	-0.04	-0.02	0.27	0.04	2.05	0.04
b	-0.32	1	-0.01	-0.51	0.04	0.01	4.56	0.05
c	-0.04	-0.01	1	-0.10	0.33	-1	-8,065	80
d	-0.02	-0.51	-0.10	1	-0.44	0.10	1.84	0.05
e	0.27	0.04	0.33	-0.44	1	-0.33	0.65	0.06
f	0.04	0.01	-1	0.10	-0.33	1	-23,260	2
	Standard deviation of the fit (1σ)/ mm s^{-1}						23.1	

For data fitting, ADCP velocity data recorded during OCE1 Bin 1 (3.2 masf) have been used.

Supplementary Table IV.4: Fitting resultant velocity data (u_r in mm s^{-1}) as a function of time (t in s) at 3.2 m distance from the seafloor. The fit has been used as velocity condition at the inlet boundary of the GRE model, constraining the numerically-derived advective flow during the experiment (for details see Supp. Tab. IV.11).

$$u_r(t, 3.2) = a + b\ t + c\ Sin(\frac{\pi\ t}{8000})$$

	Correlation matrix for parameters			Least squares estimates of parameters	Standard error (1-σ)
	a	b	c		
a	1	-0.94	-0.80	120	4
b	-0.95	1	0.83	0.0062	0.0006
c	-0.80	0.83	1	-36	3
	Standard deviation of the fit (1σ)/ mm s^{-1}			20.2	

For data fitting, ADCP velocity data recorded during OCE2 Bin 1 (3.2 masf) have been used.

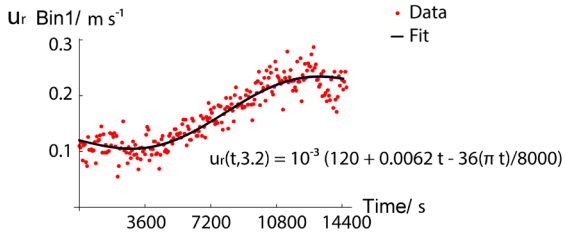

Supplementary Figure IV.1: Resultant current velocity data (red dots) during the 4h ROV observation of the GRE and the least-squares data fit (black curve) used as normal velocity inlet boundary condition to run the GRE model.

S.IV.1.1.2 Fitting transfer functions to derive carbonate system parameters of interest

Supplementary Table IV.5: pCO_2 signals (µatm) derived from applying an analytical solution (Section IV.2.2.3) were fitted as a function of DIC excess concentration (DICex in µM) assuming constant TA. This transfer function has been used to convert computed DICex concentrations into pCO_2 signals in order to compare results of the GRE plume dispersion model with pCO_2 signals observed in the field.

$$pCO2 = \frac{1}{1+e^{DIC_{ex}-50}}(430 + aDIC_{ex} + b\,DIC_{ex}^2) + \frac{1}{1+e^{50-DIC_{ex}}}(480 + c\,DIC_{ex} + d\,DIC_{ex}^2 + f\,DIC_{ex}^3)$$

	Correlation matrix for parameters					Least squares estimates of parameters	Standard error (1-σ)
	a	b	c	d	f		
a	1	-0.93	0.03	-0.03	0.03	3.9	8
b	-0.93	1	-0.05	0.50	-0.04	-0.03	0.2
c	0.03	-0.04	1	-0.95	-0.89	2.1	0.4
d	-0.03	0.05	-0.95	1	-0.98	0.030	0.001
f	0.03	-0.04	0.89	-0.98	1	$-1.6\cdot10^{-5}$	$1\cdot10^{-6}$
	Standard deviation of the fit (1σ)/ mm s^{-1}					124.5	

For data fitting, pCO_2 data predicted by an analytical solution have been used (details on the parameterization of the carbonate system parameters are given in Tab. IV.5).

Supplementary Table IV.6: pH levels derived from applying an analytical solution (Section IV.2.2.3) were fitted as a function of DIC excess concentration (DICex in µM) assuming constant TA. This transfer function has been used to covert modeled DICex concentrations in pH units in order to evaluate the environmental impact of the three leaky well scenarios.

$$pH = 8 + a\ DIC_{ex} + b\ DIC_{ex}^2$$

	Correlation matrix for parameters a	b	Least squares estimates of parameters	Standard error (1-σ)
a	1	0.96	0.00321	0.00005
b	0.96	1	$1.73*10^{-6}$	$7.0*10^{-8}$
	Standard deviation of the fit (1σ)/ units		0.03	

For data fitting, pH data predicted by an analytical solution have been used (details on the parameterization of the carbonate system parameters are given in Tab. IV.5).

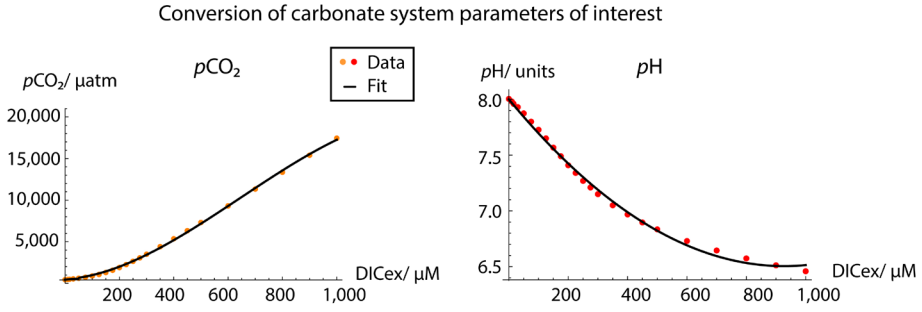

Supplementary Figure IV.2: Results showing pH (red dots) and pCO_2 values (orange dots) as a function of excess DIC concentration and the applied data fit (black curve) in order to convert plume model-derived DIC excess concentrations into carbonate system parameters of interest.

S.IV.1.1.3 Initial bubble size distributions

Supplementary Table IV.7: Fitting the dimensionless volumetric contribution (V_0/V_ψ) of initial bubble sizes (r_0) generated during the GRE (results are shown in Fig. IV.4a). The fit has been used to calculate the combined rate of CO_2 bubble dissolution (Eq. IV.2) in order to simulate the GRE.

$$V_0/V\psi_{GRE} = c \cdot e^{-(\frac{r_{eq}-a}{c})\text{^}2}$$

	Correlation matrix for parameters			Least squares estimates of parameters	Standard error (1-σ)
	a	b	c		
a	1	-0.003	-0.002	2.14	0.07
b	-0.003	1	0.58	-0.44	0.09
c	-0.002	0.58	1	0.12	0.02
	Standard deviation of the fit (1σ)/ 1			0.04	

For data fitting, HD image-derived initial bubble sizes and calculated bubble volumes have been used.

Supplementary Table IV.8: Fitting the dimensionless volumetric contribution (V_0/V_ψ) of initial bubble sizes (r_0 in mm) found at methane leaking wells (Vielstädte et al., 2015; results are shown in Fig. IV.4a). The fit has been used to calculate the combined rate of CO_2 bubble dissolution (Eq. IV.2) in order to run the leaky well scenarios.

$$V_0/V\psi_{\mathrm{LW}} = c \cdot e^{-(\frac{r_{eq}-a}{c})\text{^}2}$$

	Correlation matrix for parameters			Least squares estimates of parameters	Standard error (1-σ)
	a	b	c		
a	1	-0.03	0.05	2.74	0.02
b	-0.03	1	-0.62	0.497	0.003
c	0.05	-0.62	1	0.105	0.007
	Standard deviation of the fit (1σ)/ 1			0.01	

For data fitting, video-derived initial bubble sizes and calculated bubble volumes as described in Vielstädte et al., 2015 have been used.

S.IV.1.1.4 Rate of bubble dissolution

Supplementary Table IV.9: Fitting model-derived rates of CO_2 bubble dissolution (BD in m^{-1}) as a function of the bubble distance from the seafloor (z in m) based on the initial bubble size distribution (Ψ_{GRE}) and water depth at which bubbles were released (81.8 m) during the GRE. The fit has been used to calculate the source rate of CO_2 (S) in the GRE plume dispersion model (Eq. IV.4).

$$BD(\psi_{GRE}, 81.8) = IF[z < 2.21, 0, a \cdot e^{-b\,z^2}]$$

	Correlation matrix for parameters a	b	Least squares estimates of parameters	Standard error (1-σ)
a	1	0.97	7.6	0.9
b	0.97	1	0.31	0.02
	Standard deviation of the fit (1σ)/ m^{-1}		0.08	

For data fitting, combined CO_2 bubble dissolution rates have been used (details on the parameterization of the bubble dissolution model are given in Tab. IV. 2).

Supplementary Table IV.10: Fitting model-derived rates of CO_2 bubble dissolution (BD in m^{-1}) as a function of the bubble distance from the seafloor (z in m) based on the initial bubble size distribution (Ψ_{LW}) and water depth at which bubbles are released (81.8 m) during the leaky well simulations. The fit has been used to calculate the source rate of CO_2 (S) of the leaky well scenarios (Eq. IV.4).

$$BD(\psi_{LW}, 81.8) = a \cdot e^{-b\,z^2}$$

	Correlation matrix for parameters a	b	Least squares estimates of parameters	Standard error (1-σ)
a	1	0.53	1.16	0.03
b	0.53	1	1.06	0.07
	Standard deviation of the fit (1σ)/ m^{-1}		0.04	

For data fitting, combined CO_2 bubble dissolution rates have been used (details on the parameterization of the bubble dissolution model are given in Tab. IV.2).

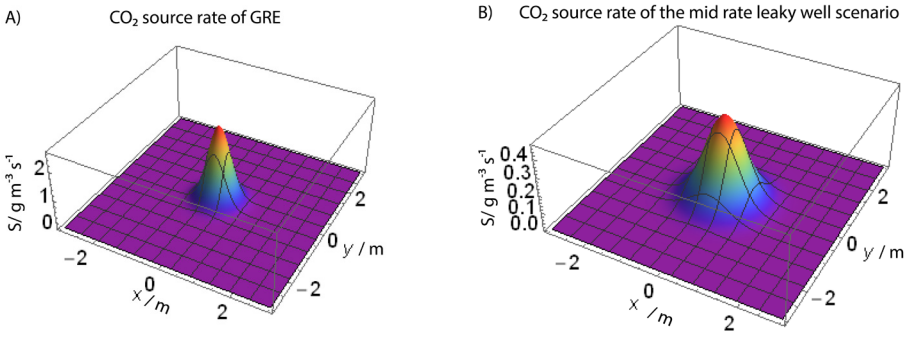

Supplementary Figure IV.3:
Parameterization of the CO_2 source term, $S(t,x,y,z) = \frac{1}{\pi \cdot w} \cdot e^{\frac{-(x^2+y^2)}{w}} \cdot R_{CO2} \cdot BD(\psi, 81.8)$,

at the depth of gas release (81.8 m) for the simulation of the GRE (**A**) and the mid-range leaky well scenario (R_{CO2}=20 t yr^{-1} of CO_2) (**B**). The gas flux during the GRE was higher than during the leaky well scenarios due to the higher leakage rate (i.e. R_{CO2}=31 t yr^{-1} of CO_2) and the smaller area from which bubbles were released (details on the parameterization of the source term are given in Tab. IV.3 and IV.4 for the GRE and leaky well scenarios, respectively).

S.IV.1.2 Setup of the COMSOL model to simulate the GRE

Supplementary Table IV.11: Setup of the plume dispersion model in COMSOL Multiphysics in order to simulate the GRE by coupling the k-ε turbulence model (spf) and transport of diluted species (tds) physics interfaces.

	Coupled physics interfaces to simulate the GRE	
Physics Interface	k-ε turbulence model (spf) with Turbulent Mixing subnode	Transport of Dilutes Species (tds)
Model Inputs	**Fluid Properties:** Seawater density and Dyn. Viscosity of seawater **Turbulence Parameters:** I_T and L_T prescribed as Inlet Boundary Condition	**Velocity field** (u, from spf solution) **Diffusion Coefficient**: $D_M=10^{-9}$ m^2 s^{-1} D_T (from spf solution) **Source Rate**: S
Initial Values	u=0	C=0
Boundary Conditions	**Inlet**: Velocity Condition (Normal Velocity: Fit to ADCP Data) **Outlet**: Pressure Condition (Normal stress P=f0=0) **Wall**: slip (no viscous stress at the sides and top) **Wall**: no-slip (Boundary Condition of the Lander geometry and seafloor), Wall roughness length= k_{seq}	**Inflow** through northern Boundary (B.): C=0 **Outflow** through southern B.: n (-D∇C)=0 (ignores diffusion) **No Flux**: at all other boundaries
Model Geometry	Rectangle model domain of 50x20x20 m^3 in x,y,z with a smaller rectangle of 2.2x0.7x2.2 m^3 in x,y,z in its center (in accordance to the geometry of the Ocean Elevator).	
Mesh (user-defined)	Extra Fine: Free Tetrahedal (dx_{min}=0.075 m; dx_{max}=1.75 m) Local Mesh Refinement along Lander Boundaries (dx_{min}=0.075 m; dx_{max}=0.2 m) Boundary Layers along the no-slip BC at the seafloor	
Model Simulations	Rotation of Ocean Elevator: 40°, 70°	

S.IV.1.3 Robustness of numerical results

The simulation of a point-source CO_2 leak which is transported within a large-scale domain exhibits some numerical difficulties. In the advection-dominated case, that is, the advective term is relatively large compared to the diffusion coefficient (i.e. Pe>10), there may occur unphysical oscillations of the discrete solution. A stable numerical scheme can be obtained by adding artificial diffusion in streamline and crosswind direction to the advection-diffusion-equation weighted by a mesh-dependent parameter (Brooks et al., 1982; Do Cramo et al., 2003; Codina, 1998). However, the discrete solution may become unphysical, if the effect of the stabilization term is too large. Therefore, a sufficiently small local mesh size is of importance in order to guarantee accuracy of numerical predictions.

To examine the extent to which the numerical solution might have been impacted by any unphysical diffusivity, we evaluate the reproducibility of numerical results by comparing the output of two numerical codes (i.e. the described COMSOL model and the Gascoigne model (http://www.gascoigne.uni-hd.de). The two numerical models were forced by the same CO_2 source rate (20 t yr^{-1} of CO_2), advection and diffusion parameters for the dispersion of the CO_2 leak (those given in Tab. IV.4) but used different advection stabilization schemes (i.e. streamline-upwind (Brooks et al., 1982) in the Gascoigne model and a combination of streamline-upwind and crosswind stabilization (Do Carmo and Alvarez, 2003; Codina, 1998) in the COMSOL model) and different spatial discretization methods, i.e. local mesh refinement (COMSOL) and adaptive mesh refinement methods (Gascoigne) with a highest resolution of the finite element mesh of 0.6 m. We compare three output parameters 1) the maximum concentration of DIC (DIC_{max}) in the model domain, 2) the water volume impacted by excess DIC concentrations exceeding those of natural heterogeneity ($DICex$> 16 µM), and 3) the seafloor area impacted by those elevated DIC concentrations.

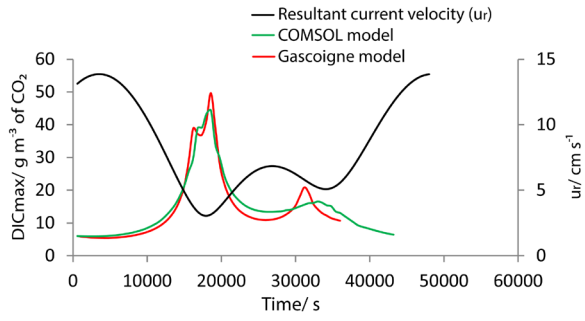

Supplementary Figure IV.4: Comparative analysis of the Gascoigne (red line) and COMSOL (red line) model showing maximum values of DIC excess concentrations in the model domain as a function of model run time. DIC excess concentrations are generally consistent for both numerical codes, with slightly sharper peak values computed by the Gascoigne model.

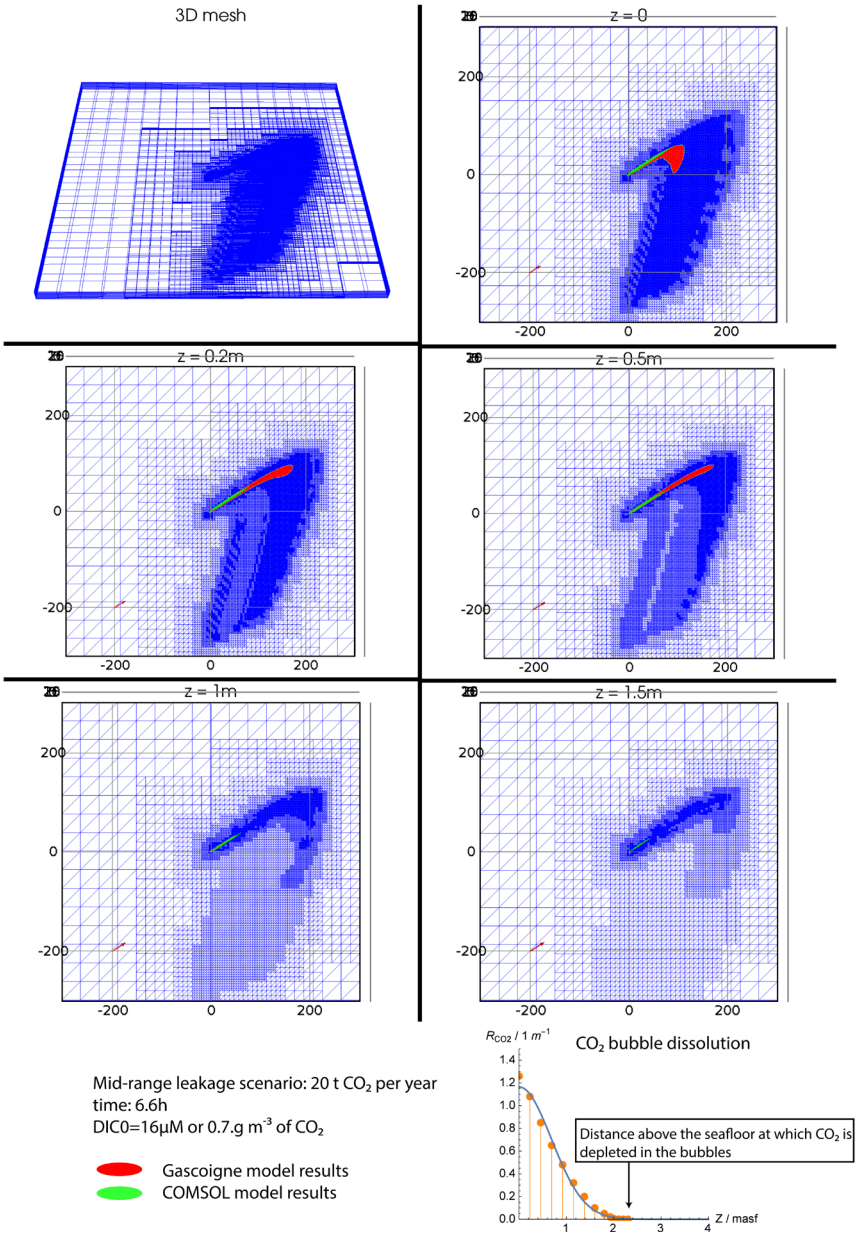

Supplementary Figure IV.5: Comparative analysis showing the results of the two numerical models (COMSOL and Gascoigne) that have been used to predict the dispersion of a detectable CO_2 plume (DIC threshold = 16 µM or 0.7 g m^{-3} of CO_2) 6.6 hours after the start of the computation for different depths above the seafloor (z). The applied models were forced by the same CO_2 source rate (20 t yr^{-1}) and input parameters for the advective and diffusive transport of DIC but used different spatial discretization and stabilizing advection schemes. The seafloor footprint predicted by the Gascoigne model, which uses adaptive mesh refinement methods (minimum mesh size of the finite elements is 60 cm) and the SUPG stabilizing advection scheme, were significantly larger than those predicted by the COMSOL model, which uses local mesh refinement methods (finite element sizes varied between 0.15 and 3 m) and a combination of streamline-upwind (SUPG) and crosswind stabilizing advection schemes instead. In contrast, 1.5 m above the seafloor there was no detectable CO_2 plume in the Gascoigne model, whereas in the COMSOL model DIC concentrations exceeding the threshold value for leak detection were still present. As model parameterizations were identical, comparative results suggest less pronounced diffusive transport in horizontal and vertical directions in the Gascoigne model, indicating that the code might be more accurate in terms of any unphysical numerical diffusivity.

Comparative analysis reveals that numerical results of DIC peak concentrations are generally consistent for both models indicating that there is no discrepancy between model parameterization and that the predictions on the level of seawater acidification are robust (Supp. Fig. IV.4). However, slightly larger and sharper DIC peak concentrations indicate that the stabilizing advection scheme and spatial discretization method of the Gascoigne model might be less diffusive than those implemented in the COMSOL model. This is consistent with larger (about one order of magnitude) seafloor areas impacted by leaking CO_2 and a reduced vertical transport of dissolved CO_2 in the Gascoigne model predictions (Supp. Fig. IV.5-6). Nonetheless, the predicted CO_2 footprints in the Gascoigne model show only a weak temporal correlation to the current flow and the state of the tides (i.e. largest footprints occur at moderate flow and not during slack water, for details see Supp. Fig. IV.6).

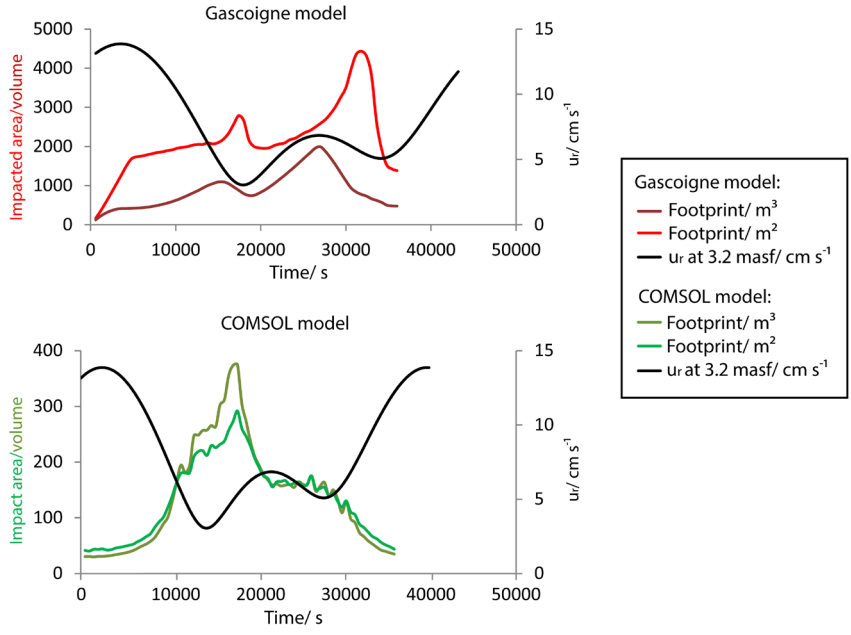

Supplementary Figure IV.6: Comparative analysis of the Gascoigne (red lines) and COMSOL model (green lines) showing CO2 footprints that are geochemically distinguishable from natural heterogeneity (i.e. DICex>16µM) as a function of model run time (the black line reflects the time series data of the resultant current velocity 3.2 masf, ur). Note, the detectable seafloor areas and water volumes that would be impacted by a well leaking CO_2 at a rate of 20 t yr^{-1} are about one order of magnitude higher in the Gascoigne model than in the COMSOL model, confirming the assumption that the Gascoigne model is less diffusive. However, the predicted CO_2 footprints in the Gascoigne model show only a weak correlation to the current flow and the state of the tides.

In summary, the discrepancy in computed CO_2 footprints between both numerical codes indicates that predictions on the sizes of environmentally harmful and detectable CO_2 plumes in seawater are less robust than the computed level of seawater acidification. The latter is considered accurate because model-derived DIC peak concentrations are generally consistent for both models (Supp. Fig. IV.4). Despite the large (about one order of magnitude) differences in model-derived CO_2 footprints both numerical codes imply that the spatial impact of a point-source CO_2 leak would be very local and arguably not significant on a regional North Sea scale. More sophisticated model runs are needed to evaluate the divergence of the applied codes, by testing and improving spatial and temporal discretization methods and stabilizing advection schemes. In addition, field data covering the far-field of a leak at low rates are needed to validate models in order to make more accurate predictions on fine-scale CO_2 leakage into a large-scale domain.

S.IV.1.4 Spatial heterogeneity of DIC concentrations in the CNS

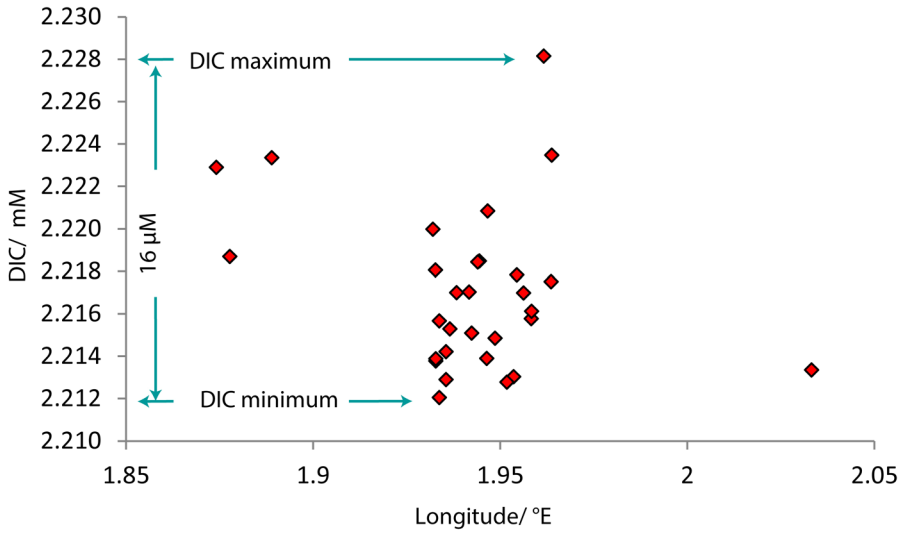

Supplementary Figure IV.7: Heterogeneity of DIC concentration measured in 78-83 m water depth during an 11 h CTD transect in the Tommeliten seepage area. The DIC heterogeneity of 16 µM was assumed to be also representative for the "nearby" Sleipner area, due to similar physicochemical conditions of seawater and was thus, used as a geochemical threshold for leak detection.

References:

McGinnis, D.F., Sommer, S., Lorke, A., Glud, R.N., Linke, P., 2014. Quantifying tidally driven benthic oxygen exchange across permeable sediments: An aquatic eddy correlation study. *J. Geophys. Res. Oceans* **119**, 6918-6932. Doi:10.1016/2014JC010303.

Vielstädte et al., 2015. Quantification of methane emissions at abandoned gas wells in the Central North Sea. *Mar. Petrol. Geol.* **68**, Part B, 848–860. Doi:10.1016/j.marpetgeo.2015.07.030.

Lisa Vielstädte

Diplom Geologin, Marine Geoscientist

Address:	Waitzstr. 41a D-24105 Kiel
Phone:	+49 (0)176 84322451
Email:	lvielstaedte@geomar.de
Date of birth:	04.08.1983
Place of birth:	Mettingen, Germany
Nationality:	German

Curriculum Vitae

Since 2/2012	Research associate at the Helmholtz Centre for Ocean Research Kiel, GEOMAR.
9/2006-5/2011	Studies of Geologie-Paläontologie at the University of Kiel